Università degli Studi di Palermo

AREA QUALITÀ, PROGRAMMAZIONE E SUPPORTO STRATEGICO
SETTORE STRATEGIA PER LA RICERCA
U. O. DOTTORATI

Dottorato di ricerca in Scienze della Terra e del Mare
Dipartimento di Scienze della Terra e del Mare (DiSTeM)
Settore Scientifico Disciplinare: BIO/05 – Zoologia

UNDER PRESSURE: ASSESSING MULTIPLE STRESS IN ANTHOZOANS. RESPONSES TO POLLUTION, INFECTION, INFLAMMATION, REGENERATION AND TEMPERATURE PLASTICITY

IL DOTTORE
Dott.ssa Claudia La Corte

IL COORDINATORE
Prof. Alessandro Aiuppa

IL TUTOR
Prof.ssa Maria Giovanna Parisi

CO TUTOR
Prof. Matteo Cammarata

CICLO XXXVI
ANNO CONSEGUIMENTO TITOLO 2023

“Lo scienziato nel suo laboratorio non è solo un tecnico, è anche un bambino davanti a fenomeni della Natura che lo affascinano come un racconto di fate.”

Marie Skłodowska Curie

INDEX

LIST OF PAPERS:

Directly connected papers with the thesis

La Corte, C., Baranzini, N., Grimaldi, A., Parisi, M.G., 2022. Invertebrate Models in Innate Immunity and Tissue Remodeling Research. https://doi.org/10.3390/ijms23126843

Parisi, M.G., Grimaldi, A., Baranzini, N., **La Corte, C.**, Dara, M., Parrinello, D., Cammarata, M., 2021a. Mesoglea extracellular matrix reorganization during regenerative process in *Anemonia viridis* (Forskål, 1775). Int. J. Mol. Sci. 22. https://doi.org/10.3390/ijms22115971

La Corte, C., Baranzini, N., Dara, M., Bon, C., Grimaldi, A., Parisi, M.G., Zizzo, M.G., Cammarata, M., Step-by-Step Regeneration of Tentacles after Injury in *Anemonia viridis*—Morphological and Structural Cell Analyses, Int. J. Mol. Sci. 24 (2023) 8860. https://doi.org/10.3390/ijms24108860

Other relevant papers

Dara, M., Carbonara, P., **La Corte, C.**, Parrinello, D., Cammarata, M., Parisi, M.G., Fish Welfare in Aquaculture: Physiological and Immunological Activities for Diets, Social and Spatial Stress on Mediterranean Aqua Cultured Species, Fishes. 8 (2023) 414. https://doi.org/10.3390/fishes8080414

La Corte, C., Dara, M., Bertini, F., Parrinello, D., Piazzese, D., Parisi, M.G., 2023. Response of *Sabella spallanzanii* to multiple stressors. The combined effect of infection and copper sulphate. Comp. Biochem. Physiol. Part C Toxicol. Pharmacol. 263, 109475. https://doi.org/10.1016/j.cbpc.2022.109475

Parisi, M.G., Baranzini, N., Dara, M., **La Corte**, C., Vizioli, J., Cammarata, M., 2022. AIF-1 and RNASET2 are involved in the inflammatory response in the Mediterranean mussel *Mytilus galloprovincialis* following *Vibrio* infection. Fish Shellfish Immunol. 127, 109–118. https://doi.org/10.1016/j.fsi.2022.06.010

Dara, M., Parisi, M.G., **La Corte, C.**, Benenati, G., Parrinello, D., Piazzese, D., Cammarata,

M., 2022. *Sabella spallanzanii* mucus bacterial agglutinating activity after arsenic exposure. The equilibrium between predation safety and immune response stability. Mar. Pollut. Bull. 181, 113833. https://doi.org/10.1016/J.MARPOLBUL.2022.113833

Dara, M., Giulianini, P.G., Manfrin, C., Parisi, M.G., Parrinello, D., **La Corte, C.**, Vasta, G.R., Cammarata, M., 2021. F-type lectin from serum of the Antarctic teleost fish *Trematomus bernacchii* (Boulenger, 1902): Purification, structural characterization, and bacterial agglutinating activity. Comp. Biochem. Physiol. Part B Biochem. Mol. Biol. 256, 110633. https://doi.org/10.1016/j.cbpb.2021.110633

Parisi, M.G., Pirrera, J., **La Corte, C.**, Dara, M., Parrinello, D., Cammarata, M., 2021b. Effects of organic mercury on *Mytilus galloprovincialis* hemocyte function and morphology. J. Comp. Physiol. B Biochem. Syst. Environ. Physiol. 191, 143–158. https://doi.org/10.1007/s00360-020-01306-0

Dara, M., Torregrossa, N., Bisanti, L., **La Corte, C.**, Bertini, F., Parrinello, D., Piazzese, D., Cammarata, M., Mohamed, B., Parisi, M.G. In vivo and in vitro effects of bioplastic materials on immune functions of mussels (*Mytilus galloprovincialis*). SUBMITTED ON: Chemosphere

Bisanti, L., **La Corte, C.**, Dara, M., Bertini, F., Parrinello, D., Chemello, R., Cammarata, M., Parisi, M.G. How does warmer sea water change the sensitivity of a Mediterranean thermophilic coral after immune-stimulation?. SUBMITTED ON: Coral Reef

SUMMARY

In this PhD thesis have been investigated the innate immunity responses and physiological biomarkers of *Anemonia viridis* (Anthozoa, Cnidaria) in the context of inflammation caused by multiple factors such as thermal stress, pathogens, pollutant, and injury. *A. viridis* could represent an excellent animal model for environmental biomonitoring validation of immunological. A battery of biomarkers, at different levels of biological organization, was used to comprehensively investigate the processes in evidence. Immunity and inflammation are the most evolutionarily widespread and conserved defence mechanism in living organisms in response to pathogens and injuries, which is why I focused on methods that specifically aimed to elucidate these aspects. Organisms have always had to deal with adverse environmental circumstances, which has resulted in the evolution of intricate biological systems to prevent or minimise functional dysregulation. Physiological and molecular mechanisms in cnidarians are not entirely clear and responses to thermal stress in literature resulted extremely different even in species that share a similar genetic pool. Marine invertebrates, including anthozoans, can "acclimate" to thermal stress by modifying some components of their cellular metabolism to better cope with high water temperatures in a climate global change scenario. The physiological acclimatization can involve the host organism, as well as symbionts, and can be modulated by protein factors such as heat shock proteins and immune system effectors. Previous studies have indicated a link between the regulation of the activity of antioxidant enzymes and acclimatization from thermal stress in coral reefs. Indeed, environmental stress can induce an increase in the production of reactive oxygen species (ROS) which damage the cnidarian-Symbiodiniaceae mutualism. The cellular response to the formation of oxygen radicals includes many defence mechanisms such as the activation of scavenger enzymes which act in concert to inactivate the radicals responsible for major cell damage. Moreover, evidence indicates that the anthozoan innate immune system is not only involved in the disruption of harmful microorganisms but is also crucial in structuring tissue-associated microbial communities, that are essential components of the cnidarian holobiont and useful to the animal's health for several functions including metabolism, immune defence, development, and behaviour. The use of the anthozoan as model will make it possible to read the responses to environmental perturbances, to acquire new knowledge on cellular and molecular mechanisms in invertebrate bioindicators which show a high tissue regeneration capacity compared to other evolutionarily more complex organisms, that due to their immunity system have limited regenerative ability. The results

obtained here highlighted how *A. viridis* can be validated as a bioindicator following exposure to heavy metals and how these are agents capable of modulating the immune response of the sea anemone. Then, thanks to the study of tentacular regeneration under constitutive conditions and following thermal stress, it was possible to identify and characterize the stages of regeneration at the macroscopic and tissue levels, the cellular components as well as to study the expression of proteins known to be involved in the inflammatory state and regeneration. Providing valuable information to corroborate the whole process, as a biomarker and also allowing to clarify the link between immunity, inflammation and regeneration. With the aim to study the adaptation to extreme environment, the first investigation on *Urticinopsis antarctica*, Antarctic species, was carried out, in which in addition to tissue and cellular analysis, *de novo* sequencing of the entire transcriptome was performed. The results can be useful to have information on the health state of our seas and to focus on molecular products of adaptative selection pressure with potential transferability to biotechnological field. The knowledge of the immunological biomarkers involved in acclimatization reactions could be important for developing monitoring programs and coordinated management of the coastline in order to cope also with the emerging environmental challenges.

Keywords: Multiple stressors; environmental perturbations; innate immunity; physiological approach; anthozoan regeneration

Chapter 1

Introduction

The marine environment is characterized by continuous changes over time in abiotic factors such as temperature, salinity, pH, and food availability with consequent impacts on organisms. Studies have shown that in temperate coastal area, organisms have developed greater thermal tolerance, implying substantial adaptations linked with climatic modifications (Cereja, 2020; Sunday et al., 2019).

Maintenance of homeostasis through structural and behavioural changes are critical to the survival of the organisms (Newell, 2013; Newell and Branch, 1980). In addition, sessile or low motility species also need modifications at the physiological level to survive in an unstable habitat in order to prevent stress (any external or physical pressure that causes a response from the body) and eliminate biomolecules, such as reactive oxygen species (ROS), which can cause cellular damage and whole body dysfunction (Halliwell and Gutteridge, 2015; Lesser, 2006). Stressors can occur at the same time (multiple stressors) and interact with marine organisms in a way that is complex to predict, and although there are numerous studies on the effects and responses to individual stressors, research based on the study of multiple stresses is still limited, and this is important because the interaction between multiple pressures is capable of producing synergistic and amplified effects with irreversible repercussions on the individual and rapid dysfunction also in the immune system (Parisi et al., 2021).

The ability to respond early to a stress is therefore critical to the survival of the individual, and to do so, organisms are equipped with defence mechanisms such as antioxidant enzymes, proteins tasked with maintaining cell structure, and processes for removing damaged cells (Kültz, 2020; Parisi et al., 2021; Tomanek, 2010).

The use of organism-scale, tissue, cellular and molecular biomarkers are commonly used in stress investigations, providing rapid information on the health status of organisms to the conditions to which they are subjected (Dara et al., 2023; La Corte et al., 2023b; Mydlarz et al., 2008; Parisi et al., 2022).

Because of the above, in the context of oxidative stress, it is useful to use antioxidant defences such as total antioxidant capacity (TOSC), which has been extensively studied in cnidarians (Richier et al., 2008, 2006; Ventura et al., 2018) or proteins that indicate cellular damage such as protein carbonylation. The latter has been widely used as a biomarker of protein oxidation in bivalves, anthozoans, arthropods, and humans (Dalle-Donne et al., 2003;

Rascón and Harrison, 2010; Richier et al., 2006), its increase has been linked to exposures to metals, UV, light, heat, and pro-oxidant agents.

Generally, stressors are capable of causing an increase in unfolded polypeptide chains (due to physiological damage or external factors) indicating the signal prompts the activation of heat shock transcription factors, which, in turn, enhance the expression of a particular group of defensive genes. The most prominent among these genes are commonly known as heat shock proteins (HSP) or chaperones (Richter et al., 2010). These are several subfamilies distinguished by molecular weight that have the function of guaranteeing proper protein folding and assembly.

HSPs are important for the preservation of cytoskeleton integrity, block apoptosis by acting on cytochrome c release pathways, are activated under conditions of cellular stress, and facilitate tissue repair or degradation following injury (Bruey et al., 2000; Mounier and Arrigo, 2002; Samali and Orrenius, 1998).

This research has as its focus, the study of the immune and physiological responses of *Anemonia viridis*, anthozoan of the phylum Cnidaria, at multiple stresses, as it has all the characteristics of a good bioindicator and can give useful information on the issues under investigation, showing interesting features such as the ability to regenerate. Multiple stresses related to pollution and bacterial infection, inflammation and regeneration also under heat stress condition were considered. An investigation, currently in progress, was then carried out on an Antarctic anemone *Urticinopsis antarctica*, in order to be able to apply the information gained through the Mediterranean animal model in an organism adapted to live in an extreme environment that will unfortunately soon face emerging environmental challenges.

Cnidarians include more than 11,000 species of radially symmetrical marine invertebrates, including sea anemones, corals, hydroids, and jellyfish. A first subdivision can be made on an anatomical basis or by DNA (Figure 1). The class Anthozoa includes two subclasses. Octocorallia e Hexacorallia. The major difference is their symmetry with division into 8 or 6 septa.

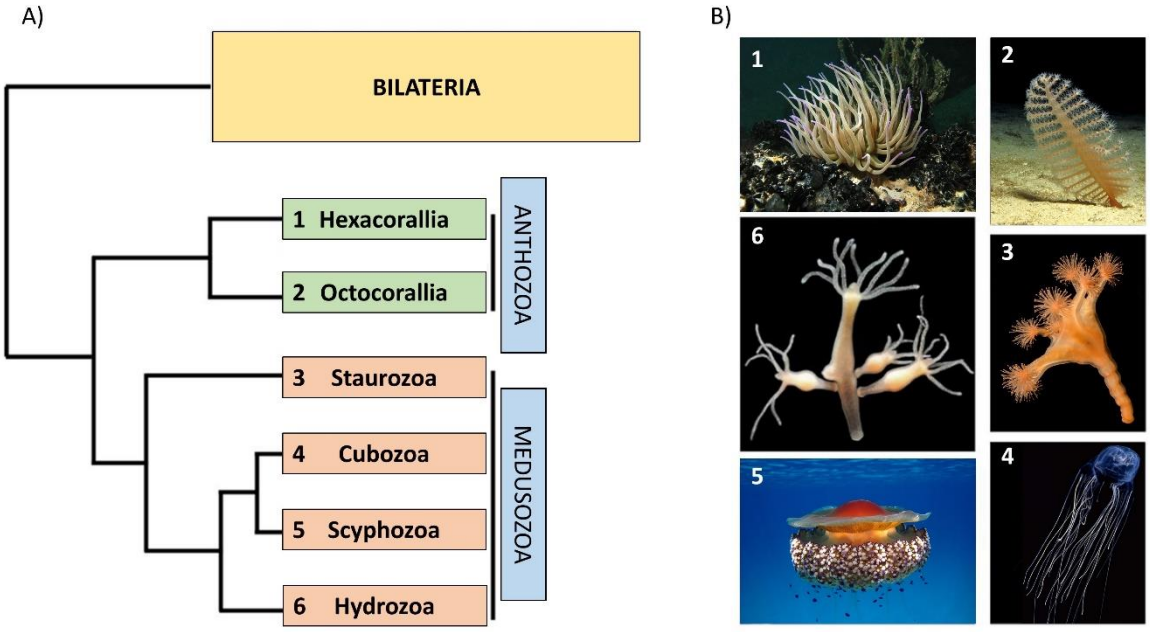

Figure 1 ***(A)*** *Cnidarian philogeny* ***(B)*** *Representative species. By order of number: 1. Anemonia viridis variety smaragdina, 2. Pennatula aculeata, 3. Lucernaria quadricornis, 4. Chironex fleckeri, 5.Cotylorhiza tuberculata, 6. Hydra vulgaris.*

At the morphological level, cnidarians among them show great variability; in general, they are characterized by a simple cavity with a gastric chamber that opens outward with a single opening, serving as both mouth and anus, which is surrounded by tentacles. The ontogeny of Cnidarians is extremely peculiar with an alternation between the polypoid (sessile) and medusoid forms (motile). Medusozoa alternate between both forms during their life cycle, in contrast anthozoans exhibit only the polypoid form (Figure 2).

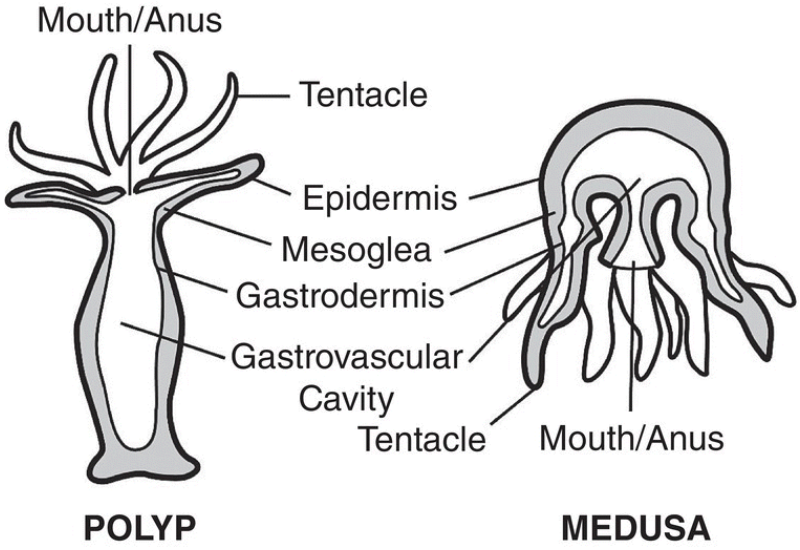

Figure 2 Cnidaria body plan: polyp and medusa. Source Kevin Seline, artist.

It is possible to find colonial species characterized by a large number of small, interconnected individuals capable of secreting a calcareous exoskeleton. These are diblastic

organisms: the endoderm produces the innermost epithelium, the gastroderm; the ectoderm produces the outermost, the epidermis. The two epithelial layers are separated by the mesoglea, a gelatinous matrix almost entirely devoid of cells (Figure 3).

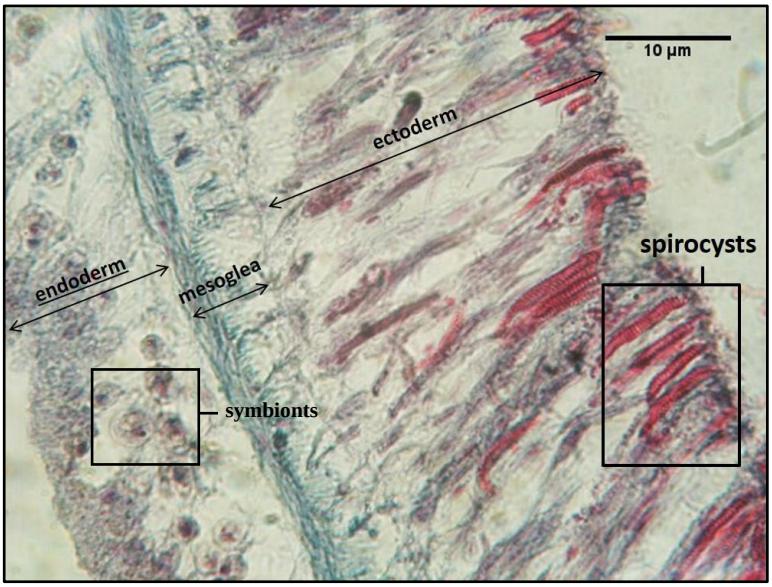

Figure 3 Longitudinal section of Anemonia viridis tentacle stained in Gomori's Trichrome. Are visible the tissue layers, spyrocists and symbiont cells.

They have heterotrophic feeding behavior with specialized cells useful for predatory and defensive activity. They are considered hubs of diverse life forms that hold significance in both ecological and economic contexts, are in fact a source of food, protection and nursery for hundreds of species (Dubinsky, 1992). These are species found in almost all aquatic environments (freshwater and marine), accustomed to wide temperature, salinity and depth conditions. This contrasts with their morphological simplicity if not considered the entire life cycle, symbiosis and regeneration ability; therefore, they have also developed remarkable adaptations at the genetic level to resist stress. Many species benefit from symbiosis with dinoflagellate algae of the genus *Symbiodinium*, commonly called zooxanthellae as well as having an extensive microbial community associated. This allows the species to succeed in colonizing even oligotrophic environments, however, causing the host to adapt to the pro-oxidant conditions caused by photosynthesis (Furla et al., 2005).

The term "holobiont" could be used to refer to the complete set of organisms: the host, symbiont and associated microbial community (Rosenberg et al., 2007). They are also extremely long-lived organisms, and there are known cases of trans-differentiation, reverse development, and absence of senescence processes in addition to the fact that numerous studies have investigated the remarkable capacity for regeneration (Galliot and Schmid,

2002; Parisi et al., 2020; Piraino et al., 1996). These organisms have a number of physiological properties that can be applied to different fields of research beyond environmental research, such as biomedical research; indeed, they possess several fluorescent proteins used as markers in the histological field as well as bioactive molecules with antimicrobial capabilities (Nicosia et al., 2018; Palmer et al., 2009; Trapani et al., 2016, 2014; Wiedenmann et al., 2009).

The research model chosen in this dissertation, *A. viridis*, as an invertebrate, it possesses only innate immunity, meaning that its defence system is based on self/non-self recognition, with humoral and cellular effectors allowing it to respond to infection caused by pathogens and heal from wounds. Many of these components have been identified and characterized in cnidarians and include: recognition and toll-like receptors, peptidoglycan binding proteins, prophenoloxidase and melanin synthesis, antimicrobial proteins and wound repair systems (Mydlarz et al., 2016; Parisi et al., 2020). Advances on molecular and cellular level studies have also supported investigations of the mechanisms of defence systems of cnidarians to the extent that they can be compared with species of the same phylum, but also belonging to others, opening the door to the discovery of genes related to immunity, in non-model animals (Miller et al., 2007; Shinzato et al., 2011).

Currently, there are clear limitations in our understanding of the regulation and timing of these processes and the subsequent impacts on traits and characteristics associated with these pathways. Consequently, another objective of this work is to fill in, as far as possible, these knowledge gaps. In relation to the mechanisms that enable the organism to detect a threat, destroy a pathogen, and repair an injury, four fundamental functions emerge in the immune system of these animals: immune recognition, intracellular signalling, effector reaction, and the process of tissue repair. Recognition of a pathogen induces activation of the immune system. This process occurs through membrane-bound receptors that bind promptly to molecular patterns present in pathogens (Rast and Messier-Solek, 2008). This is interesting if we focus on the mechanisms that regulate the establishment and maintenance of symbiosis, which are mostly to be found in immunity-related processes used to protect the host from pathogens (Rodriguez-Lanetty et al., 2006; Schwarz et al., 2008; Vidal-Dupiol et al., 2009). Therefore, these elements are of considerable interest when analysing the immune system of cnidarians.

The well-being of the holobiont is based on the balance of the symbiosis, and the breakdown of the symbiosis can lead to death. The loss of symbiosis is known as

"bleaching". This phenomenon can occur when the holobiont undergoes stress due to high temperatures, excessive exposure to ultraviolet light, or attack by pathogens (Baird et al., 2009; Lesser et al., 1990). Changes in microbial communities, due to variations in environmental conditions, may contribute to the increase of pathogenic microorganisms capable of causing disease. Maintaining an intact epithelial layer is crucial event for defending against pathogens and other stressors. Unlike hydrozoans, anthozoans possess circulating populations of amoebocytes that can move to injured areas and ingest foreign cells, resulting in exposure to proteolytic enzymes and free radicals (Mullen et al., 2004). Cnidarians are able to activate an inflammatory response in order to destroy or isolate the source of injury (Figure 4).

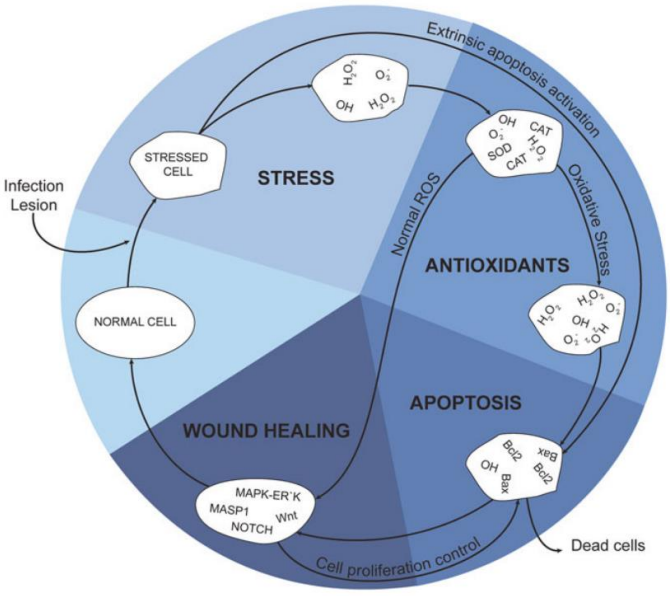

Figure 4 A visual diagram illustrating the sequential stages of tissue restoration and wound recovery subsequent to a pathogen assault or tissue damage (From Mydlarz et al. 2016).

Usually, this process involves the rapid infiltration of immune cells into damaged tissues and the initiation of phagocytosis. Elimination also occurs with the help of ROS or antimicrobial compounds they produce, creating a barrier between affected and healthy tissues (Palmer et al., 2008). Precisely phagocytosis is a mechanism involved in nutrition and symbiosis (Mullen et al., 2004). The wound-healing process is crucial as it restores function to impaired areas and prevents infection. In sessile cnidarians, which are constantly subject to physical damage caused by both non-living and living factors, this process assumes vital significance (Galliot, 2012; Poss, 2010; Reitzel et al., 2008). Following injury, the individual's immune response is activated in order to prevent infection and initiate the process of eliminating damaged cells in the injured area (Peiris et al., 2014). Several stages

have been recognized in the wound-healing process: plug formation, inflammation, tissue proliferation and maturation (Palmer et al., 2011). These depend on the activation of components belonging to different signalling pathways, and in fact the differences found among different taxa even for the regenerative event can be attributed to the increased complexity of the immune system (Godwin and Brockes, 2006; Godwin and Rosenthal, 2014). In *Actinia equina* and in *Anemonia viridis* several cell types related to the wound-healing process have been identified (Hutton and Smith, 1996) as well as the different steps related to the crucial moments of regeneration (La Corte et al., 2023a). It can be concluded that scientific evidence shows that there is a direct link between innate immunity, maintenance of homeostasis, inflammation and regeneration. Given, moreover, the increasingly strict restrictions on the use of vertebrates for experimental purposes, invertebrates are increasingly being used as alternative animal models, which are also convenient from an economic and management perspective (La Corte et al., 2022). It should also be considered that the ability to regenerate organs and body parts developed with the advent of multicellularity. Many invertebrates demonstrate remarkable regenerative capacities, whereas in vertebrates this capacity is limited. This, once again, highlights the enormous potential for using a peculiar organism such as *Anemonia viridis* even in species comparisons with a high degree of sharing between seemingly distant scientific fields.

REFERENCES

Baird, A.H., Bhagooli, R., Ralph, P.J., Takahashi, S., 2009. Coral bleaching: the role of the host. Trends Ecol. Evol. 24, 16–20. https://doi.org/10.1016/J.TREE.2008.09.005

Bruey, J.M., Ducasse, C., Bonniaud, P., Ravagnan, L., Susin, S.A., Diaz-Latoud, C., Gurbuxani, S., Arrigo, A.P., Kroemer, G., Solary, E., Garrido, C., 2000. Hsp27 negatively regulates cell death by interacting with cytochrome c. Nat. Cell Biol. 2, 645–652. https://doi.org/10.1038/35023595

Cereja, R., 2020. Critical thermal maxima in aquatic ectotherms. Ecol. Indic. 119. https://doi.org/10.1016/J.ECOLIND.2020.106856

Dalle-Donne, I., Giustarini, D., Colombo, R., Rossi, R., Milzani, A., 2003. Protein carbonylation in human diseases. Trends Mol. Med. 9, 169–176.

Dara, M., Carbonara, P., La Corte, C., Parrinello, D., Cammarata, M., Parisi, M.G., 2023. Fish Welfare in Aquaculture: Physiological and Immunological Activities for Diets, Social and Spatial Stress on Mediterranean Aqua Cultured Species. Fishes 8, 414. https://doi.org/10.3390/fishes8080414

Dubinsky, Z., 1992. Coral reefs. Ecosystems of the world (Z. Dubinsky [ed.]). Limnol. Oceanogr. 37, 915–915. https://doi.org/10.4319/lo.1992.37.4.0915

Furla, P., Allemand, D., Shick, J.M., Ferrier-Pagès, C., Richier, S., Plantivaux, A., Merle, P.L., Tambutté, S., 2005. The symbiotic anthozoan: A physiological chimera between alga and animal. Integr. Comp. Biol. 45, 595–604. https://doi.org/10.1093/icb/45.4.595

Galliot, B., 2012. *Hydra*, a fruitful model system for 270 years. Int. J. Dev. Biol. 56, 411–423. https://doi.org/10.1387/ijdb.120086bg

Galliot, B., Schmid, V., 2002. Cnidarians as a model system for understanding evolution and regeneration. Int. J. Dev. Biol. 46, 39–48.

Godwin, J.W., Brockes, J.P., 2006. Regeneration, tissue injury and the immune response, in: Journal of Anatomy. https://doi.org/10.1111/j.1469-7580.2006.00626.x

Godwin, J.W., Rosenthal, N., 2014. Scar-free wound healing and regeneration in amphibians: Immunological influences on regenerative success. Differentiation. https://doi.org/10.1016/j.diff.2014.02.002

Halliwell, B., Gutteridge, J.M.C., 2015. Free Radicals in Biology and Medicine. Free Radicals Biol. Med. https://doi.org/10.1093/ACPROF:OSO/9780198717478.001.0001

Hutton, D., Smith, V.J., 1996. Antibacterial Properties of Isolated Amoebocytes From the Sea Anemone *Actinia equina*. Biol. Bull. 191, 441–451. https://doi.org/10.2307/1543017

Kültz, D., 2020. Evolution of cellular stress response mechanisms. J. Exp. Zool. Part A Ecol. Integr. Physiol. 333, 359–378. https://doi.org/10.1002/JEZ.2347

La Corte, C., Baranzini, N., Dara, M., Bon, C., Grimaldi, A., Parisi, M.G., Zizzo, M.G., Cammarata, M., 2023a. Step-by-Step Regeneration of Tentacles after Injury in *Anemonia viridis*—Morphological and Structural Cell Analyses. Int. J. Mol. Sci. 24, 8860. https://doi.org/10.3390/ijms24108860

La Corte, C., Baranzini, N., Grimaldi, A., Parisi, M.G., 2022. Invertebrate Models in Innate Immunity and Tissue Remodeling Research. Int. J. Mol. Sci. 23, 6843. https://doi.org/10.3390/ijms23126843

La Corte, C., Dara, M., Bertini, F., Parrinello, D., Piazzese, D., Parisi, M.G., 2023b. Response of *Sabella spallanzanii* to multiple stressors. The combined effect of infection and copper sulphate. Comp. Biochem. Physiol. Part C Toxicol. Pharmacol. 263, 109475. https://doi.org/10.1016/j.cbpc.2022.109475

Lesser, M.P., 2006. Oxidative stress in marine environments: biochemistry and physiological ecology. Annu. Rev. Physiol. 68, 253–278. https://doi.org/10.1146/annurev.physiol.68.040104.110001

Lesser, M.P., Stochaj, W.R., Tapley, D.W., Shick, J.M., 1990. Bleaching in coral reef anthozoans: effects of irradiance, ultraviolet radiation, and temperature on the activities of protective enzymes against active oxygen. Coral Reefs 8, 225–232. https://doi.org/10.1007/BF00265015

Miller, D.J., Hemmrich, G., Ball, E.E., Hayward, D.C., Khalturin, K., Funayama, N., Agata, K., Bosch, T.C.G., 2007. The innate immune repertoire in cnidaria--ancestral complexity and stochastic gene loss. Genome Biol. 8, R59. https://doi.org/10.1186/gb-2007-8-4-r59

Mounier, N., Arrigo, A.P., 2002. Actin cytoskeleton and small heat shock proteins: how do they interact? Cell Stress Chaperones 7, 167. https://doi.org/10.1379/1466-1268(2002)007<0167:acashs>2.0.co;2

Mullen, K.M., Peters, E.C., Harvell, C.D., 2004. Coral Resistance to Disease. Coral Heal. Dis. 377–399. https://doi.org/10.1007/978-3-662-06414-6_22

Mydlarz, L.D., Fuess, L., Mann, W., Pinzón, J.H., Gochfeld, D.J., 2016. Cnidarian immunity: From genomes to phenomes. Cnidaria, past, Present Futur. World Medusa her Sisters. https://doi.org/10.1007/978-3-319-31305-4_28

Mydlarz, L.D., Holthouse, S.F., Peters, E.C., Harvell, C.D., 2008. Cellular responses in sea fan corals: Granular amoebocytes react to pathogen and climate stressors. PLoS One 3. https://doi.org/10.1371/journal.pone.0001811

Newell, R.C., 2013. Adaptation to environment: essays on the physiology of marine animals.

Elsevier.

Newell, R.C., Branch, G.M., 1980. The Influence of Temperature on the Maintenance of Metabolic Energy Balance in Marine Invertebrates, in: Advances in Marine Biology. pp. 329–396. https://doi.org/10.1016/S0065-2881(08)60304-1

Nicosia, A., Mikov, A., Cammarata, M., Colombo, P., Andreev, Y., Kozlov, S., Cuttitta, A., 2018. The *Anemonia viridis* venom: Coupling biochemical purification and rna-seq for translational research. Mar. Drugs 16, 1–15. https://doi.org/10.3390/md16110407

Palmer, C. V, Modi, C.K., Mydlarz, L.D., 2009. Coral fluorescent proteins as antioxidants. PLoS One 4, e7298. https://doi.org/10.1371/journal.pone.0007298

Palmer, C. V, Mydlarz, L.D., Willis, B.L., 2008. Evidence of an inflammatory-like response in non-normally pigmented tissues of two scleractinian corals. Proceedings. Biol. Sci. 275, 2687–2693. https://doi.org/10.1098/rspb.2008.0335

Palmer, C. V, Traylor-Knowles, N.G., Willis, B.L., Bythell, J.C., 2011. Corals Use Similar Immune Cells and Wound-Healing Processes as Those of Higher Organisms. PLoS One 6, e23992.

Parisi, M.G., Baranzini, N., Dara, M., Corte, C. La, Vizioli, J., Cammarata, M., 2022. AIF-1 and RNASET2 are involved in the inflammatory response in the Mediterranean mussel *Mytilus galloprovincialis* following *Vibrio* infection. Fish Shellfish Immunol. 127, 109–118. https://doi.org/10.1016/j.fsi.2022.06.010

Parisi, M.G., Giacoletti, A., Mandaglio, C., Cammarata, M., Sarà, G., 2021. The entangled multi-level responses of *Mytilus galloprovincialis* (Lamarck, 1819) to environmental stressors as detected by an integrated approach. Mar. Environ. Res. 168. https://doi.org/10.1016/j.marenvres.2021.105292

Parisi, M.G., Parrinello, D., Stabili, L., Cammarata, M., 2020. Cnidarian immunity and the repertoire of defense mechanisms in anthozoans. Biology (Basel). 9, 1–26. https://doi.org/10.3390/biology9090283

Peiris, T.H., Hoyer, K.K., Oviedo, N.J., 2014. Innate immune system and tissue regeneration in planarians: An area ripe for exploration. Semin. Immunol. https://doi.org/10.1016/j.smim.2014.06.005

Piraino, S., Boero, F., Aeschbach, B., Schmid, V., 1996. Reversing the life cycle: Medusae transforming into polyps and cell transdifferentiation in *Turritopsis nutricula* (Cnidaria, Hydrozoa). Biol. Bull. https://doi.org/10.2307/1543022

Poss, K.D., 2010. Advances in understanding tissue regenerative capacity and mechanisms in animals. Nat. Rev. Genet. 2010 1110 11, 710–722. https://doi.org/10.1038/nrg2879

Rascón, B., Harrison, J.F., 2010. Lifespan and oxidative stress show a non-linear response

to atmospheric oxygen in *Drosophila*. J. Exp. Biol. 213, 3441–3448. https://doi.org/10.1242/JEB.044867

Rast, J.P., Messier-Solek, C., 2008. Marine invertebrate genome sequences and our evolving understanding of animal immunity. Biol. Bull. 214, 274–283. https://doi.org/10.2307/25470669

Reitzel, A.M., Sullivan, J.C., Traylor-Knowles, N., Finnerty, J.R., 2008. Genomic survey of candidate stress-response genes in the estuarine anemone *Nematostella vectensis*. Biol. Bull. 214, 233–254. https://doi.org/10.2307/25470666

Richier, S., Rodriguez-Lanetty, M., Schnitzler, C.E., Weis, V.M., 2008. Response of the symbiotic cnidarian *Anthopleura elegantissima* transcriptome to temperature and UV increase. Comp. Biochem. Physiol. - Part D Genomics Proteomics 3, 283–289. https://doi.org/10.1016/j.cbd.2008.08.001

Richier, S., Sabourault, C., Courtiade, J., Zucchini, N., Allemand, D., Furla, P., 2006. Oxidative stress and apoptotic events during thermal stress in the symbiotic sea anemone, *Anemonia viridis*. FEBS J. 273, 4186–4198. https://doi.org/10.1111/j.1742-4658.2006.05414.x

Richter, K., Haslbeck, M., Buchner, J., 2010. The Heat Shock Response: Life on the Verge of Death. Mol. Cell 40, 253–266. https://doi.org/10.1016/j.molcel.2010.10.006

Rodriguez-Lanetty, M., Phillips, W.S., Weis, V.M., 2006. Transcriptome analysis of a cnidarian - Dinoflagellate mutualism reveals complex modulation of host gene expression. BMC Genomics 7, 1–11. https://doi.org/10.1186/1471-2164-7-23/TABLES/2

Rosenberg, E., Koren, O., Reshef, L., Efrony, R., Zilber-Rosenberg, I., 2007. The role of microorganisms in coral health, disease and evolution. Nat. Rev. Microbiol. 2007 55 5, 355–362. https://doi.org/10.1038/nrmicro1635

Samali, A., Orrenius, S., 1998. Heat shock proteins: regulators of stress response and apoptosis. Cell Stress Chaperones 3, 228. https://doi.org/10.1379/1466-1268(1998)003<0228:hspros>2.3.co;2

Schwarz, J.A., Brokstein, P.B., Voolstra, C., Terry, A.Y., Miller, D.J., Szmant, A.M., Coffroth, M.A., Medina, M., 2008. Coral life history and symbiosis: functional genomic resources for two reef building Caribbean corals, *Acropora palmata* and *Montastraea faveolata*. BMC Genomics 9, 97. https://doi.org/10.1186/1471-2164-9-97/FIGURES/6

Shinzato, C., Shoguchi, E., Kawashima, T., Hamada, M., Hisata, K., Tanaka, M., Fujie, M., Fujiwara, M., Koyanagi, R., Ikuta, T., Fujiyama, A., Miller, D.J., Satoh, N., 2011. Using the *Acropora digitifera* genome to understand coral responses to environmental change. Nature 476, 320–323. https://doi.org/10.1038/nature10249

Sunday, J., Bennett, J.M., Calosi, P., Clusella-Trullas, S., Gravel, S., Hargreaves, A.L., Leiva, F.P., Verberk, W.C.E.P., Olalla-Tárraga, M.Á., Morales-Castilla, I., 2019. Thermal tolerance patterns across latitude and elevation. Philos. Trans. R. Soc. Lond. B. Biol. Sci. 374. https://doi.org/10.1098/RSTB.2019.0036

Tomanek, L., 2010. Environmental Proteomics: Changes in the Proteome of Marine Organisms in Response to Environmental Stress, Pollutants, Infection, Symbiosis, and Development. https://doi.org/10.1146/annurev-marine-120709-142729 3, 373–399. https://doi.org/10.1146/ANNUREV-MARINE-120709-142729

Trapani, M.R., Parisi, M.G., Maisano, M., Mauceri, A., Cammarata, M., 2016. Old Weapons for New Wars: Bioactive Molecules From Cnidarian Internal Defense Systems. Cent. Nerv. Syst. Agents Med. Chem. 16, 183–196. https://doi.org/10.2174/1871524915666150710120650

Trapani, M.R., Parisi, M.G., Toubiana, M., Coquet, L., Jouenne, T., Roch, P., Cammarata, M., 2014. First evidence of antimicrobial activity of neurotoxin 2 from *Anemonia sulcata* (Cnidaria). Invertebr. Surviv. Journal; Vol 11 No 1.

Ventura, P., Toullec, G., Fricano, C., Chapron, L., Meunier, V., Röttinger, E., Furla, P., Barnay-Verdier, S., 2018. Cnidarian Primary Cell Culture as a Tool to Investigate the Effect of Thermal Stress at Cellular Level. Mar. Biotechnol. 20, 144–154. https://doi.org/10.1007/s10126-017-9791-3

Vidal-Dupiol, J., Adjeroud, M., Roger, E., Foure, L., Duval, D., Mone, Y., Ferrier-Pages, C., Tambutte, E., Tambutte, S., Zoccola, D., Allemand, D., Mitta, G., 2009. Coral bleaching under thermal stress: putative involvement of host/symbiont recognition mechanisms. BMC Physiol. 9, 14. https://doi.org/10.1186/1472-6793-9-14

Wiedenmann, J., Oswald, F., Nienhaus, G.U., 2009. Fluorescent proteins for live cell imaging: Opportunities, limitations, and challenges. IUBMB Life 61, 1029–1042. https://doi.org/10.1002/iub.256

The first main topic presented here is about a multiple stress condition caused by exposure to a pollutant and bacterial infection. The goal is to try to answer the questions: Given the sessile *A. viridis* lifestyle, can it be validated as an environmental bioindicator following acute exposure to an heavy metal with immunomodulatory activity? What happens in combination with a bacterial infection?

Chapter 2

Sea anemone, Methylmercury, Bacterial infection, Multiple Stress: A Closer Look

ABSTRACT

Specimens of the Mediterranean sea anemone *Anemonia viridis*, were exposed to methylmercury (MeHg) and bacterial infection in order to investigate their immune responses in presence of a well-known toxic pollutant. The singular and the multiple stress triggered by the combined effect of these stressors using molecular immunological markers were evaluated. Anemones were housed in laboratory and distributed into five experimental groups: 1. Control (no microinjected), 2. filtered seawater + TBS injection (control of point 3), 3. filtered seawater + *E. coli* injection (control of point 4), 4. MeHg + TBS injection (control of point 5), and 5. MeHg + *E. coli* injection. Immune and physiological markers like lysozyme, esterase and alkaline phosphatase activity and detoxifying/antioxidant enzymes such as glutathione peroxidase were evaluated in total body extracts of the animals. Here, was demonstrated the immunomodulating effect of this pollutant related to oxidative stress and immune system in order to validate the species as a model organism in marine-coastal biomonitoring programmes.

Keywords: sea anemones, methylmercury, multiple stressors, infection, immunomodulating agent

INTRODUCTION

Mercury (Hg) is a highly toxic pollutant in coastal environments and its presence is due to industrial and agricultural emissions. It exists in soil, atmospheric and aquatic compartment as metallic, inorganic and organic form (Zhang and Wong, 2007) and evidences show that Hg, and particularly the organic form - methylmercury (MeHg) - can bioaccumulate and biomagnified in food chains reaching higher levels in top predatory species (Guardiola et al., 2015; Wu et al., 2018). MeHg interacts with the structure and activity of several protein and molecules (Cappello et al., 2016; dos Santos et al., 2018; Parisi et al., 2021b). Indeed, MeHg can affect cells functions such as membrane stability, metabolism and detoxifying processes (Cappello et al., 2016). However, pathways and mechanisms underlying MeHg-induced oxidative stress in Cnidaria still need to be explained. Only few information about toxicity and bioaccumulation of mercury are available on this phylum and some research highlighting also the relevance in aquaculture field and their economic and social values, evidenced the potential risks related to jellyfish as human food resource and also to their position in the trophic network (Raposo et al., 2022). Most of the studies dealing with the topic in coelenterates have focused on the localization of metals in corals, the toxic effects on their physiology and the measurement of the metal concentration on organisms, as proxy of the environment concentration (Bastidas and García, 2004; Cossa et al., 2009; Reichelt-Brushett and McOrist, 2003).

Cnidaria are a large group of marine invertebrates (over 11,000 species) widespread all over the world both in freshwater and marine ecosystems. They display two kind of body forms: one with pelagic habitus as swimming medusae, and the other sessile, as polyp. Due to this peculiar lifecycle and their predatory feeding behaviour, can be exposed to pollutants present in their different chemical forms. Among the polyps, there is *Anemonia viridis*, a Mediterranean benthonic hexacoral, living on rocky bottom from 0 to 10 meters deep or deeper in case of waters with high transparency. It is a cosmopolitan species of warm water, able to attach to the substrate with the pedal disc that has remarkable physiological features and it is involved in symbiosis with unicellular algae of the genus *Symbiodinium*. In recent years, the remarkable regenerative capabilities of this species have also been explored in stressed conditions (Childs, 2013; La Corte et al., 2023a; Parisi et al., 2021a). Interestingly, Harland and Nganro (1990) showed that symbionts are implied in the uptake of trace metals, as zinc (Zn), cadmium (Cd) and copper (Cu) in *Anemonia viridis* and *Actinia equina* suggesting the metal accumulation and the consequent elimination through zooxanthellae

(Harland and Nganro, 1990). The aim of the research is to evaluate the effect of methylmercury and the combined stress caused by the injection of *E. coli* in the macroinvertebrate *A. viridis* providing new data on immune response and to validate the anthozoan as bioindicator of aquatic environment, and the immunological biomarkers as good markers of early response. Our hypothesis is that MeHg and the MeHg + bacteria are able to induce an alteration on immune response in the sea anemone. In detail, were considered the activities of several biomarkers, which are antioxidants as well as inflammatory enzymes (glutathione peroxidase, esterase, alkaline phosphatase). Moreover, modulation of lysozyme, well-known antimicrobial proteins that recognize and bind the bacterial wall (Fiołka et al., 2012) , the production of protease molecules and the general protein patterns were investigated.

MATERIAL AND METHODS

Chemicals, molecular biology reagents

Chemicals and reagents were from Sigma-Aldrich (USA). *E. coli* (ATCC 25922) was obtained from Chrisope Technologies (Louisiana, USA). *Micrococcus lysodeikticus* (ATCC 4698) was supplied by Sigma- Aldrich (USA).

Sampling and experimental plan

Animal collection took place on spring 2021 in Mongerbino (Palermo, Italy) a site not particularly subjected to anthropogenic impact. The organisms (N = 15) were then carried to the Department of Earth and Marine Sciences, University of Palermo, and housed in the Marine Immunobiology laboratories. Animals were acclimatised to laboratory conditions for 7 days at 18 ± 1 °C before proceeding with the experiments. Methylmercury solutions $[CH_3Hg]^+$ were prepared at a sub-lethal concentration of 0.4 mg/l (Bastidas and García, 2004; Wang and Fisher, 1999); TBS solution (150 mM NaCl, 10 mM Tris-HCl, pH 7.4) was prepared for the control of bacterial injection; *Escherichia coli* bacterial suspension was prepared at a concentration of 1×10^7 bacteria. Three "naive" controls were considered, animals not subjected to microinjections and from which the tissues were stored at −20 °C. The following procedures were applied to the remaining 12 organisms: 6 were placed in tanks containing filtered seawater, while the other 6 were placed in tanks containing filtered seawater and organic mercury (for a total of 4 tanks with 3 organisms each, at a fixed temperature of 18 °C) for a period of 4 days. Then, 3 animals were taken from filtered seawater only and 3 animals which had been exposed to the pollutant, were inoculated with *E. coli*, while the other 6 were injected with TBS only. Injections of *E. coli* and TBS were made in the middle of the columnar body. The animals were sacrificed three hours after the bacterial injection and tissues stored for further study (Fig. 1).

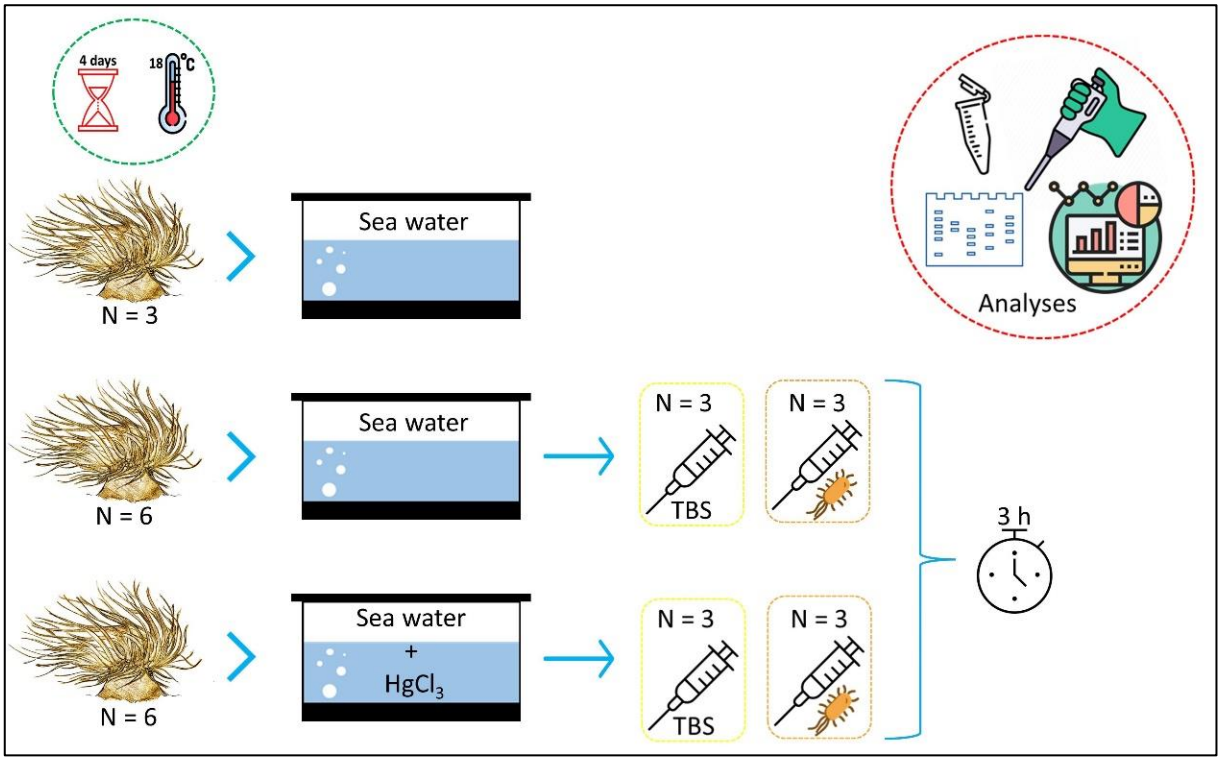

Figure 1 Illustration of experimental plan.

Sample treatment

Tissues were homogenized in polycarbonate tubes adding TBS buffer (NaCl 150 mM, Tris-HCl 10 mM, pH 7.4) and centrifuged (12,000 rpm for 30 min at 4 ◦C). The supernatant was collected and stored in Eppendorf tubes at −20 ◦C. Extracts were adjusted at 0.5 mg/ml before performing enzymatic assays.

Protein concentration

Protein concentration measurement was conducted on tissue extracts according to the method found in Bradford (1976). TBS was used for blank (NaCl 150 mM, Tris-HCl 10 mM, pH 7.4). Absorbance was read at 595 nm (RAYTO RT-2100C), and a calibration curve defined through bovine serum albumin (BSA) was used to obtain protein concentration expressed in mg/ml.

Glutathione peroxidase activity (GPx)

Enzymatic activity was measured in triplicate on *A. viridis* extracts according to Ross *et alii* (2000). In 96-well flat-bottomed plates, 50 µl of sample at standard concentration (0.5 mg/ml) was incubated with 100 µl TMB (3,3′ 5,5′-tetramethylbenzidine). The reaction was stopped after 30 min of dark incubation with sulphuric acid (H_2SO_4) 2 M. The absorbance was read spectrophotometrically at 450 nm in a microplate reader (RT-2100C) and the GPx

produced was expressed in U/mg of protein according to the equation: U/mg = Abs * Vf / CP where Vf is the final volume of the well and CP is the protein concentration of the sample.

Esterase activity (EST)

According to the method of Ross *et al.* (2000), the same volume of sample was incubated with 0.4 mM p-nitrophenylmyristate substrate in 100 mM ammonium bicarbonate containing 0.5 % of Triton X-100 (pH 7.8, 30 ◦C). The increase of the optical density and the determination of the activity were quantified as for ALP.

Alkaline phosphatase activity (ALP)

Samples were incubated in an equal volume of 4 mM p-nitrophenyl phosphate liquid in 100 mM ammonium bicarbonate containing 1 mM $MgCl_2$ (pH 7.8). The enzymatic kinetic was evaluated according to Ross *et al.* (2000) at regular intervals of 5 min to 1 h at 405 nm with a microplate reader (RAYTO RT-2100C). One unit (U) of activity was defined as the amount of enzyme required to release 1 µmol of p-nitrophenol produced in 1 min.

Lysozyme (LYS)

Lysozyme activity was evaluated using a turbidimetric assay modified for microplate reader (Sutton et al., 2006). In a suspension (0.025% in phosphate buffer 0.06M, pH 6.2) of *Micrococcus lysodeikticus* was measured reduction (*M. lysodeikticus* lysis) in absorbance at 450 nm. Absorbance was measured before and after the incubation (20 min at 37°C) and compared with a standard curve constructed using Lyophilized Hen Egg Lysozyme (HEWL; Sigma–Aldrich, St. Louis, MO, USA). The results were expressed as µg/mL.

SDS-PAGE and Protease activity

Protein extracts were separated by SDS-PAGE on 7.5% polyacrylamide gel in non-reducing conditions according to (Laemmli, 1970), using a Mini Protean II cell (Bio-Rad), in order to evidence proteins in their functional structure. Gels were calibrated with high molecular weight range standard protein (S8445, Sigma-Aldrich, USA). Migration was performed in running buffer (Trizma base 25 mM, Glycine 192 mM, 1% w/v SDS, pH 8.3) at 60 V for the first 10 min and 160 V for approximately 1 h and the apparent molecular weight of the band was calculated. Gel was stained at room temperature with Coomassie Blue dye (Coomassie Brillant Blue G250 0.1%, 40% Methanol, Acetic Acid 1%). The gel was destained with destaining solution (0.1% acetic acid; methanol 0.4% in distilled water). Reaction was stopped with distilled water. Further gels were prepared under the same

conditions by adding fibrinogen (0.5mg/ml) as substrate to investigate the protease activity of samples. In this case, migration was followed by three washing for three minutes with 10 mM Ca TBS (150 mM NaCl, 10 mM Tris HCl, 10 mM $CaCl_2$, pH 8) in the presence of 2% Triton X- 100. After incubation overnight with TBS Ca 10 mM pH 8, the gels were washed for 4 min in 50% methanol and stained in Coomassie Blue and then destained and reaction blocked (Trapani et al., 2016b). Densitometric analysis was carried out on SDS-PAGE with fibrinogen substrate using the open source software for biological-image analyses "FIJI" (Schindelin et al., 2012)

Statistical analysis

After performing a normality test on the dataset to verify the distribution of the data and the homoscedasticity assumption, one-way ANOVA was conducted. The analysis of multiple comparisons was performed using the Tukey post-hoc test to highlight differences between treatments. The analyses were carried out using GraphPad Prism Version 8.0.0. for Windows (www.graphpad.com) (accessed on 22 August 2021). All experiments were performed in triplicate, and the values used were the mean of the three assays ± standard deviation (SD). Differences between means were considered significant for $*p < 0.05$, $**p < 0.01$ and $***p < 0.001$.

RESULTS

Macroscopic observations

No mortality was recorded in any specimens regardless of the experimental treatment. The morphological alterations resulting from the four treatments were evaluated. Anemones exposed to the pollutant were less motile in tank and turgid than control animals. Following bacterial inoculation + MeHg, a slight swelling with formation of yellowish parts was found near the injection area, as indicated in Fig. 2. None of these anomalies were visible in other treatments.

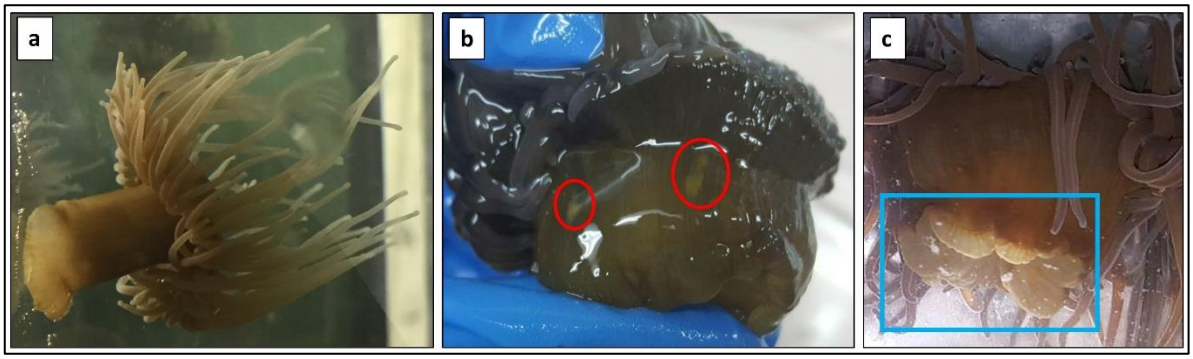

*Figure 2 A.viridis control organism in **(a)**. Anemones injected with E. coli in **(b, c)**. Red circles = yellowish parts in injection area. Blue rectangle = Pedal disk swelling.*

Enzymatic Analyses

Graphics in figure 3 show the evaluation of enzymatic activities. Regarding peroxidase (Fig. 3a), the measured amount of the enzyme increase in treated groups compared to control organisms (naive), reaching highest values in samples subjected to the combined exposure. Multiple comparison analysis showed significant results for animals subjected to multiple stressors, compared to naive (p value = 0.0084). The ordinary one-way ANOVA analysis showed a 0.0038 p value for the variables "treatment" (T). As regards LYS (Fig. 3b), the ANOVA showed a significant difference between treatment groups (p value <0.0001). The greatest amount of LYS produced was measured in samples injected with *E. coli* suspension. The presence of methyl mercury seems to affect lysozyme modulation; indeed, organisms exposed only to the chemical show a decrease in activity compared to the naive group. In combined stressor, LYS amount is slightly higher to the naive and TBS treatment, probably due to the presence of bacteria. Tukey post-hoc test underlined significant differences between organisms treated (except for *E. coli* + CH_3HgCl) respect to naive and TBS injection. Moreover, statistically significant differences between samples inoculated with TBS and *E. coli* (p = 0.0015), *E. coli* vs TBS + MeHg groups (<0.0001), and between

samples exposed only to the organometallic vs *E. coli* + MeHg (p = 0.0015) have been quantified. Alkaline phosphatase (Fig. 3c) activity is higher in treated samples respect to naive (one-way ANOVA p value = 0.0015). The post-hoc Tukey test highlighted, differences between controls vs samples exposed to CH_3HgCl (p = 0.0285), between naive vs combined stress (p = 0.0100) and TBS vs TBS + CH_3HgCl (p = 0.0356). As regard EST analysis (Fig. 3d), the activity increase compared to the control group, especially for specimens *E. coli* injected. The one-way ANOVA highlighted a p-value of <0.0001 between treatments. Statistically significant differences have been founded in particular between naive and bacterial injection (p < 0.0001), between TBS injected versus TBS + MeHg (p = 0.0037) and in bacterial injection versus *E. coli* + MeHg (p = 0.0283) experimental condition.

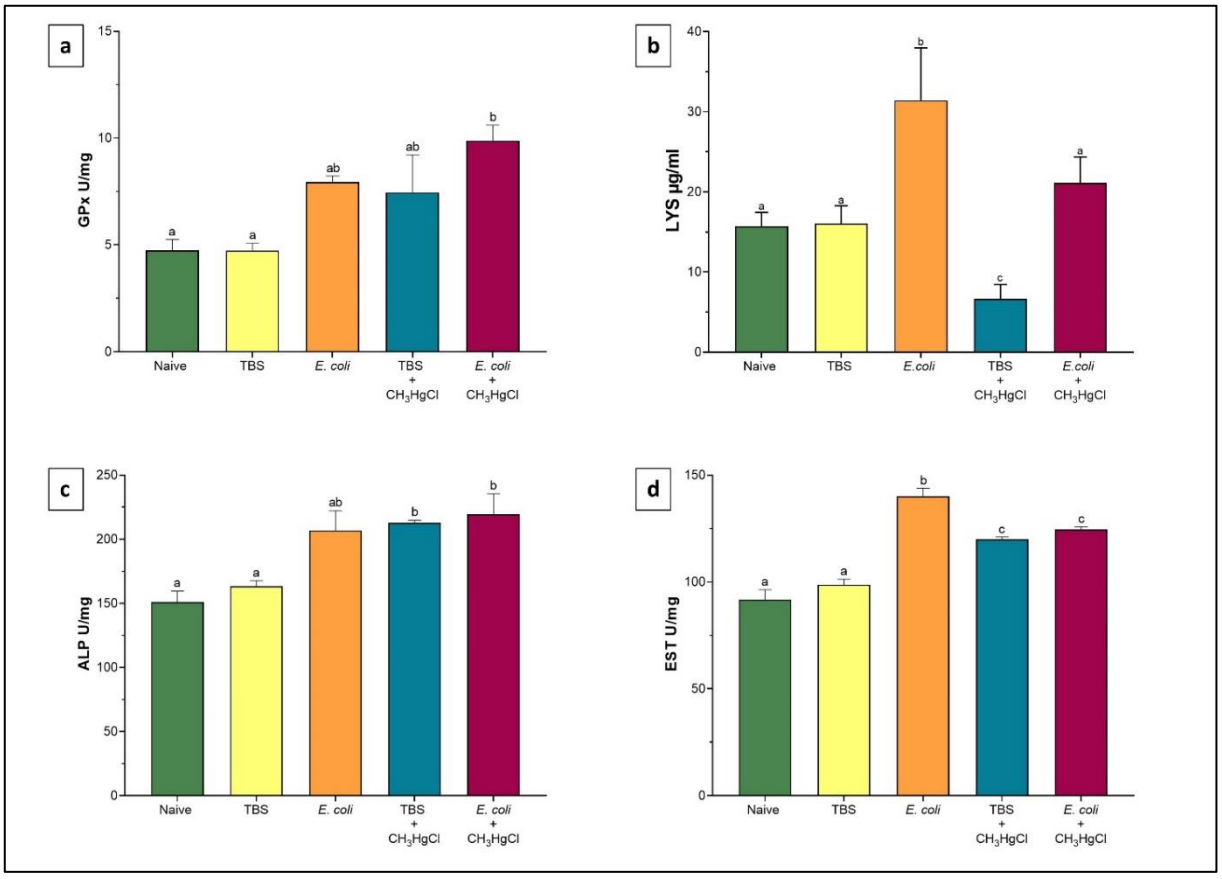

Figure 3 Panel show the enzymatic activity modulation in A. viridis of: ***(a)*** *peroxidase (GPx);* ***(b)*** *lysozyme (LYS);* ***(c)*** *alkaline phosphatase (ALP);* ***(d)*** *esterase (EST). Data were tested for normality, and differences between groups were shown by one-way ANOVA as mean ± standard deviation. Letters indicate statistically significant differences between treatments. Differences between means were considered significant for p < 0.05.*

Electrophoretic patterns

SDS-PAGE was conducted on *A. viridis tissues* extracts. The bands resulting from densitometric analysis are those having molecular weights around 24, 50 and 100 kDa.

SDS electrophoretic analysis enabled a comparison of tissues extracts subjected to the various experimental treatments. As observed in Fig 4a, in naive extracts (Lane 1), a 50 kDa band was less detectable compared to the inoculated samples with TBS (Lane 2), *E. coli* suspension (Lane 3), exposed to the pollutant (Lane 4) and subjected to the combined effect (Lane 5). Higher integrated density values were measured in sample *E. coli* inoculated with an increase of 16% compared to the naive. MeHg exposure increase for 5% and the combined bacteria + methylmercury for 12% (Fig 4b). Despite the band of 50 kDa, there were no other differences in protein patterns.

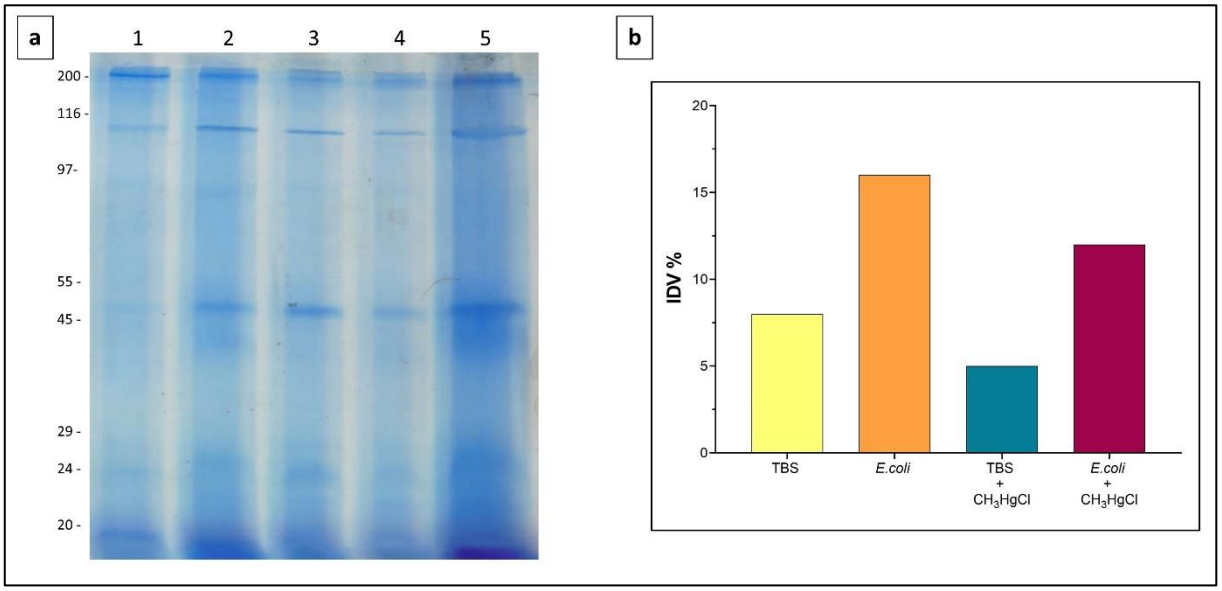

Figure 4 SDS-PAGE (7.5%) under non-reducing conditions of A. viridis extracts ***(a)****. Lane 1 = naive; Lane 2 = TBS inoculum; Lane 3 = E. coli inoculum; Lane 4 = TBS inoculum + CH_3HgCl; Lane 5 = E. coli inoculum + CH_3HgCl.* ***(b)*** *Densitometric analysis carried on 50 kDa band using Fiji software. Integrated density values (IDV) have been normalized for naive and then here reported as the increase in percentage of IDV respect to the naive.*

Evaluation of fibrinolytic activity

Fibrinolytic activity was assayed in the several treatments by SDS-PAGE using fibrinogen as substrate (Fig. 5). Fibrinolytic protein component was more clearly expressed in TBS inoculated samples and those injected with *E. coli* suspension (Lane 2-3 respectively). Were detected active bands around 50 kDa and around 25 kDa also for the sample exposed only to the pollutant (Lane 4). The lightest, albeit labile, molecular weight band was also highlighted for samples subjected to multiple stress (Lane 5). No bands were present in naive samples.

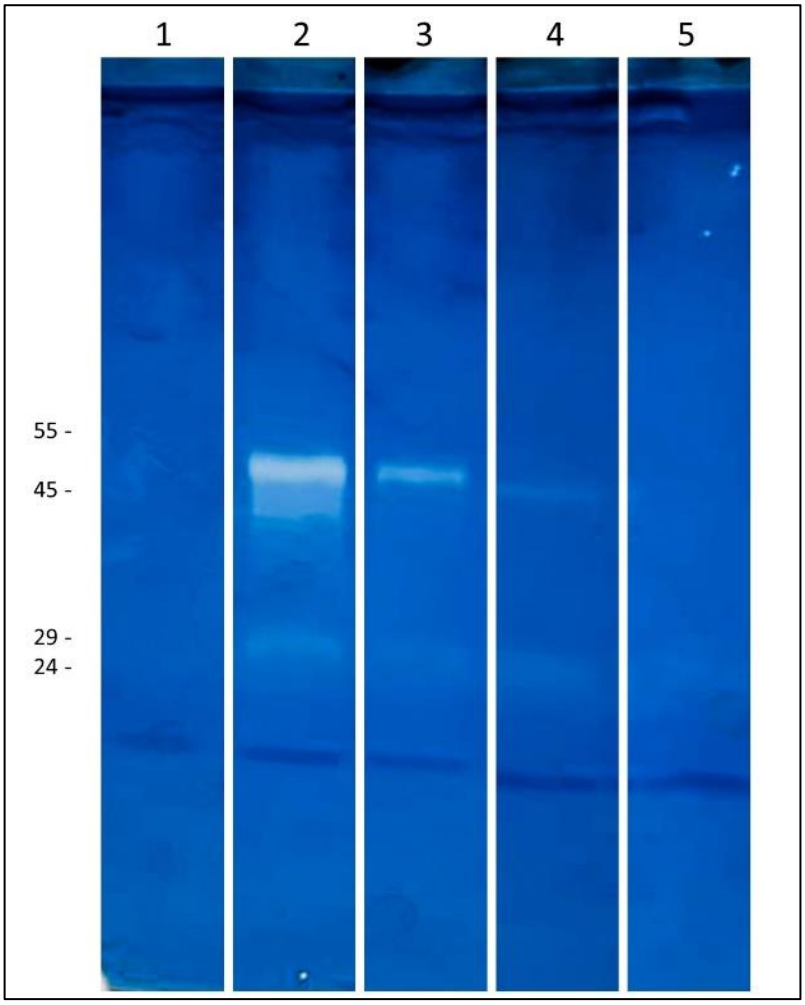

Figure 5 Protease activity. SDS-PAGE (7.5%) in non-reducing conditions with fibrinogen substrate of extracts of A. viridis. Samples loading: Lane 1 = naive; Lane 2 = TBS inoculum; Lane 3 = E. coli inoculum; Lane 4 = TBS inoculum + CH_3HgCl; Lane 5 = E. coli inoculum + CH_3HgCl.

DISCUSSION

This study analysed immunological and physiological parameters of the sea anemone *Anemonia viridis* in a context of single (chemical or bacterial exposure) and multiple stressor (chemical + bacteria). The effects were estimated using biomarkers related to oxidative stress and the inflammatory process. Many studies have shown that metals at high concentrations are able to induce alteration on invertebrates homeostasis with consequent modification in immune system responses (Cammarata et al., 2019, 2007; La Corte et al., 2023b; Parisi et al., 2021b). A first macroscopic evaluation allowed to obtain an overview about the effects of experimental treatments.

The morphological change in the injection zone and the appearance of a bulge in the aboral area corresponding to the foot of the animal is coherent with the observations of Trapani et *alii* (2016b), in which the bacterial injection caused an area of swelling, something also observed in other invertebrates such as *Sabella spallanzanii* (La Corte et al., 2023b). Electrophoresis evidenced the presence and modulation of proteins with a molecular weight between 20 and 50 kDa; these bands may be attributed to cytolytic proteins like toxins characterized from *Actinia equina* and *A. viridis* with antimicrobial properties described in Trapani et al. (2016a, 2014). Furthermore, their modulation, investigated by fibrinolytic activity assay could rely on the exposure at methylmercury and its affinity with different proteins (Lee et al., 2020). Further analyses could elucidate these proteins bands are and understand the mechanism that causes their modulation in the presence of methylmercury. Metalloproteases zinc-dependent have been found in the transcripts of the nematocysts of anthozoans, scyphozoa and hydrozoa suggesting a certain degree of conservation of these toxins (Ponce et al., 2016; Rachamim et al., 2015). Moreover, matrix metalloproteases involved in the spatial reorganisation of tissue during regenerative processes (Parisi et al., 2021a). It must also be pointed out that the question of which components actively respond to the presence of heavy metals in Cnidaria remains not entirely resolved. Really, the known critical components related to the metal-stress pathways in metazoans are absent in Cnidaria. Although the metal transcription factor-1 (Mtf1) has been identified in *Nematostella vectensis* and in *Hydra*, it does not exist in all genera of the phylum. This is of particular interest because the major target of the molecule are metallothioneins, a group of small cysteine-rich proteins involved in heavy metal detoxification, and these last are also not found in the genomes of corals, sea anemones or hydra, suggesting that they might be absent in all cnidarians and that the metal signal is transduced through different pathways (Andersen

et al., 1988; Reitzel et al., 2008; Shinzato et al., 2012), like phytochelatins family, that in *N. vectensis* is up-regulated as a result of exposure to mercury and copper (Elran et al., 2014). Furthermore, the presence of bands in the electrophoretic pattern that might suggest the release of toxins and the presence of proteases from the fibrinogen-substrate gel, which are differentially visible with respect to the type of treatment, allows us to hypothesise the involvement of these molecules during the bacterial challenge and in the response to organometal exposure. The latter may cause them to be inhibited, especially during multiple stress where the bands are faint, resulting in a major difficult for organisms to respond to stress.

Lysozyme is defensive element of protection against pathogens and the modulation of its enzymatic activity has been experimentally observed in this study. Indeed, as just evidenced in literature, the bacterial inoculum immediately provoked the increase of the lysozyme activity of the animal, reaching a two-up production of the enzyme compared to the naive. Exposure to methylmercury appears to inhibit the production of the enzyme which decreases by two thirds compared to normal conditions. The inhibition is still visible in the combined treatment in fact even if the presence of the pathogen stimulates the production, this is however less than about 10 µg/ml respect to samples *E. coli* injected. Differential expression of detoxifying enzymes and lysozyme in presence of heavy metals, and in particular mercury, has been widely addressed in the literature, e.g. in *Mactra veneriformis* lysozyme, superoxide dismutase and metallothionein genes were up-regulated in earlier moment after exposure to heavy metals and bacteria, leading also to an increase in clams mortality (Fang et al., 2013).

Consistent with what was observed by Elran *et al.* (2014) in *N. vectensis*, gluthatione has high affinity for toxic metals and the antioxidant genes, glutathione peroxidases (GPx) and Cu/Zn superoxide dismutase (SOD) were overexpressed and this is correlated with formation of the metal-binding peptides like phytochelatins from glutathione. Moreover, the exposure to methylmercury induced the EST and ALP up-regulation.

The combined treatment trend reflects a particular response pattern where it can be assumed that pathogen incursion lead to a synergistic or additive interaction in the presence of a pollutant (Fang et al., 2013). The results could also be explained by the symbiotic relationship between *A. viridis* and the zooxanthellae of *Symbiodinium* genus, which contribute to the detoxification from the metal by storing it and thus delaying the occurrence of the effective oxidative stress as explained in other research (Harland and Nganro, 1990;

Main et al., 2010). Indeed, previous work on animal filter models has shown that exposure to mercury can lead to cellular changes at the cytoskeletal and pseudopod level and to a consequent increase in cellular mortality (Parisi et al., 2021b; Parrinello et al., 2017), opening to a new possible observation scenario of multistress phenomenon.

CONCLUSIONS

Due to the exponential employing of heavy metals in many contexts, which affect estuaries and coastal areas, environmental pollution has rapidly grown. This study focuses on the effects of four different treatments on the whole body of the benthic macroinvertebrate model *A. viridis*, organism previously used by the research team that has once again proven to be effective in ecotoxicological and immunological studies, having all the qualities of perfect bioindicators. The markers investigated were also good biomarkers for investigating multiple stressors: metals and bacterial inoculum. The alteration of LYS activity and enzyme responses, which are recognised stress indicators, has effectively brought out the distinctions between the various treatments. Similar to earlier research, MeHg modulate the immunological responses, particularly after bacterial inoculation. In order to uncover more about the immune mechanisms that are activated and how animals are able to manage the energies intended for the maintenance of internal homeostasis, the Mediterranean sea anemone was validated and subjected to four different treatments, including one combined treatment with stressogenic effects detectable on several structural levels.

Studies on the sub-lethal effects of MeHg on organisms are critical for motivating earlier action in circumstances of pollution exposure. We believe that, due to the intrinsic characteristics of the molecule and also of the animal model used here, it would be interesting to observe the phenomenon from other points of view such as the cellular and molecular, seen also the symbiotic bond between anthozoan and dinoflagellate, in order to compare it with what is observed in other models commonly used for the study of the pollutants effects, such as molluscs, ascidians and polychaetes.

REFERENCES

Andersen, R.A., Wiger, R., Daae, H.L., Eriksen, K.D.H., 1988. Is the metal binding protein metallothionein present in the coelenterate *Hydra attenuata*? Comp. Biochem. Physiol. Part C Comp. Pharmacol. 91, 553–557.

Bastidas, C., García, E.M., 2004. Sublethal effects of mercury and its distribution in the coral Porites astreoides. Mar. Ecol. Prog. Ser. 267, 133–143. https://doi.org/10.3354/meps267133

Bradford, M.M., 1976. A rapid and sensitive method for the quantitation of microgram quantities of protein utilizing the principle of protein-dye binding. Anal. Biochem. https://doi.org/10.1016/0003-2697(76)90527-3

Cammarata, M., Benenati, G., Dara, M., Parisi, M.G., Piazzese, D., Falco, F., Stabili, L., 2019. *Sabella spallanzanii* mucus contain a galactose-binding lectin able to agglutinate bacteria. Purification and characterization. Invertebr. Surviv. J. 16, 15–24.

Cammarata, M., Parisi, M.G., Benenati, G., Arizza, V., Cillari, T., Piazzese, D., Gianguzza, A., Vazzana, M., Vizzini, A., Parrinello, N., 2007. In vitro effects of methylmercury on ascidian (*Styela plicata*) immunocyte responses. Appl. Organomet. Chem. 21, 1022–1028. https://doi.org/10.1002/aoc.1335

Cappello, T., Brandão, F., Guilherme, S., Santos, M.A., Maisano, M., Mauceri, A., Canário, J., Pacheco, M., Pereira, P., 2016. Insights into the mechanisms underlying mercury-induced oxidative stress in gills of wild fish (*Liza aurata*) combining 1H NMR metabolomics and conventional biochemical assays. Sci. Total Environ. 548–549, 13–24. https://doi.org/https://doi.org/10.1016/j.scitotenv.2016.01.008

Childs, K., 2013. The effect of copper-induced oxidative stress on regeneration in *Anemonia viridis* (Forskäl , 1775). Plymouth Student Sci. 6, 31–55.

Cossa, D., Averty, B., Pirrone, N., 2009. The origin of methylmercury in open mediterranean waters. Limnol. Oceanogr. 54, 837–844. https://doi.org/10.4319/lo.2009.54.3.0837

dos Santos, A.A., Ferrer, B., Gonçalves, F.M., Tsatsakis, A.M., Renieri, E.A., Skalny, A. V., Farina, M., Rocha, J.B.T., Aschner, M., 2018. Oxidative stress in methylmercury-induced cell toxicity. Toxics 6, 1–15. https://doi.org/10.3390/toxics6030047

Elran, R., Raam, M., Kraus, R., Brekhman, V., Sher, N., Plaschkes, I., Chalifa-Caspi, V.,

Lotan, T., 2014. Early and late response of *Nematostella vectensis* transcriptome to heavy metals. Mol. Ecol. 23, 4722–4736. https://doi.org/10.1111/mec.12891

Fang, Y., Yang, H., Liu, B., Zhang, L., 2013. Transcriptional response of lysozyme, metallothionein, and superoxide dismutase to combined exposure to heavy metals and bacteria in *Mactra veneriformis*. Comp. Biochem. Physiol. - C Toxicol. Pharmacol. 157, 54–62. https://doi.org/10.1016/j.cbpc.2012.10.002

Fiołka, M.J., Zagaja, M.P., Hułas-Stasiak, M., Wielbo, J., 2012. Activity and immunodetection of lysozyme in earthworm *Dendrobaena veneta* (Annelida). J. Invertebr. Pathol. 109, 83–90. https://doi.org/10.1016/j.jip.2011.10.002

Guardiola, F.A., Dioguardi, M., Parisi, M.G., Trapani, M.R., Meseguer, J., Cuesta, A., Cammarata, M., Esteban, M.A., 2015. Evaluation of waterborne exposure to heavy metals in innate immune defences present on skin mucus of gilthead seabream (*Sparus aurata*). Fish Shellfish Immunol. 45, 112–123.

Harland, A.D., Nganro, N.R., 1990. Copper uptake by the sea anemone *Anemonia viridis* and the role of zooxanthellae in metal regulation. Mar. Biol. 104, 297–301. https://doi.org/10.1007/BF01313271

La Corte, C., Baranzini, N., Dara, M., Bon, C., Grimaldi, A., Parisi, M.G., Zizzo, M.G., Cammarata, M., 2023a. Step-by-Step Regeneration of Tentacles after Injury in *Anemonia viridis*—Morphological and Structural Cell Analyses. Int. J. Mol. Sci. 24, 8860. https://doi.org/10.3390/ijms24108860

La Corte, C., Dara, M., Bertini, F., Parrinello, D., Piazzese, D., Parisi, M.G., 2023b. Response of *Sabella spallanzanii* to multiple stressors. The combined effect of infection and copper sulphate. Comp. Biochem. Physiol. Part C Toxicol. Pharmacol. 263, 109475. https://doi.org/10.1016/j.cbpc.2022.109475

Laemmli, U.K., 1970. Cleavage of Structural Proteins during the Assembly of the Head of Bacteriophage T4. Nature 227, 680–685. https://doi.org/10.1038/227680a0

Lee, J.Y., Hwang, G.W., Naganuma, A., Satoh, M., 2020. Methylmercury toxic mechanism related to protein degradation and chemokine transcription. Environ. Health Prev. Med. 25, 3–7. https://doi.org/10.1186/s12199-020-00868-3

Main, W.P.L., Ross, C., Bielmyer, G.K., 2010. Copper accumulation and oxidative stress in the sea anemone, *Aiptasia pallida*, after waterborne copper exposure. Comp. Biochem.

Physiol. Part C Toxicol. Pharmacol. 151, 216–221.

Parisi, M.G., Grimaldi, A., Baranzini, N., La Corte, C., Dara, M., Parrinello, D., Cammarata, M., 2021a. Mesoglea extracellular matrix reorganization during regenerative process in *Anemonia viridis* (Forskål, 1775). Int. J. Mol. Sci. 22. https://doi.org/10.3390/ijms22115971

Parisi, M.G., Pirrera, J., La Corte, C., Dara, M., Parrinello, D., Cammarata, M., 2021b. Effects of organic mercury on Mytilus galloprovincialis hemocyte function and morphology. J. Comp. Physiol. B 191, 143–158. https://doi.org/10.1007/s00360-020-01306-0

Parrinello, D., Bellante, A., Parisi, M.G., Sanfratello, M.A., Indelicato, S., Piazzese, D., Cammarata, M., 2017. The ascidian *Styela plicata* hemocytes as a potential biomarker of marine pollution: In vitro effects of seawater and organic mercury. Ecotoxicol. Environ. Saf. 136, 126–134. https://doi.org/10.1016/j.ecoenv.2016.11.001

Ponce, D., Brinkman, D.L., Potriquet, J., Mulvenna, J., 2016. Tentacle transcriptome and venom proteome of the pacific sea nettle, *Chrysaora fuscescens* (Cnidaria: Scyphozoa). Toxins (Basel). 8. https://doi.org/10.3390/toxins8040102

Rachamim, T., Morgenstern, D., Aharonovich, D., Brekhman, V., Lotan, T., Sher, D., 2015. The dynamically evolving nematocyst content of an Anthozoan, a scyphozoan, and a hydrozoan. Mol. Biol. Evol. 32, 740–753. https://doi.org/10.1093/molbev/msu335

Raposo, A., Alasqah, I., Alfheeaid, H.A., Alsharari, Z.D., Alturki, H.A., Raheem, D., 2022. Jellyfish as Food: A Narrative Review. Foods 11, 1–20. https://doi.org/10.3390/foods11182773

Reichelt-Brushett, A.J., McOrist, G., 2003. Trace metals in the living and nonliving components of scleractinian corals. Mar. Pollut. Bull. 46, 1573–1582. https://doi.org/10.1016/S0025-326X(03)00323-0

Reitzel, A.M., Sullivan, J.C., Traylor-Knowles, N., Finnerty, J.R., 2008. Genomic survey of candidate stress-response genes in the estuarine anemone *Nematostella vectensis*. Biol. Bull. 214, 233–254. https://doi.org/10.2307/25470666

Ross, N.W., Firth, K.J., Wang, A., Burka, J.F., Johnson, S.C., 2000. Changes in hydrolytic enzyme activities of naive Atlantic salmon *Salmo salar* skin mucus due to infection with the salmon louse Lepeophtheirus salmonis and cortisol implantation. Dis. Aquat.

Organ. 41, 43–51. https://doi.org/10.3354/dao041043

Schindelin, J., Arganda-Carreras, I., Frise, E., Kaynig, V., Longair, M., Pietzsch, T., Preibisch, S., Rueden, C., Saalfeld, S., Schmid, B., Tinevez, J.-Y., White, D.J., Hartenstein, V., Eliceiri, K., Tomancak, P., Cardona, A., 2012. Fiji: an open-source platform for biological-image analysis. Nat. Methods 9, 676–682. https://doi.org/10.1038/nmeth.2019

Shinzato, C., Hamada, M., Shoguchi, E., Kawashima, T., Satoh, N., 2012. The repertoire of chemical defense genes in the coral *Acropora digitifera* genome. Zoolog. Sci. 29, 510–517.

Sutton, J., Balfry, S., Higgs, D., Huang, C.-H., Skura, B., 2006. Impact of iron-catalyzed dietary lipid peroxidation on growth performance, general health and flesh proximate and fatty acid composition of Atlantic salmon (*Salmo salar* L.) reared in seawater. Aquaculture 257, 534–557.

Trapani, M.R., Parisi, M.G., Maisano, M., Mauceri, A., Cammarata, M., 2016a. Old Weapons for New Wars: Bioactive Molecules From Cnidarian Internal Defense Systems. Cent. Nerv. Syst. Agents Med. Chem. 16, 183–196. https://doi.org/10.2174/1871524915666150710120650

Trapani, M.R., Parisi, M.G., Toubiana, M., Coquet, L., Jouenne, T., Roch, P., Cammarata, M., 2014. First evidence of antimicrobial activity of neurotoxin 2 from A*nemonia sulcata* (Cnidaria). Invertebr. Surviv. Journal; Vol 11 No 1.

Trapani, M.R., Parisi, M.G.G., Parrinello, D., Sanfratello, M.A.A., Benenati, G., Palla, F., Cammarata, M., 2016b. Specific inflammatory response of *Anemonia sulcata* (Cnidaria) after bacterial injection causes tissue reaction and enzymatic activity alteration. J. Invertebr. Pathol. 135, 15–21. https://doi.org/10.1016/j.jip.2016.01.010

Wang, W.X., Fisher, N.S., 1999. Assimilation efficiencies of chemical contaminants in aquatic invertebrates: A synthesis. Environ. Toxicol. Chem. 18, 2034–2045. https://doi.org/10.1897/1551-5028(1999)018<2034:AEOCCI>2.3.CO;2

Wu, F., Huang, W., Liu, Q., Xu, Xiaoqun, Zeng, J., Cao, L., Hu, J., Xu, Xudan, Gao, Y., Jia, S., 2018. Responses of antioxidant defense and immune gene expression in early life stages of large yellow croaker (*Pseudosciaena crocea*) under methyl mercury exposure. Front. Physiol. 9, 1–10. https://doi.org/10.3389/fphys.2018.01436

Zhang, L., Wong, M.H., 2007. Environmental mercury contamination in China: sources and impacts. Environ. Int. 33, 108–121.

The focus shifted to the characterization of the regenerative event under constitutive conditions. This was in order to implement the knowledge base on this organism and topic, exploit this capability as a biomarker, and highlight the link between immunity and regeneration.

Chapter 3

Mesoglea Extracellular Matrix Reorganization during Regenerative Process in *Anemonia viridis* (Forskål, 1775)

International Journal of
Molecular Sciences

MDPI

Article

Mesoglea Extracellular Matrix Reorganization during Regenerative Process in *Anemonia viridis* (Forskål, 1775)

Maria Giovanna Parisi [1,*], Annalisa Grimaldi [2,*], Nicolò Baranzini [2], Claudia La Corte [1], Mariano Dara [1], Daniela Parrinello [1] and Matteo Cammarata [1]

ABSTRACT

Given the anatomical simplicity and the extraordinary ability to regenerate missing parts of the body, Cnidaria represent an excellent model for the study of the mechanisms regulating regenerative processes. They possess the mesoglea, an amorphous and practically acellular extracellular matrix (ECM) located between the epidermis and the gastrodermis of the body and tentacles and consists of the same molecules present in the ECM of vertebrates, such as collagen, laminin, fibronectin and proteoglycans. This feature makes cnidarians anthozoans valid models for understanding the ECM role during regenerative processes. Indeed, it is now clear that its role in animal tissues is not just tissue support, but instead plays a key role during wound healing and tissue regeneration. This study aims to explore regenerative events after tentacle amputation in the Mediterranean anemone *Anemonia viridis*, focusing in detail on the reorganization of the ECM mesoglea. In this context, both enzymatic, biometric and histological experiments reveal how this gelatinous connective layer plays a fundamental role in the correct restoration of the original structures by modifying its consistency and stiffness. Indeed, through the deposition of collagen I, it might act as a scaffold and as a guide for the reconstruction of missing tissues and parts, such as amputated tentacles.

Keywords: *Anemonia viridis*; regeneration; morphology; histology; enzymatic activity; collagen

INTRODUCTION

The ability to restore the correct tissue architecture after injuries requires a series of closely connected cellular and molecular events. Defects in the early steps of wound healing and the tissue remodelling program can interfere with regeneration (DuBuc et al., 2014), even in low invertebrates with a high regenerative capacity (Bely and Nyberg, 2010; Bosch, 2007; Holstein et al., 2003). Therefore, understanding the mechanisms regulating tissue regeneration capacity can help shed light on factors related to the loss of vertebrate regenerative ability, which is reduced to only a few structures and tissues.

Although in the animal kingdom different mechanisms exist, in the last decades it has become clear that the extracellular matrix (ECM) plays a pivotal role during different physiological processes, including wound healing and tissue regeneration (Mason et al., 2012).

Since the Cnidaria, a sister group to Bilateria, possess high body regeneration capacities and can regrow missing body parts when dissected (Holstein et al., 2003), is it is likely that knowledge in this group of organisms can drive the perspective on bilaterian regeneration.

Cnidarians are among the simplest living metazoans and evolved approximately 700 million years ago. They consist of two body layers derived from the endoderm (gastrodermis) and ectoderm (epidermis) of the embryo. Between these two cellular layers is an amorphous, jelly-like mesoglea connective layer. This generally contains no cellular elements other than some scattered amoebocytes and local genital cells.

The majority and most detailed cellular and molecular regeneration studies have been carried out using Hydra (Bosch, 2009, 2008; Frank et al., 2009; Galliot, 2012; Watanabe et al., 2009), and the colonial hydrozoan Hydractinia (Bradshaw et al., 2015; DuBuc et al., 2020). However, the regenerative potential has been described also in other medusozoa (Fischer and Hofmann, 2004; Sinigaglia et al., 2020) and in anthozoan sea anemone *Nematostella vectensis* (Amiel et al., 2015; Bossert et al., 2013; DuBuc et al., 2014; Schaffer et al., 2016), in which a structure responsible for the repair and regeneration program and stem cell populations was identified (Amiel et al., 2019).

Unlike the freshwater polyp Hydra, where regeneration is based on three distinct populations of multipotent stem cells, the I-cells, the ectodermal and endodermal epithelial cells (Augustin and Bosch, 2010; Bosch et al., 1991; Campbell and Bode, 1983; Galliot et al., 2009; Technau and Steele, 2011), in anthozoans, another type of undifferentiated cell, called the amoebocyte, regulates this process (Gold and Jacobs, 2013; Palmer et al., 2011; Palmer and Traylor-Knowles, 2018; Parisi et al., 2020). These agranular hyaline cells are scattered

in the mesoglea and can differentiate into fibroblast-like cells, characterized by extended pseudopodia and by the ability to control extracellular matrix production and collagen deposition (Palmer et al., 2011).

The ultrastructure of the mesoglea in hexacoral anthozoan polyps shares some properties with that of various Hydra species, having a basal lamina composed of a lattice of fine filaments and containing collagen IV orthologs (Davis, 1975; Davis and Haynes, 1968). However, the role of this matrix in the regeneration of tissues, particularly in that of the tentacles, is not yet fully understood. For this purpose, we used the Mediterranean *Anemonia viridis* as an in vivo model for the study of the matrix/cell interaction.

A. viridis is a Mediterranean hexacoral anthozoan (from Atlantic Portugal up to the Irish coasts) belonging to the family Actinidae, that inhabits benthic rocky bottoms from 0 to10 m deep. Like many anthozoans, it harbors zooxanthellae, photosynthetically active unicellular algae belonging to the genus *Symbiodinium*, within its gastrodermal cells. This association represents a trophic mutualistic endosymbiosis, in which zooxanthellae provide their cnidarian host with reduced organic carbon, resulting from their photosynthetic activity, while the host provides unicellular algae with inorganic carbon, inorganic nitrogen, and inorganic phosphate, as well as a refuge from herbivory (Muller-Parker et al., 1990; Muscatine and Pool, 1979). The anatomy is distinguish- able into three parts—the tentacles, the body column, in which the gastrovascular cavity is divided into several chambers by longitudinal partition called septa or mesenteries, and the base foot that binds to a solid surface.

The broader objective of the study was to analyse the mesoglea ECM, from a biochemical, biometric and morphological point of view, in unamputated and injured polyps after amputation of their oral tentacles. Specifically, we evaluated changes in mesoglea stiffness during regeneration, both in tentacles and the body's mesenteries. The possible role of fibroblast-like cells, differentiated from hyaline amoebocytes, in the remodelling of the ECM through the production of metalloproteases, the deposition and spatial organization of new collagen I fibrils in the mesoglea matrix were investigated.

MATERIALS AND METHODS

Experimental Plan and Reagents

Considering previous studies on the seasonal changes in morphology of *A. viridis*, the specimens have been collected between October and November, when biometric variations are less influenced by thermal stress (Parisi et al., 2017). Adult organisms were harvested in Termini Imerese, located near Palermo (Italy), maintained at 20° C under controlled laboratory conditions until experimental use, fed twice a week with mussels and clams and left to acclimate for two weeks before starting the experiments. Each animal was amputated to the level of 25% of the total tentacles, to be then placed and fed in the tank. After 1, 7 and 14 days after the first amputation, three replicates of animals, respectively, were used for morphological, biometric, biochemical and histological analyses. Not amputated specimens were used as control. Chemicals were from Sigma-Aldrich (USA).

Tissues Extraction and Estimation of the Proteins Content

For each experimental time, protein extraction was performed separately for body and tentacles cut in the basal zone, near the oral disk using the protocol. Tissues were homogenized in polycarbonate tubes with 10 mL TBS buffer (150 mM NaCl, 10 mM Tris-HCl, pH 7.4) and centrifuged at 12,000 rpm for 30 min at 4° C (Beckman Allegra 64R Centrifuge, rotor F1202). Supernatant was collected and stored in Eppendorf tubes at - 20° C. The protein content was measured by Bradford method (1976) using bovine serum albumin (BSA) as standard and samples were adjusted at the concentration of 500 µg/mL to perform enzymatic assays.

Alkaline Phosphatase Activity (ALP)

Samples were incubated in an equal volume of 4 mM p-nitrophenyl phosphate liquid in 100 mM ammonium bicarbonate containing 1 mM $MgCl_2$ (pH 7.8). The enzymatic kinetic was evaluated (Ross et al., 2000) at regular intervals of 5 min to 1 h at 405 nm with a microplate reader (RAYTO RT-2100C). One unit (U) of activity was defined as the amount of enzyme required to release 1 micromole of p-nitrophenol produced in 1 min.

Protease Activity

The polyacrylamide electrophoretic run of tentacle and body extracts was performed under non-reducing conditions (7.5%) using gelatin (2 mg/mL) and fibrinogen (0.5 mg/mL) as substrates. Migration took place at 160 V for about 1 h. Gels were washed in TBS Ca^{2+}

(150 mM NaCl, 10 mM di Tris-HCl, 10 mM $CaCl_2$, pH 8.0) adjusted with 2% Triton X-100. Gels were left to stir overnight in TBS Ca^{2+} (pH 8.0) at room temperature, immersed in 50% methanol, stained in Coomassie Blue (0.1% Coomassie Brillant Blue G250, 40% Methanol, 1% Acetic acid) for an hour and finally decoloured (0.1% acetic acid, 0.4% methanol). The reaction was stopped with distilled water and densitometric analysis was carried out using the open-source software Image J (http://rsbweb.nih.gov/ij/download.html) (accessed on 20 May 2021).

Biometry of the Regenerative Area

Animals were placed in a plate and biometric parameters were measured (pedal and oral disc, length of tentacle) using a millimeter gauge, to select specimens of comparable size. Pictures of the part in regeneration were taken using a stereoscopic microscope (Eurotek NB50T, Milano, Italy). The thickness of the different tentacle layers and of the lumen area were calculated in micrometers and then the percentage increase or decrease through mathematical transformation compared to a tentacle of a control animal was also calculated. The biometric evaluation system for tentacles in regeneration was carried out using Image J software.

Light and Transmission Electron Microscopy (TEM)

Embedding Tissue in Paraffin

The budding area (cutting site with regrowth tissues) of three organisms subjected to the cut of 25% of the total number of tentacles at three times point (1, 7 and 14 dpa) was fixed in Bouin's solution until complete sinking. Subsequently, samples were dehydrated in an increasing scale of ethanol (30%, 50%, 70%, 90%, 96%, 100%) and paraffin-embedded. Sections (7 µm in thickness) have been cut in series with a rotary microtome (Microm HM 350S, GMBH,Walldorf, Germany) and processed for the Masson's and Gomori's and Trichrome stains.

Gomori's Trichrome

Sections were stained with Carazzi's emalume (200 mL—10 g $KAl(SO_4)$, 0.2 g hematoxylin, 0.04 g KIO_3, 40 mL glycerol) for 10 min at room temperature, washed in distilled water for 15 min, and been left in Gomori's trichrome solution (100 m—0.6 g chromotropium 2R, 0.3 g fast green FCF, 0.6 g of phosphotungstic acid, 1 mL acetic acid, pH 3.4) and finally washed in acidified water (0.2% acetic acid).

Masson’s Trichrome

Masson’s trichrome assays were performed using a specific colorimetric kit (Trichromica kit, Bio Optica, Milan, Italy) and specimens were treated as suggested by the datasheet, in order to highlight the presence of both collagen and the reticular fibers with aniline blue, while the cell cytoplasm was in red. Images were recorded with a Nikon Digital Sight DS-SM optical Microscope (Nikon, Tokyo, Japan).

Embedding Tissues in Epoxy Resin

A. viridis tissues, dissected from the area in regeneration, were fixed in 0.1Mcacodylate buffer (pH 7.4) containing 4% glutaraldehyde for 2 h. Specimens were then washed in the same buffer and post-fixed for 1 h with 1% osmium tetroxide in cacodylate buffer (pH 7.4). After standard serial ethanol dehydration, specimens were embedded in an Epon-Araldite 812 mixture. Sections were obtained with a Reichert Ultracut S ultratome (Leica, Wien, Austria). Data were recorded with a DS-5 M-L1 digital camera system (Nikon). Ultrathin sections (0.7 µm in thickness) were placed on copper grids (300 mesh), stained by uranyl acetate and lead citrate and observed with a Jeol 1010 EX transmission electron microscope (Jeol, Tokyo, Japan).

Immunofluorescence Analyses

After etching with 3% NaOH in 100% ethanol (Causton, 1984), ultrathin sections were treated pre-incubated for 30 min in BSA blocking solution (2% Bovine Serum Albumin and 0.1% Tween20 in PBS), which was also used to dilute both the primary and secondary antibodies. Subsequently, samples were incubated with anti-COL1α1 (rabbit polyclonal, EMD Milli- pore, ABT257) and anti-bFGF receptor Flg (rabbit polyclonal, Santa Cruz Biotechnology, sc-121) primary antibodies, diluted 1:200, for 1 h at room temperature. After several washes in PBS (137 mM NaCl, 2.7 mM KCl, 10 mM Na_2HPO_4, pH 7.4), specimens were incubated with and goat anti-rabbit Cy3-conjugated secondary antibody (goat, Jackson ImmunoRe- search Laboratories, Baltimore Pike, West Grove, PA, USA), diluted 1:200, for 45 min. Cell nuclei were counterstained with DAPI (4,6-diamidino-2-Phenylinedole, 0.1 mg/mL in PBS) for 2 min and slides were mounted with Cityfluor (Cityfluor Ltd., London, UK). Negative control experiments were performed omitting primary antibodies.

Immunogold

Ultrathin sections were obtained as above and collected on gold grids (300 mesh). After etching with NaOH 3% and methanol, specimens were pre-incubated for 30 min in BSA blocking solution and then for 1 h with the anti-bFGF receptor Flg primary antibody, diluted 1:50. After two washings with PBS, the goat anti-rabbit IgG (H + L)-gold conjugate secondary antibody (GE Healthcare, Amersham, UK; particle size, 10 nm), diluted at 1:40, was used for 30 min. In control experiments, the primary antibody was omitted, and sections were incubated with the secondary antibody alone. After washings with PBS, samples were treated for 5 min with 0.5% glutaraldehyde in PBS solution, counterstained with uranyl acetate for 8 min and observed at TEM.

Statistical Analyses

All the experiments were performed in triplicate and the values used were the mean of the three assays ± SEM. To assess multiple comparisons, a parametric two-way analysis of variance (ANOVA) was performed on the data, with a post hoc Tukey test. Differences between means were considered significant for * $p < 0.05$, ** $p < 0.01$ and *** $p < 0.001$. The analyses were carried out using the GraphPad Prism Version 8.0.0. for Windows (www.graphpad.com) (accessed on 20 May 2021). The mesoglea area and the number of elongated amoebocytes were evaluated both in intact and injured tentacles by analysing five different slides, using the ImageJ software. The software GraphPad Prism 7 (GraphPad Software, La Jolla, CA, USA) was used to perform statistical analyses and differences between treatments were calculated by one-way ANOVA, followed by Fisher's post-hoc test. Values of $p < 0.05$ were considered statistically significant.

RESULTS

Macroscopic Assessment of A. viridis Recovery

The anemones survived the stress of injury. The tentacles hexamerously were arranged in several cycles moderately long (to 20–30 mm length), smooth, slender, tapering distally, inner ones longer than outer ones, contractile, dark-yellow to light-brown, sometimes with whitish or light pink tips.

In Figure 1a, the black boxed area indicated where in the *A. viridis* adult specimen the tentacles were amputated. A lateral view of the amputated tentacle is shown in Figure 1b, in which the arrow indicates the magnification of the injury reported in inset.

After 1 day post-amputation (dpa), the injured terminal parts of tentacles appeared lighter in colour than the rest of tentacles and the body (Figure 1c). The black box area indicated the non-pigmented area shown at a greater magnification in Figure 1d in which the terminal portion of the tentacle closed but without colouring is visible. The white pigmentation indicated by the arrow in the magnification is due to the absence the symbiont zooxanthellae in the wound closure area (Figure 1d). In the amputated specimens, a normal macroscopic tissue morphology was detected, and pigmentation occurred within 7 days (Figure 1e). In Figure 1f, a visible tentacle bud of about 2 mm was indicated by the yellow arrow. The regenerative event appeared clear at macroscopic level after 14 dpa (Figure 1g) when a remarkable regrowth of about 3–4 mm was measured (Figure 1h).

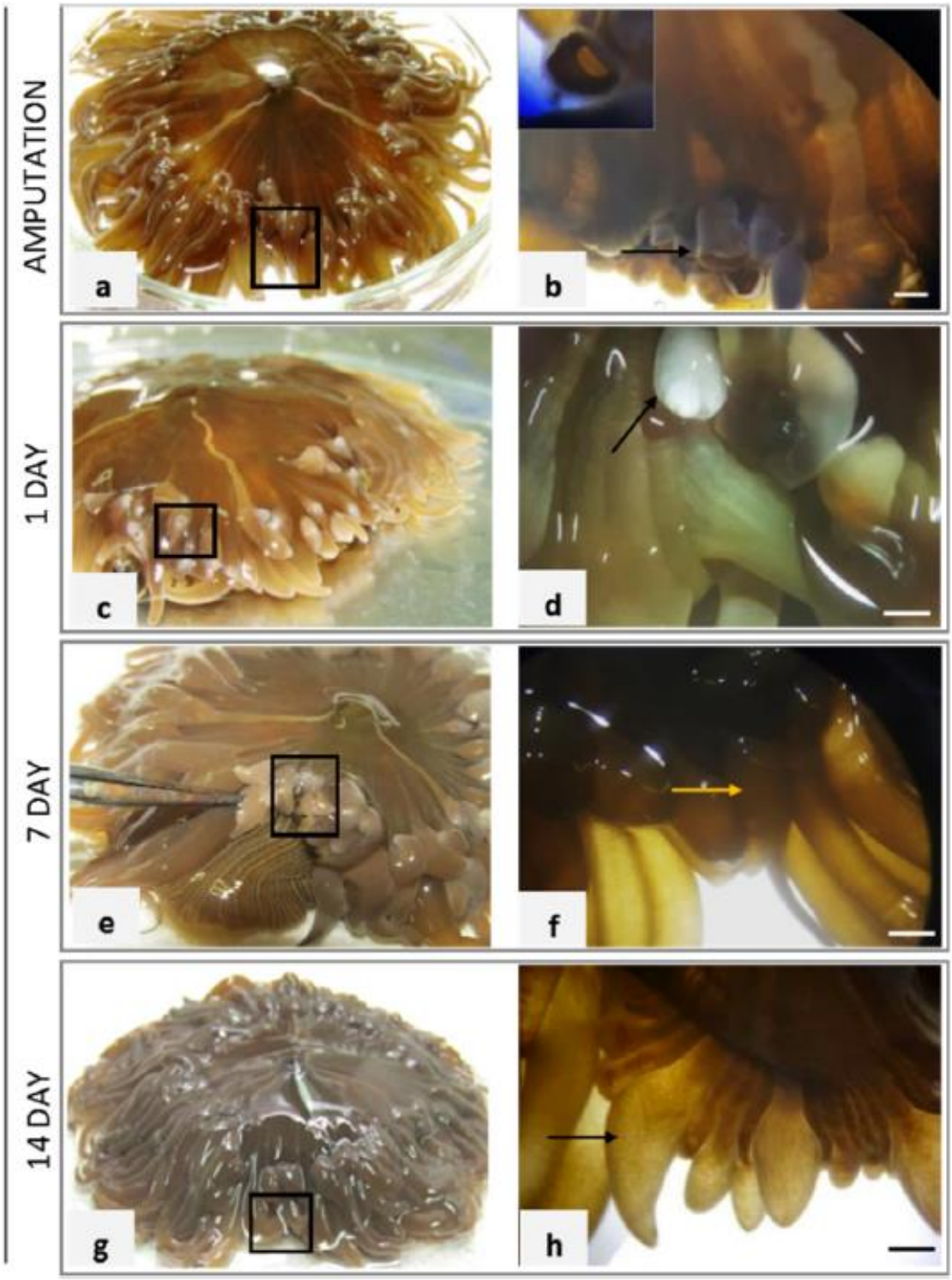

Figure 1 Morphological detection of the wound of A. viridis and regrowth of the amputated tentacles. Specimens injured in the black box area ***(a)****, wound area observed after 6 h with magnification of amputated tentacles indicated by the arrow* ***(b)****. After 1 day post-amputation (dpa), the wound in the tentacles appear closed but avoid of pigment* ***(c)****. Magnification of the closed terminal part of the tentacles with white pigmentation indicated by the arrow* ***(d)****. At 7 dpa, the black boxed area includes the regenerated tentacles* ***(e)****, and the small 2 mm long regrown tentacles showed a yellow–brown color like the global tentacular component* ***(f)****. At 14 dpa, the tentacles continue to grow (g) in length and diameter with yellow–brown pigmentation* ***(h)****. The arrow indicates a 4 mm long tentacle. Bar = 2 mm.*

Biochemical Response

Alkaline phosphatase enzyme measured both in *A. viridis* tentacles and body extracts increased over time in amputated samples with respect to unamputated animals (Figure 2a,b). Particularly, in the tentacles (Figure 2a), the production of the enzyme constantly increased during the three observation step points. Multiple comparison analysis provided significant results for samples analysed after 1 and 14 dpa with respect to control unamputated specimens. On the other hand, in the body extracts (Figure 2b), the enzymatic values result was consistently and significantly higher than the control samples at all time step points. Significant results were detected for each treated group. In both tissues, the two-way ANOVA analysis reported in Table 1 showed a p-value (< 0.05) for the interaction of time (T) and injury (I) factors (TxI). In the body, both time (T) and injury (I) factors resulted in significance (p-value < 0.05) as well as their interaction (TxI). The proteolytic activity was investigated in tentacles and body extracts using SDS-PAGE with gelatin and fibrinogen as substrates (Figure 2c,d). The gelatinolytic and fibrinolytic activity, assayed by the densitometric analysis and based on the calculated integrated value of density (IDV), grew over the time in the tentacles (Figure 2c). In the body, the fibrinolytic activity was present only at 1 day while the gelatinolytic activity was found from 1 to 14 dpa (Figure 2d).

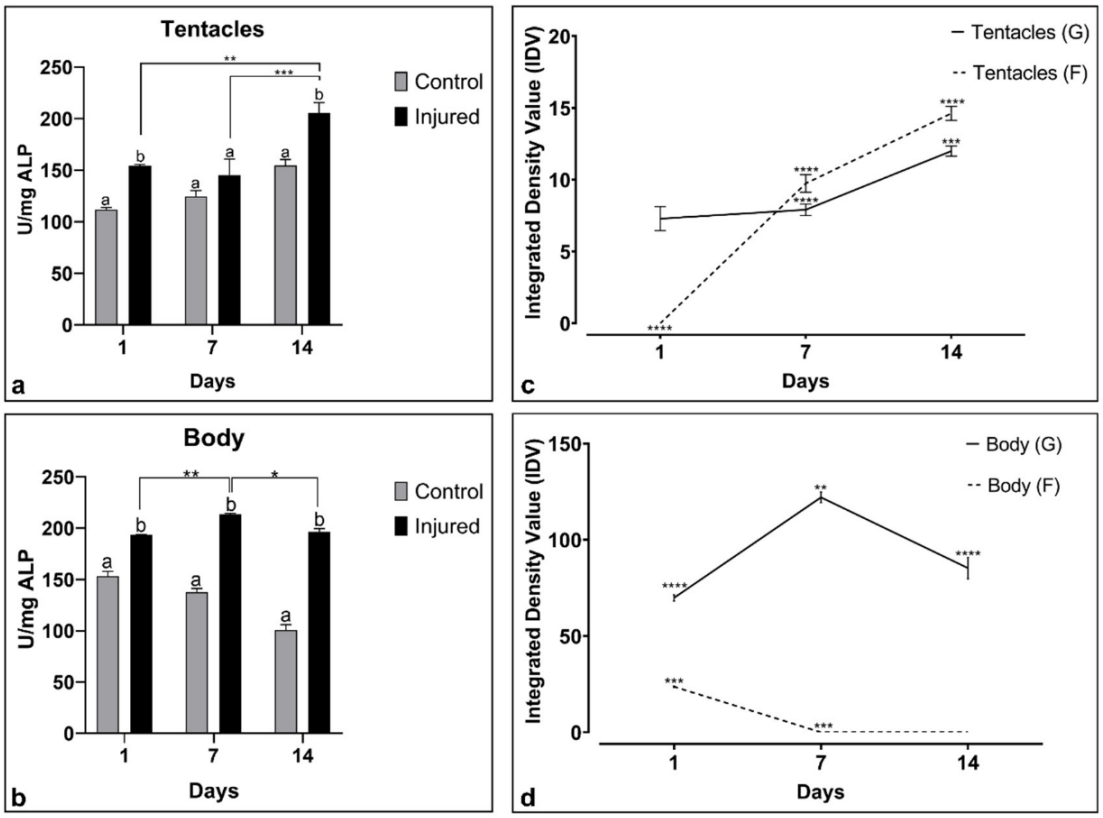

*Figure 2 Alkaline phosphatase activity (ALP) and proteolytic activity in tentacles and in the body extracts of A. viridis. ALP in tentacles **(a)** and in the body **(b)** extracts of A. viridis of injured (amputated) and control samples. Kinetics of ALP was expressed as U*mg^{-1} of protein. Densitometric analysis of the proteolytic activity based on the integrated value of density (IDV) calculated on SDS-PAGE carried out with gelatin and fibrinogen as substrates using the tentacles **(c)** and the body tissue extracts of amputated specimens **(d)**. Data were statistically analysed using analysis of variance to determine differences between groups and showed mean ± standard error. The letters indicate statistically significant differences between control and its respective treated group. * Indicates differences between groups at each time. Significant differences were detected by Tukey post hoc test—* p < 0.05, ** p < 0.01, *** p < 0.001, **** p < 0.0001.*

Table 1 Two-way ANOVA analysis results of alkaline phosphatase activity (ALP) measured in the tentacles and body extracts of A. viridis. Statistically significant effects of the following variables— Time (T) and Injury (I) and interactions (TxI). The analyses were carried out using the GraphPad Prism Version 8.0.0. for Windows (www.graphpad.com (accessed on 1 March 2021)). Differences between means were considered significant for p < 0.05.

		Tentacles		Body	
Activity	**Variables**	**F Value**	**p Value**	**F Value**	**p Value**
ALP	T	1.668	0.229	5.417	0.0089
	I	2.716	0.125	39.83	<0.0001
	T x I	4.996	0.026	6.625	0.003

The two-way ANOVA results regarding proteolytic activity were reported in Table 2. A

significant p-value (<0.05) in both body and tentacle tissue extracts was revealed for the variables Time (T), Substrate (S) and their interaction (TxS).

Table 2 Two-way ANOVA analysis results of Proteolytic activities (Fibrinolytic and Gelanolytic) measured in the tentacles and body extracts of A. viridis. Statistically significant effects were seen in the following variables—Time (T) and Substrate (S) and interactions (TxS). Bold numbers indicate the significant p-value. The analyses were carried out using the GraphPad Prism Version 8.0.0. for Windows (www.graphpad.com (accessed on 1 March 2021)). Differences between means were considered significant for p < 0.05.

		Tentacles		Body	
Activity	**Variables**	**F Value**	**p Value**	**F Value**	**p Value**
PROTEOLYTIC	T	173.5	<0.0001	26.51	<0.0001
	S	4.984	0.00454	1527	<0.0001
	T x S	56.22	<0.0001	102.8	<0.0001

Biometry of Unamputated and Regenerating Tentacle Tissues

In order to evaluate biometric parameters of regenerating tissues, longitudinal sections, stained with Gomori's Trichrome, of control (unamputated) (Figure 3a,b) and 7 dpa tentacles (Figure 3c,d) were observed under a light microscope. Dimensional analysis of the different tissue layers in both control and post-injury specimens was carried out by image J software (Figure 3e–g).

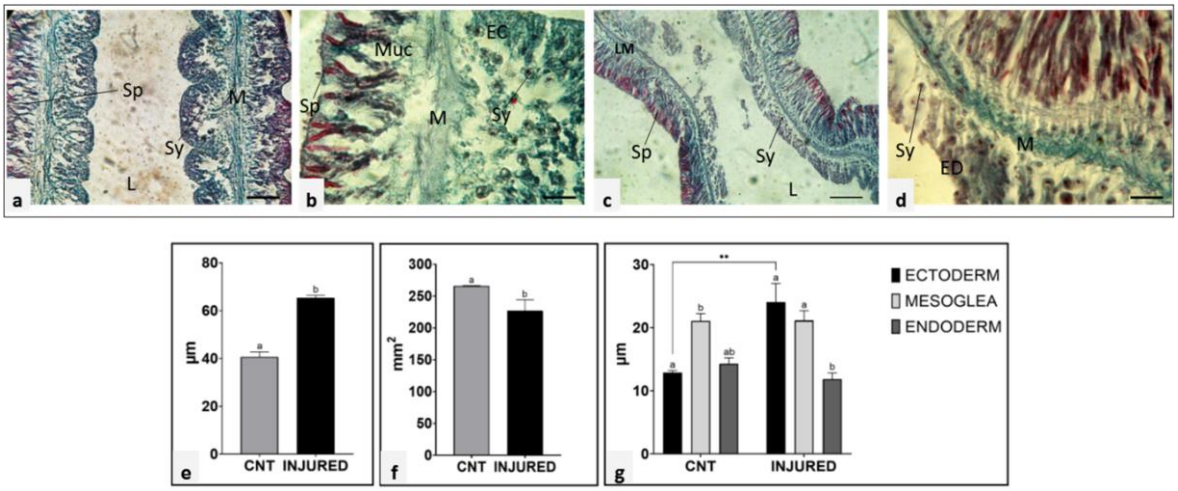

*Figure 3 Gomori stain of tentacle transversal sections from uninjured specimens (a,b) and after 7 dpa (c,d). In light microscopy, Ectoderm (EC), Mesoglea (M), Endoderm (ED), Lumen (L), Spirocysts (Sp), Mucocytes (Muc), longitudinal muscle (LM), and Symbiodinium symbiont (Sy) were identified. The different dimensions of the tissue layers are evident in the magnifications of the sections of the control (c) and amputated (d) tentacles. Bars—50 (a,c) and 100 µm (b,d). Plots report that the biometric quantification of tentacular thickness increases (e) and the lumen decreases (f) in regenerating organisms post-amputation (injured) compared to the unamputated specimens (cnt). (g) shows the thickness of three body layers (ectoderm, mesoglea and endoderm). The Mesoglea and the Endoderm maintain constant size while the ectodermal layer increases in injured specimens with respect to the control (cnt). Analysis of variance was carried out. The letters (a,b) indicate statistically significant differences between control and its respective treated group. * Indicates differences between groups at each time. Significant differences were detected by Tukey post hoc test—** $p < 0.01$.*

Of note, in the 7 dpa tentacle, both the ectoderm and the gastrodermis layers appeared thicker than in the unamputated tentacle, while the mesoglea size remained constant during all the regenerative phases. However, a pronounced variation in the mesoglea connective tissue density was appreciated. Indeed, after 7 dpa (Figure 3c,d) the connective tissue appeared more compact and darker green coloured than that of the control tentacle.

Comparing the control tentacles with the regeneration after amputation, a significant increase in tissue thickness (Figure 3e) and a reduction in lumen (Figure 3f), were observed. The thickness of the three tissue layers (ecto-, meso-, and endoderm) appeared significantly different between control (cnt) and amputated organisms (injured) (Figure 3g). Particularly, the ectoderm shows a statistically significant variation in the injured samples compared to the unamputated specimens.

Morphological and Ultrastructural Analyses of Regenerating Tentacle

In order to shed light on morphological modification occurring in the mesoglea connective tissue during tentacle regeneration, histological and ultrastructural analyses were performed on unamputated and regenerated tentacles.

Control tentacle tissues revealed intact epithelia containing cells characteristic for each epithelium and separated by a loose mesoglea. Epidermis was formed by a single layer of densely packed columnar cells with the basal part mounted on the mesoglea. On the opposite side, the gastrodermis layer, with numerous endosymbiotic dinoflagellates zooxanthellae, was visible (Figure 4a). Mesoglea ECM appeared as an amorphous fibrous matrix (Figure 4b) in which no fibrillar collagen and only a few scattered rounded amoebocytes containing a large nucleus were detectable (Figure 4c,d).

The changes occurring in the ECM during the regenerative phase, both at the level of cellular and matrix reorganization, were evaluated in tentacles allowed to grow back for 1 and 7 days and subsequently cut from the base of the body. The epidermal layer of the tentacle regrown after one day from cutting, was formed by columnar cells arranged in a circular way and anchored with their basal side to the inner mesoglea (Figure 4e).

An increased number of elongated amoebocytes with irregularly round nuclei appeared in the mesoglea protruding in the newly formed epidermal layer (Figure 4f–h). The darker violet staining (Figure 4e,f) indicated a connective tissue remodelling, also confirmed by ultrastructural electron transmission microscopy (TEM) analysis. Indeed, bundles of collagen fibrils were clearly detectable surrounding the elongated amoebocytes, especially concentrated just to the outside of these cells (Figure 4g,h), strongly suggesting their fibroblastic nature.

After 7 days, the mesoglea infiltrating the newly formed epidermis increased in length together with the tentacle growth (Figure 4i). Bands of collagen fibrils were organized to form a robust scaffold in which aggregates of spindle-shaped fibroblast-like cells were observed (Figure 4j,k).

The ECM area and the number of elongated amoebocytes in both noninjured (Cnt) and amputated tentacles (Figure 5a) were quantified using ImageJ (see material and methods) and the graphs showed an increased ECM area after 1- and 7-days post-amputation (dpa) (Figure 5b). A greater number of elongated amoebocytes was found 1 day after amputation. These data suggested that these cells might be implicated in the ECM neo-synthesis and reorganization.

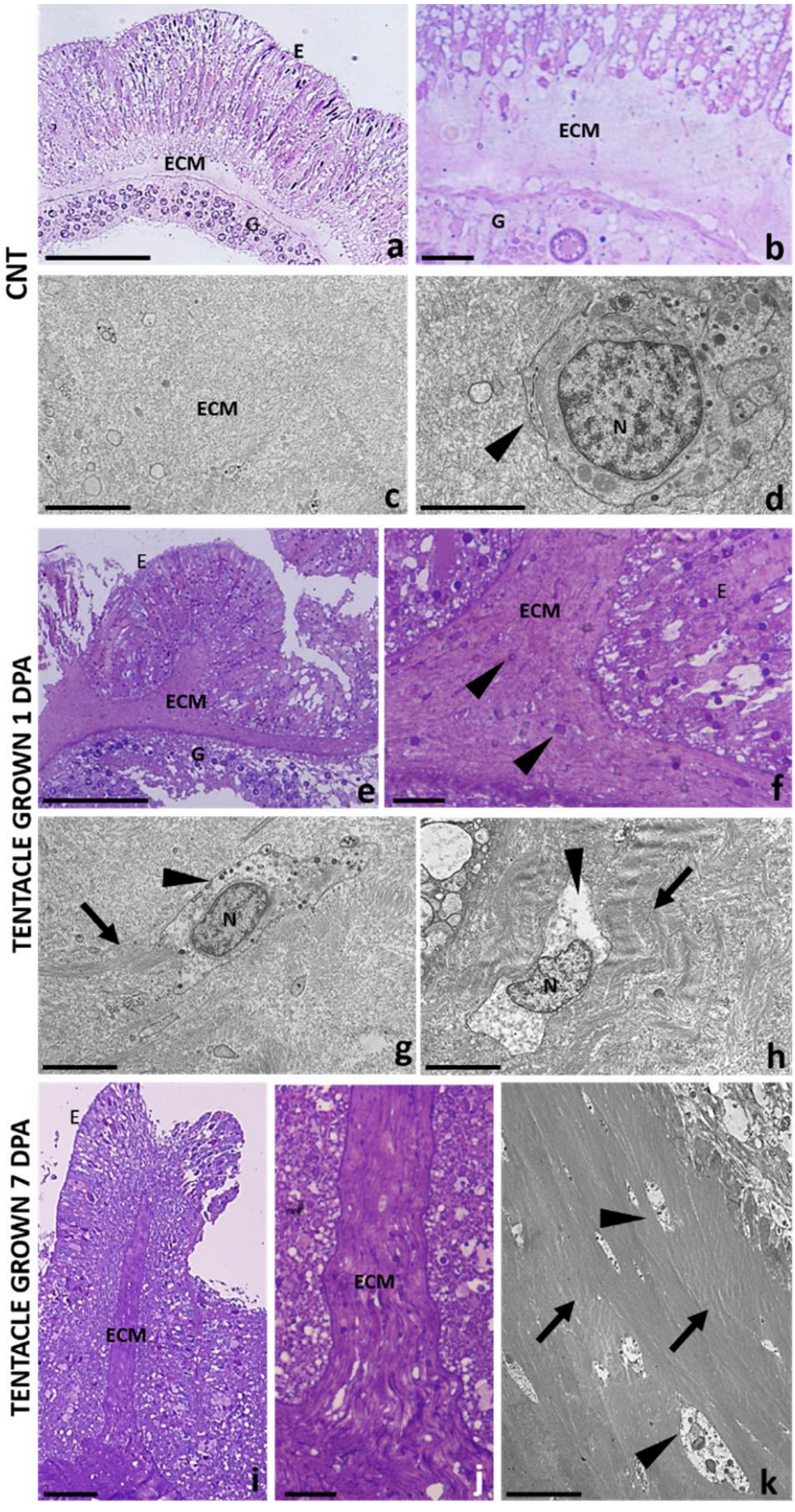
CNT
TENTACLE GROWN 1 DPA
TENTACLE GROWN 7 DPA
E
ECM
G
N
a
b
c
d
e
f
g
h
i
j
k

Figure 4 Light and electron transmission microscopy analyses of control and amputated organisms. In the control tentacle (a–d), mesoglea ECM, localized between the epidermis and gastrodermis, appears as a loose matrix. Ultrastructural TEM images (c,d) show that it is composed of a meshwork of thin filaments in which no fibrillar collagen and only few round shape amoebocytes (arrowhead) are detectable. After one day from amputation (e–h), epithelial columnar cells of the regrowth tentacle are arranged in a circular way surrounding the inner mesoglea. Elongated amoebocytes (arrowheads) with irregular nuclei (g,h) and collagen fibrils (arrows) concentrated on their outer surface are visible. After 7 dpa (i–k), the regenerated tentacle increased in length, supported by a robust and extended collagenic scaffold, in which spindle-shaped fibroblast-like cells (arrowheads) have migrated. ECM, Mesoglea; E, Epidermis; G, Gastrodermis; N, nuclei. Scale bars—(a,e) 100 µm; (i) 50 µm; (b,f,j) 10 µm; (c,k) 5 µm; (d,g,h) 2 µm.

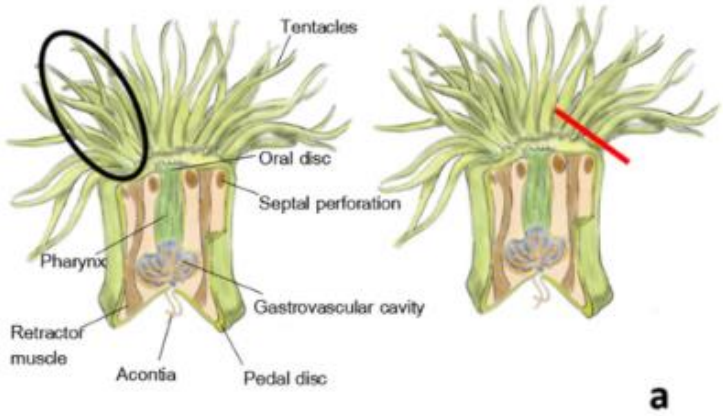

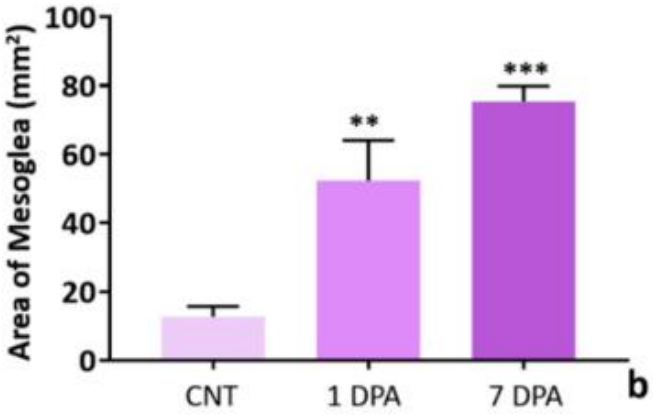

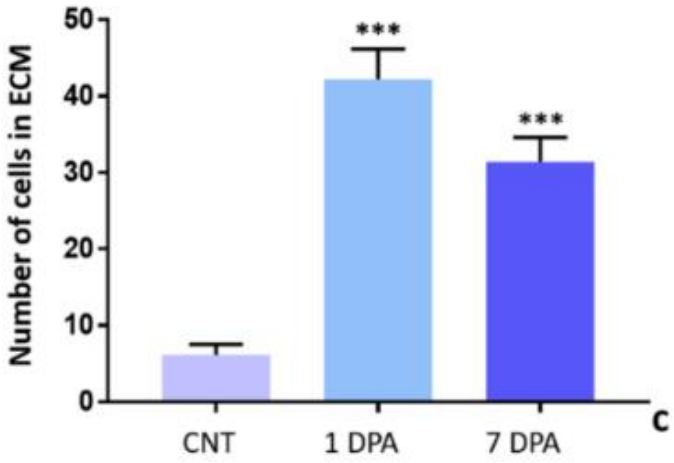

Figure 5 Comparison of ECM area and cell number between unamputated (black encircled) and amputated (red line) regenerating tentacles (a). The graphs show the quantification of the mesoglea area (b) and of elongated amoebocytes

*number (c) in noninjured (Cnt) and regenerating tentacles at 1 and 7 days post-amputation (dpa). Significant differences were detected by Fisher post hoc test—** $p < 0.01$, and *** $p < 0.001$.*

Mesoglea Matrix Reorganization and Collagen Neo-Synthesis Based

Based on the morphological observation, we were further interested in evaluating a possible interaction between tentacle regeneration and mesoglea expansion from the body's mesenteries and whether the mesoglea ECM remodelling would be correlated to collagen neo-synthesis and fibroplasia events. To this aim, Masson's trichrome staining with blue aniline, immunofluorescence and immunogold assays using anti-pro-collagen1α1 (COL1α1), to detect collagen I and bFGFR, a specific fibroblast marker in both vertebrates and invertebrates (Baranzini et al., 2020), was performed in the area of the body where the tentacles were cut and allowed to grow back for 1 and 7 days (Figure 6).

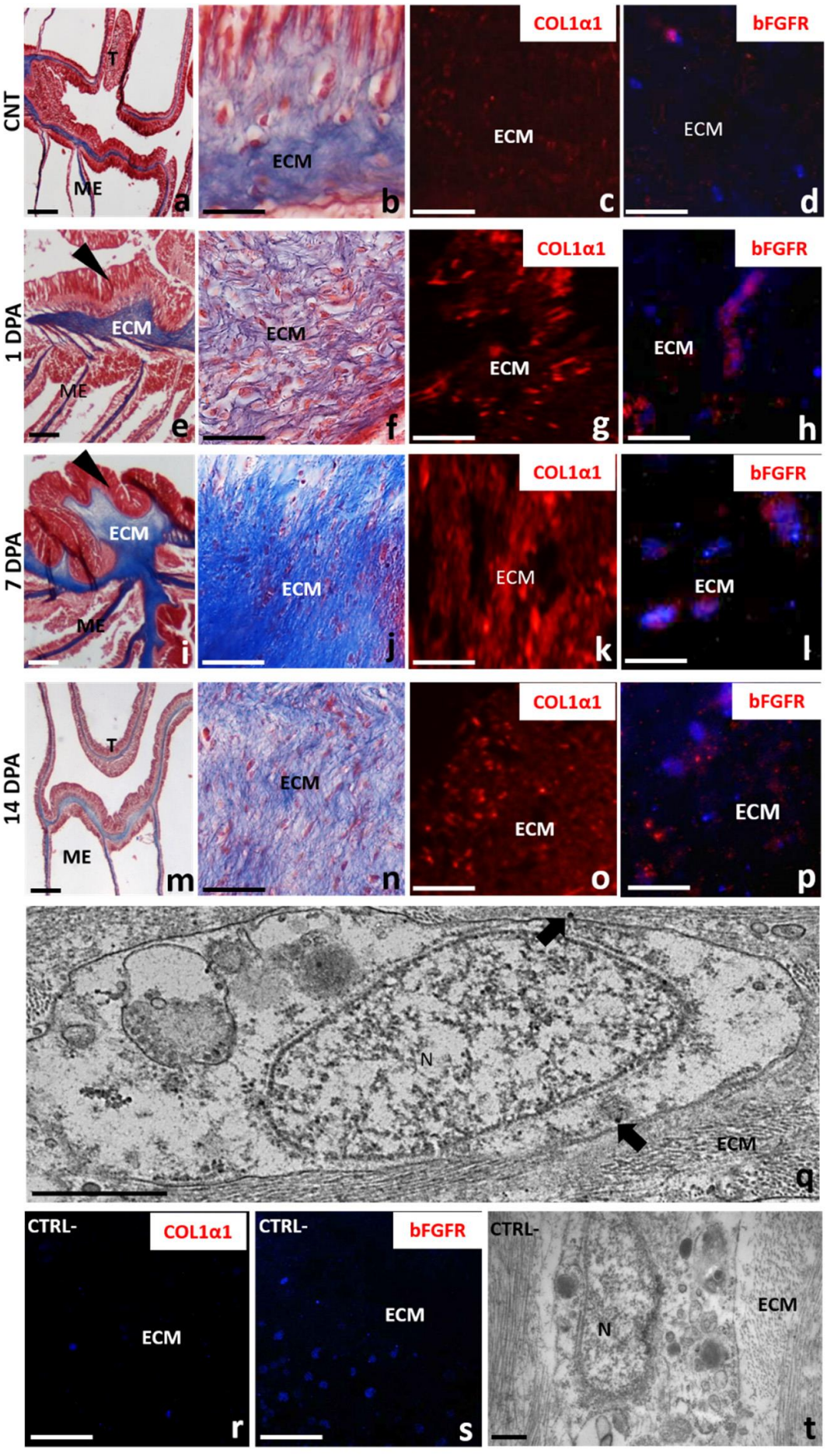
CNT
1 DPA
7 DPA
14 DPA
T
ME
ECM
COL1α1
bFGFR
N
CTRL-
a
b
c
d
e
f
g
h
i
j
k
l
m
n
o
p
q
r
s
t

Figure 6 Masson's trichrome and COL1α1/bFGFR immunolocalization assays. In control animals (a–d), Masson's trichrome colorimetric assays highlighted the presence of a slightly coloured ECM both in tentacles (T) and in the body wall (B) (a,b). A low immunofluorescent signal is detected for both anti-COL1α1 (red in c) bFGFR (red in (d)) primary antibodies, indicating the presence of few fibroblast-like cells involved in collagen production. After 1 dpa (e–h), an intensely blue-coloured ECM (e,f), numerous dispersed COL1α1+ fibrils (g) and bFGFR+ fibroblast-like cells (g) are detectable in the tentacle bud (arrowhead) and in the mesenteries (ME). After 7 dpa (i–l), a compact scaffold formed by collagen fibrils in which aggregates of COL1α1+ (k) and bFGFR+ (l) spindle-shaped fibroblast-like cells are present in the ECM of both tentacle buds (arrow) and mesenteries. After 14 days (m–p), the ECM appears looser, less blue-staining (m,n) and low COL1α1 (o) and bFGFR (p) fluorescent signals are visible. (q) Immunogold localization at TEM showing the localization of bFGFR (arrows) on the fibroblast-like cell membrane. Nuclei are counterstained in blue by DAPI. No signals were detected in negative control experiments, in which primary antibodies are omitted (r–t). ECM, extracellular matrix of mesoglea; E, Epidermis; ME, mesenteries N-nuclei; T, tentacle. Scale bars—(a,e,i,m) 100 µm; (b,f,j,n,r,s) 20 µm; (c,d,g,h,k,l,o,p) 5 µm; (q,t) 500 nm.

In both tentacles and mesenteries of healthy animals, the ECM had an amorphous and nonfibrotic appearance and was slightly coloured by aniline blue (Figure 6a,b). Moreover, a low signal (Figure 5c) was detected for the antibody anti-COL1_1.

By contrast, after 1 day from injury, a remarkable rearrangement of the mesoglea collagen-based connective tissue was evident. Indeed, the ECM, now more intensely coloured in blue, was clearly organized in fibrils, both in the mesoglea of mesenteries adjacent to the regenerating area and in that infiltrating the tentacle bud, likely deriving from the mesentery itself (Figure 6e,f). Furthermore, COL1_1+ fibrils dispersed in the ECM were detected by immunofluorescence assay (Figure 6g).

The fibrillar organization of the mesoglea matrix became even more evident especially in the sprawling bud regrown at 7 dpa, as also demonstrated by the significant increase of collagen I deposition (Figure 6i–k).

After 14 dpa (Figure 6m,n), the tentacle had almost completely regrown and the mesoglea matrix was looser both in the regenerated tentacle and in the mesenteries, appearing less intensely blue-coloured and had a lower expression of COL1_1 (Figure 6o).

In order to better characterize the elongated and migrating amoebocytes found in the mesoglea connective tissue, immunofluorescence analysis using the anti-bFGFR antibody was performed. A basal level of bFGFR expression was found from a few resident cells located in the mesoglea of the control polyp (Figure 6d), whereas following tentacle amputation, an increased number of elongated bFGFR+ cells appeared in the ECM (Figure 6h,l,p) of both tentacles and mesenteries. The immunogold assay confirmed that the bFGFR was localized on the surface of hyaline amoebocytes (Figure 6q), indicating the differentiation of these cells involved in new collagen production activity as fibroblast-like cells. In all the negative control experiments, no signals were detected (Figure 6r–t).

DISCUSSION AND CONCLUSIONS

In this study, we aimed to shed light on the structural and cellular mechanisms of the recovery of the mesoglea after injury, a key aspect of the regenerative process in cnidarians (Sarras, 2012), using as a model the symbiotic anemone snakelocks *A. viridis*.

We first evaluated the regrowth of the oral tentacles after their amputation from the base of the body for 14 days, through a constant observation at a macroscopic level. At the same time, we quantified the activity of alkaline phosphatase and protease enzymes, typical biochemical markers associated with regenerative events. After 24 h, the closure of the wound is complete, and the injured part appears devoid of pigment probably due to the absence of zooxanthellae, lost from the tissues after injury. The sprawling regrowth was already noticeable after 7 days and new pigmented 5-mm-sized tentacles were visible after 14 days from injury. The return of pigmentation after 14 days is probably correlated to the repopulation of the tissues by the symbionts, which also seem to have an important role in the lengthening of the regenerating tentacles (Ferrier-Pagès et al., 2016).

In vertebrates, one of the first events triggered during wound healing, inflammation and regeneration, is the alkaline phosphatase (ALP) activity, especially by fibroblasts localized in the connective tissue (Abe et al., 2001). This enzyme is usually highly expressed also during tissue regeneration in cnidarian and in Hydra, and it has been described as one of the main enzymatic markers related to nematocyte and epithelial cell differentiation during tentacle regeneration (De Petrocellis et al., 1999).

Here, we showed that ALP in *A. viridis* increases significantly in tentacle extracts after amputation in all three time points considered, while the enzyme amount remains at a constant level in the body extract.

Algae convert dissolved organic phosphorus (DOP) in the environment into dissolved inorganic phosphorus (DIP), which is used by animal organisms for their metabolic activities. The symbiotic zooxanthellae, abundant in the tentacles, play a crucial role in the absorption of phosphate dissolved in water (Annis and Cook, 2002; Parisi et al., 2017; Rader, 2017; Stabili et al., 2018). The different amount of ALP present in the tentacles compared to the body may be explained with their more effective absorption and bioaccumulation capacity of phosphorus.

Wound healing, occurring immediately after an injury and involving cell contraction and re-adhesion, is the phase that precedes the regeneration of the lost structures. During both of

these phases, the immune response facilitates protection against microbes, maintaining homeostasis and preventing infections that might compromise fitness (Brown and Rodriguez-Lanetty, 2015; Van De Water et al., 2015). Alongside immune system activation, in response to injury, protease enzymes, normally minimally active in adult tissues are upregulated during regeneration and tissue remodelling (Trapani et al., 2016). Matrix metalloproteinases (MMPs) are a family of endopeptidases collectively able to degrade the components of the extracellular matrix. They play important roles in propeptides and collagen fibril formation and normal tissue remodelling, embryogenesis, angiogenesis, and wound healing (Parisi et al., 2020; Ricci and Srivastava, 2018). In cnidarian, several typical components of vertebrate ECM, such as fibronectin, laminin and different types of collagen are involved in cell adhesion (Adams, 1978; Barzansky et al., 1975; Barzansky and Lenhoff, 1974; Haller, 1989; Miura and Kimuras, 1985; Schmid and Bally, 1988), and several matrix proteases with gelatinolytic and fibrinolytic activities have been cloned and characterized (Jouiaei et al., 2015; Lee et al., 2011; Li et al., 2014; Yan et al., 2000, 1995).

Here we found a significant increase of protease activity (both gelatinolytic and fibrinolytic) in the regenerating tissue after wound closure from 1 to 14 dpa. Our results suggested that these metalloproteases could play an essential role in the degradation and remodelling of mesoglea connective tissue during tissue regrowth. These findings are consistent with the results obtained by tissue biometric analysis performed on sections of new formed tentacles 7 days after injury and show that during regeneration the thickness of the mesoglea did not increase, as it did for the epidermis and gastrodermis. However, the consistency of the mesoglea changed visibly and shifted from a loose matrix to a compact one. The change in stiffness was probably due to the ECM remodelling mediated by proteases, secreted by immune cells during wound healing and tissue regeneration phases (Tomlin and Piccinini, 2018). The close interplay between the ECM and the innate immune system in cnidarian is mediated by the granular and hyaline amoebocytes that use the mesoglea as a territory to move to the wound site, where they infiltrate and aggregate to spread out along the lesion edge that occurs during the inflammation phase in vertebrates (Palmer et al., 2011). During this process, it is likely that they not only release antimicrobial and cytotoxic material, including melanin, which can destroy pathogen invaders, but they might also produce proteases to facilitated cell migration (Grimaldi et al., 2004) and secrete new collagen used as a scaffold for tissue reconstruction (Sarras, 2012; Tettamanti et al., 2005).

Our morphological analyses under an optical and electron microscope, and Masson's trichrome-specific colorimetric assays for ECM, seem to support this hypothesis, showing for the first time that during the tentacle regenerative process, mesoglea shift from a lax network to a lattice organized in bundles of collagen fibrils. Furthermore, immunolocalization assays, using polyclonal antibodies directed against the pro-collagen1α1 and bFGFR antigens, indicate that the visco-elastic behaviour of mesoglea is obtained by the neo-synthesis of type I collagen from bFGFR+ hyaline amoebocytes, acting as fibroblast-like cells. These cells, interacting with the neosynthesized collagen fibrils, appear to be involved in the formation and spatial organization of a compact collagen scaffold.

In conclusion, basing on the obtained evidence, we suggest that in *A. viridis*, the mesoglea ECM provides not only a mechanical support to maintain the shape and integrity of tissues, but also plays a fundamental role in tissue morphogenesis, cell migration and differentiation during tentacle regeneration (Godwin et al., 2014). Indeed, as already proposed for *N. vectensis*, after tentacle amputation, the change of mesoglea stiffness, obtained through metalloprotease activity, could initially play the role of a barrier against the entry of pathogens into the lesion site. Subsequently, the production of new collagen ECM by fibroblast-like cells, differentiated from amoebocytes, could act as a scaffold to guide the correct regrowth of the tentacle.

REFERENCES

Abe, T., Abe, Y., Aida, Y., Hara, Y., Maeda, K., 2001. Extracellular matrix regulates induction of alkaline phosphatase expression by ascorbic acid in human fibroblasts. J. Cell. Physiol. 189, 144–151. https://doi.org/10.1002/jcp.10011

Adams, E., 1978. Invertebrate collagens. Science (80-.). 202, 591 LP – 598. https://doi.org/10.1126/science.212833

Amiel, A.R., Foucher, K., Ferreira, S., Röttinger, E., 2019. Synergic coordination of stem cells is required to induce a regenerative response in anthozoan cnidarians. bioRxiv 2019.12.31.891804. https://doi.org/10.1101/2019.12.31.891804

Amiel, A.R., Johnston, H.T., Nedoncelle, K., Warner, J.F., Ferreira, S., Röttinger, E., 2015. Characterization of morphological and cellular events underlying oral regeneration in the sea anemone, *Nematostella vectensis*. Int. J. Mol. Sci. 16, 28449–28471. https://doi.org/10.3390/ijms161226100

Annis, E., Cook, C.B., 2002. Alkaline phosphatase activity in symbiotic dinoflagellates (zooxanthellae) as a biological indicator of environmental phosphate exposure. Mar. Ecol. Ser. - MAR ECOL-PROGR SER 245, 11–20. https://doi.org/10.3354/meps245011

Augustin, R., Bosch, T.C.G., 2010. Cnidarian immunity: A tale of two barriers, Advances in Experimental Medicine and Biology. https://doi.org/10.1007/978-1-4419-8059-5_1

Baranzini, N., Weiss-Gayet, M., Chazaud, B., Monti, L., de Eguileor, M., Tettamanti, G., Acquati, F., Grimaldi, A., 2020. Recombinant HvRNASET2 protein induces marked connective tissue remodelling in the invertebrate model *Hirudo verbana*. Cell Tissue Res. 380, 565–579. https://doi.org/10.1007/s00441-020-03174-0

Barzansky, B., Lenhoff, H.M., 1974. On the chemical composition and developmental role of the mesoglea of Hydra. Am. Zool. 14, 575–581.

Barzansky, B., Lenhoff, H.M., Bode, H., 1975. Hydra mesoglea: similarity of its amino acid and neutral sugar composition to that of vertebrate basal lamina. Comp. Biochem. Physiol. Part B Comp. Biochem. 50, 419–424.

Bely, A.E., Nyberg, K.G., 2010. Evolution of animal regeneration: re-emergence of a field. Trends Ecol. Evol. 25, 161–170. https://doi.org/https://doi.org/10.1016/j.tree.2009.08.005

Bosch, T.C.G., 2009. Hydra and the evolution of stem cells. BioEssays 31, 478–486. https://doi.org/https://doi.org/10.1002/bies.200800183

Bosch, T.C.G., 2008. Stem Cells in Immortal Hydra BT - Stem Cells: From Hydra to Man, in: Bosch, T.C.G. (Ed.), . Springer Netherlands, Dordrecht, pp. 37–57.

https://doi.org/10.1007/978-1-4020-8274-0_3

Bosch, T.C.G., 2007. Why polyps regenerate and we don't: towards a cellular and molecular framework for Hydra regeneration. Dev. Biol. 303, 421–433. https://doi.org/10.1016/j.ydbio.2006.12.012

Bosch, T.C.G., Rollbühler, R., Scheider, B., David, C.N., 1991. Role of the cellular environment in interstitial stem cell proliferation in Hydra. Roux's Arch. Dev. Biol. 200, 269–276. https://doi.org/10.1007/BF00241296

Bossert, P.E., Dunn, M.P., Thomsen, G.H., 2013. A staging system for the regeneration of a polyp from the aboral physa of the anthozoan Cnidarian *Nematostella vectensis*. Dev. Dyn. an Off. Publ. Am. Assoc. Anat. 242, 1320–1331. https://doi.org/10.1002/dvdy.24021

Bradford, M.M., 1976. A rapid and sensitive method for the quantitation of microgram quantities of protein utilizing the principle of protein-dye binding. Anal. Biochem. https://doi.org/10.1016/0003-2697(76)90527-3

Bradshaw, B., Thompson, K., Frank, U., 2015. Distinct mechanisms underlie oral vs aboral regeneration in the cnidarian *Hydractinia echinata*. Elife 2015, 1–19. https://doi.org/10.7554/eLife.05506

Brown, T., Rodriguez-Lanetty, M., 2015. Defending against pathogens – immunological priming and its molecular basis in a sea anemone, cnidarian. Sci. Rep. 5, 17425. https://doi.org/10.1038/srep17425

Campbell, R.D., Bode, H.R., 1983. Terminology for Morphology and Cell Types BT - Hydra: Research Methods, in: Lenhoff, H.M. (Ed.), . Springer US, Boston, MA, pp. 5–14. https://doi.org/10.1007/978-1-4757-0596-6_2

Causton, B., 1984. The choice of resins for electron immunocytochemistry, in: Polak, J., Varndell, I. (Eds.), Immunolabelling for Electron Microscopy. Elsevier Science Limited, Amsterdam New York Oxford, pp. 29–36.

Davis, L.E., 1975. Histological and ultrastructural studies of the basal disk of Hydra. III. The gastrodermis and the mesoglea. Cell Tissue Res. 162, 107–118. https://doi.org/10.1007/bf00223266

Davis, L.E., Haynes, J.F., 1968. An ultrastructural examination of the mesoglea of Hydra. Zeitschrift für Zellforsch. und Mikroskopische Anat. 92, 149–158. https://doi.org/10.1007/BF00335643

De Petrocellis, L., Orlando, P., Pierobon, P., De Falco, M., Ruggiero, A.M., Stefano, G.S., Tino, A., Grippo, P., 1999. Kelletinin A, from the marine mollusc *Buccinulum corneum*, promotes differentiation in *Hydra vulgaris*. Res. Commun. Mol. Pathol. Pharmacol. 103, 17–28.

DuBuc, T.Q., Schnitzler, C.E., Chrysostomou, E., McMahon, E.T., Febrimarsa, Gahan, J.M., Buggie, T., Gornik, S.G., Hanley, S., Barreira, S.N., Gonzalez, P., Baxevanis, A.D., Frank, U., 2020. Transcription factor AP2 controls cnidarian germ cell induction. Science 367, 757–762. https://doi.org/10.1126/science.aay6782

DuBuc, T.Q., Traylor-Knowles, N., Martindale, M.Q., 2014. Initiating a regenerative response; cellular and molecular features of wound healing in the cnidarian *Nematostella vectensis*. BMC Biol. 12. https://doi.org/10.1186/1741-7007-12-24

Ferrier-Pagès, C., Godinot, C., D'Angelo, C., Wiedenmann, J., Grover, R., 2016. Phosphorus metabolism of reef organisms with algal symbionts. Ecol. Monogr. 86, 262–277. https://doi.org/https://doi.org/10.1002/ecm.1217

Fischer, A.B., Hofmann, D.K., 2004. Budding, bud morphogenesis, and regeneration in *Carybdea marsupialis* Linnaeus, 1758 (Cnidaria: Cubozoa), in: Fautin, D.G., Westfall, J.A., Cartwrigh, P., Daly, M., Wyttenbach, C.R. (Eds.), Hydrobiologia. Springer Netherlands, Dordrecht, pp. 331–337. https://doi.org/10.1007/s10750-004-2658-4

Frank, U., Plickert, G., Müller, W.A., 2009. Cnidarian interstitial cells: The dawn of stem cell research, in: Stem Cells in Marine Organisms. Springer, pp. 33–59. https://doi.org/10.1007/978-90-481-2767-2_3

Galliot, B., 2012. Hydra, a fruitful model system for 270 years. Int. J. Dev. Biol. 56, 411–423. https://doi.org/10.1387/ijdb.120086bg

Galliot, B., Quiquand, M., Ghila, L., de Rosa, R., Miljkovic-Licina, M., Chera, S., 2009. Origins of neurogenesis, a cnidarian view. Dev. Biol. 332, 2–24. https://doi.org/https://doi.org/10.1016/j.ydbio.2009.05.563

Godwin, J., Kuraitis, D., Rosenthal, N., 2014. Extracellular matrix considerations for scar-free repair and regeneration: insights from regenerative diversity among vertebrates. Int. J. Biochem. Cell Biol. 56, 47–55. https://doi.org/10.1016/j.biocel.2014.10.011

Gold, D.A., Jacobs, D.K., 2013. Stem cell dynamics in Cnidaria: Are there unifying principles? Dev. Genes Evol. 223, 53–66. https://doi.org/10.1007/s00427-012-0429-1

Grimaldi, A., Tettamanti, G., Rinaldi, L., Perletti, G., Valvassori, R., Eguileor, M. De, 2004. Role of cathepsin B in leech wound healing. Invertebr. Surviv. J. 38–46.

Haller, M., 1989. Isolation and partial purification of hydrozoan collagen and its relevance for species-specific cell adhesion. University of Basel.

Holstein, T.W., Hobmayer, E., Technau, U., 2003. Cnidarians: An evolutionarily conserved model system for regeneration? Dev. Dyn. 226, 257–267. https://doi.org/10.1002/dvdy.10227

Jouiaei, M., Yanagihara, A.A., Madio, B., Nevalainen, T.J., Alewood, P.F., Fry, B.G., 2015.

Ancient Venom Systems: A Review on Cnidaria Toxins. Toxins (Basel). 7, 2251–2271. https://doi.org/10.3390/toxins7062251

Lee, H., Jung, E., Kang, C., Yoon, W.D., Kim, J.-S., Kim, E., 2011. Scyphozoan jellyfish venom metalloproteinases and their role in the cytotoxicity. Toxicon 58, 277–284. https://doi.org/10.1016/j.toxicon.2011.06.007

Li, R., Yu, H., Xue, W., Yue, Y., Liu, S., Xing, R., Li, P., 2014. Jellyfish venomics and venom gland transcriptomics analysis of *Stomolophus meleagris* to reveal the toxins associated with sting. J. Proteomics 106, 17–29. https://doi.org/10.1016/j.jprot.2014.04.011

Mason, B.N., Califano, J.P., Reinhart-King, C.A., 2012. Matrix Stiffness: A Regulator of Cellular Behavior and Tissue Formation BT - Engineering Biomaterials for Regenerative Medicine: Novel Technologies for Clinical Applications, in: Bhatia, S.K. (Ed.), . Springer New York, New York, NY, pp. 19–37. https://doi.org/10.1007/978-1-4614-1080-5_2

Miura, S., Kimuras, S., 1985. the evolution of mesogloea collagen in Coelenterates. J. Biol. Chem.

Muller-Parker, G., Cook, C.B., D'elia, C.F., 1990. Feeding affects phosphate fluxes in the symbiotic sea anemone Aiptasia pallida. Mar. Ecol. Prog. Ser. 283–290.

Muscatine, L., Pool, R.R., 1979. Regulation of Numbers of Intracellular Algae. Proc. R. Soc. Lond. B. 204, 131–139.

Palmer, C.V., Traylor-Knowles, N.G., 2018. Cnidaria: Anthozoans in the hot seat, Advances in Comparative Immunology. https://doi.org/10.1007/978-3-319-76768-0_3

Palmer, C.V., Traylor-Knowles, N.G., Willis, B.L., Bythell, J.C., 2011. Corals use similar immune cells and wound-healing processes as those of higher organisms. PLoS One 6. https://doi.org/10.1371/journal.pone.0023992

Parisi, M.G., Lentini, A., Cammarata, M., 2017. Seasonal changes in morpho-functional aspects of two *Anemonia sulcata* (Pennant, 1777) wild populations. Mar. Biodivers. 47, 561–573. https://doi.org/10.1007/s12526-017-0695-2

Parisi, M.G., Parrinello, D., Stabili, L., Cammarata, M., 2020. Cnidarian immunity and the repertoire of defense mechanisms in anthozoans. Biology (Basel). 9, 1–26. https://doi.org/10.3390/biology9090283

Rader, B.A., 2017. Alkaline Phosphatase, an Unconventional Immune Protein. Front. Immunol. 8, 897. https://doi.org/10.3389/fimmu.2017.00897

Ricci, L., Srivastava, M., 2018. Wound-induced cell proliferation during animal regeneration. Wiley Interdiscip. Rev. Dev. Biol. 7, 1–17.

https://doi.org/10.1002/wdev.321

Ross, N.W., Firth, K.J., Wang, A., Burka, J.F., Johnson, S.C., 2000. Changes in hydrolytic enzyme activities of naive Atlantic salmon *Salmo salar* skin mucus due to infection with the salmon louse *Lepeophtheirus salmonis* and cortisol implantation. Dis. Aquat. Organ. 41, 43–51. https://doi.org/10.3354/dao041043

Sarras, M.P., 2012. Components, structure, biogenesis and function of the Hydra extracellular matrix in regeneration, pattern formation and cell differentiation. Int. J. Dev. Biol. 56, 567–576. https://doi.org/10.1387/ijdb.113445ms

Schaffer, A.A., Bazarsky, M., Levy, K., Chalifa-Caspi, V., Gat, U., 2016. A transcriptional time-course analysis of oral vs. aboral whole-body regeneration in the Sea anemone *Nematostella vectensis*. BMC Genomics 17, 1–22. https://doi.org/10.1186/s12864-016-3027-1

Schmid, V., Bally, A., 1988. Species specificity in cell-substrate interactions in medusae. Dev. Biol. 129, 573–581.

Sinigaglia, C., Peron, S., Eichelbrenner, J., Chevalier, S., Steger, J., Barreau, C., Houliston, E., Leclère, L., 2020. Pattern regulation in a regenerating jellyfish. Elife 9, e54868. https://doi.org/10.7554/eLife.54868

Stabili, L., Parisi, M.G., Parrinello, D., Cammarata, M., 2018. Cnidarian interaction with microbial communities: From aid to animal's health to rejection responses. Mar. Drugs 16, 1–15. https://doi.org/10.3390/md16090296

Technau, U., Steele, R.E., 2011. Evolutionary crossroads in developmental biology: Cnidaria. Development 138, 1447–1458. https://doi.org/10.1242/dev.048959

Tettamanti, G., Grimaldi, A., Congiu, T., Perletti, G., Raspanti, M., Valvassori, R., Eguileor, M., 2005. Collagen reorganization in leech wound healing. Biol. Cell 97, 557–568. https://doi.org/10.1042/bc20040085

Tomlin, H., Piccinini, A.M., 2018. A complex interplay between the extracellular matrix and the innate immune response to microbial pathogens. Immunology 155, 186–201. https://doi.org/10.1111/imm.12972

Trapani, M.R.R., Parisi, M.G.G., Parrinello, D., Sanfratello, M.A.A., Benenati, G., Palla, F., Cammarata, M., 2016. Specific inflammatory response of *Anemonia sulcata* (Cnidaria) after bacterial injection causes tissue reaction and enzymatic activity alteration. J. Invertebr. Pathol. 135, 15–21. https://doi.org/10.1016/j.jip.2016.01.010

Van De Water, J.A.J.M., Ainsworth, T.D., Leggat, W., Bourne, D.G., Willis, B.L., Van Oppen, M.J.H., 2015. The coral immune response facilitates protection against microbes during tissue regeneration. Mol. Ecol. 24, 3390–3404. https://doi.org/10.1111/mec.13257

Watanabe, H., Hoang, V.T., Mättner, R., Holstein, T.W., 2009. Immortality and the base of multicellular life: Lessons from cnidarian stem cells. Semin. Cell Dev. Biol. 20, 1114–1125. https://doi.org/10.1016/j.semcdb.2009.09.008

Yan, L., Leontovich, A., Fei, K., Sarras, M.P., 2000. Hydra metalloproteinase 1: A secreted astacin metalloproteinase whose apical axis expression is differentially regulated during head regeneration. Dev. Biol. 219, 115–128. https://doi.org/10.1006/dbio.1999.9568

Yan, L., Pollock, G.H., Nagase, H., Sarras, M.P.J., 1995. A 25.7 x 10^3 M_r hydra metalloproteinase (HMP1), a member of the astacin family, localizes to the extracellular matrix of *Hydra vulgaris* in a head-specific manner and has a developmental function. Development 121, 1591–1602.

Also in the following chapter the focus remains on characterizing the regenerative event under constitutive conditions. The aim is to emphasize what happens in the epithelial layers and more specifically, which cells are involved in regeneration and what their role is.

Chapter 4

Step-by-Step Regeneration of Tentacles after Injury in *Anemonia viridis*—Morphological and Structural Cell Analyses

International Journal of
Molecular Sciences

MDPI

Article

Step-by-Step Regeneration of Tentacles after Injury in *Anemonia viridis*—Morphological and Structural Cell Analyses

Claudia La Corte [1,†], Nicolò Baranzini [2,†], Mariano Dara [1], Camilla Bon [2], Annalisa Grimaldi [2,*], Maria Giovanna Parisi [1,*], Maria Grazia Zizzo [3,4] and Matteo Cammarata [1]

ABSTRACT

Benthic marine invertebrates, such as corals, are often subjected to injury caused by several sources. Here, the differences and characteristics in injured and health tissues in terms of cellular components are shown through a histological investigation of the soft coral *Anemonia viridis* at 0 h, 6 h, 24 h, and 7 days after injury caused by tentacle amputation. In addition, a new tool was used for the first time in invertebrates, positron emission tomography, in order to investigate the events that occur during regeneration within a longer time period (0 h, 24 h, and 14 days after the tentacles were cut). Higher integrated density values were measured through a densitometric analysis in sections stained with Fontana–Masson at 24 h after the tentacles were cut. This suggests an increase in melanin-like containing cells and a subsequent increase in fibroblast-like cells differentiated by amoebocytes that converge to the lesion site in the early stages of inflammation and regeneration. This work provides, for the first time, an elucidation of the events that occur during wound-healing and regeneration in basal metazoan, focusing on the characterisation of immune cells and their role. Our results indicate that Mediterranean anthozoan proves to be a valuable model for studying regeneration. Many events highlighted in this research occur in different phyla, suggesting that they are highly conserved.

Keywords: anthozoan regeneration; *Anemonia viridis*; PET; Histology; Immune cells; TEM analysis

INTRODUCTION

Several studies have evidenced the global decline in coral populations caused by a variety of disturbances (Bisanti et al., 2022) and events that cause wounding such as predation and natant anchorages (Boström-Einarsson et al., 2020; Raymundo et al., 2018). To date, only a few histological studies have been conducted on the mechanisms involved in the events that occur during wound-healing and regeneration in anthozoans (Meszaros and Bigger, 1999; Parisi et al., 2021; Young, 1974). This argument is better addressed in scleractinian corals, in particular for the global observation of regeneration (Van De Water et al., 2015; Work and Aeby, 2010) under different stress conditions. Although the histological aspects of wound healing have not been thoroughly investigated, they represent the first step in understanding cnidarian immune responses, resulting in better insight into the health status of these organisms. Injury could trigger diseases, facilitating microbe infection (Raymundo et al., 2018). Cnidarians have evolved and developed a suite of strategies to face these challenges, such as clotting, cell proliferation, the activation of inflammation pathways, and the production of metabolites such as melanin. Studies have also shown the clear importance of wound healing as a vital process, in which immune cells are recruited to the lesion site, not only facilitating the healing and blocking of eventual infections but also supporting tissue regeneration (La Corte et al., 2022; Parisi et al., 2021). Several research have demonstrated the conservation of the main step-points of wound-healing process along phyla (Bely and Nyberg, 2010; Dinsmore, 2007; Sánchez Alvarado and Tsonis, 2006), with four characteristic phases (Arenas Gómez et al., 2020): (i) During the coagulation process, semisolid haemolymphs form a plug and seal the injury. This phase leads to the formation of a hard clot, which in mammals, is normally constituted by aggregated platelets and stabilised by fibrin molecules while, in invertebrates, occurs via immune cell degranulation, followed by the incorporation of cellular debris, bacteria, and extracellular matrix components into extracellular aggregates (Loof et al., 2011; Robson et al., 2001). (ii) Immune cells are recruited to the site of the injury in order to engulf aggregates containing microbes and cellular debris (Loof et al., 2011). (iii) Proliferation of new immune cells, of fibroblasts-like cells and re-epithelisation. During this phase, different cell types migrate to the edge of the wound, immersed in the extracellular matrix, and join together (Krzyszczyk et al., 2018). In particular, the massive proliferation of fibroblast-like cells, characterised by extensive pseudopods essential for wound contraction and by the synthesis and deposition of new collagen, favours subsequent tissue reorganisation. (iv) During the maturation and tissue remodelling phase, the density of fibroblast-like cells decreases through apoptosis and

collagen-rich scar tissue is formed, resulting in an increase in tissue stiffness and strength (Krzyszczyk et al., 2018; Zhao et al., 2016). Although many of these processes have been well-described in vertebrates and in some invertebrates, such as annelids and molluscs (Baranzini et al., 2020; La Corte et al., 2022; Meszaros and Bigger, 1999; Parisi et al., 2022; Tettamanti et al., 2004; Traylor-Knowles, 2019), this information is still rather incomplete for many other invertebrate species, especially for anthozoan cnidarians. In order to fill this gap, in this work, we used the experimental model *Anemonia viridis* to shed light on the cellular mechanisms underlying immune response and wound healing. *A. viridis* is a Mediterranean hexacoral anthozoan that can be found in low rocky depths. Like many anthozoans, it is involved in trophic mutualistic endosymbiosis, hosting unicellular zooxanthellae algae belonging to the genus *Symbiodinium*. These organisms consist of two body layers derived from the endoderm (gastrodermis) and ectoderm (epidermis) of the embryo. Between these layers, a gelatinous and amorphous connective layer is present, called the mesoglea, which does not contain cells apart from a few amoebocytes (Parisi et al., 2021) (Figure 1).

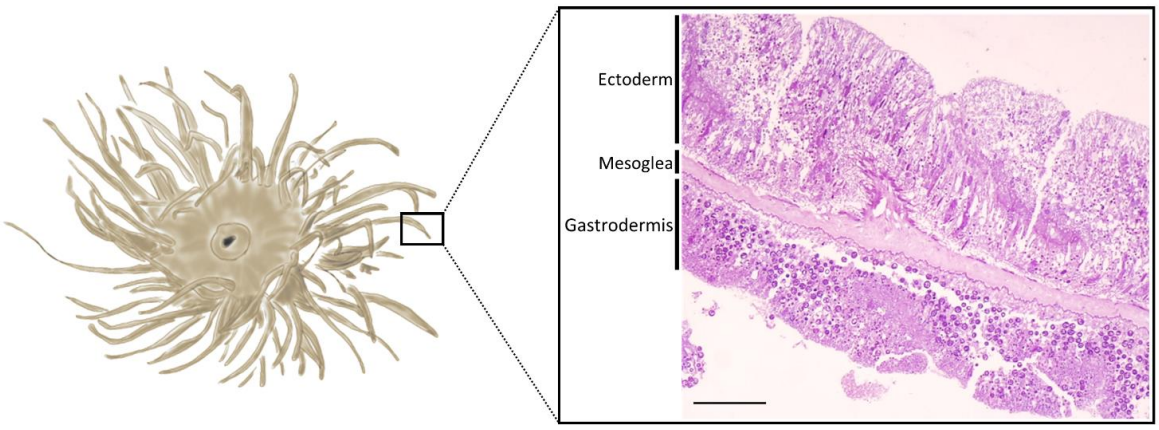

Figure 1 Illustration of the epithelial layers of Anemonia viridis tentacles. The outermost layer is the ectoderm and the innermost layer is the gastrodermis, both rich in cells. The latter also hosts zooxanthellae. The mesoglea is the central amorphous gelatinous layer and only has a few cells, predominantly amoebocytes. Scale bar: 100 µm.

Through histological and ultrastructural approaches, we morphologically and functionally characterised the different cell types involved both in the first phase of wound closure and in the regeneration and regrowth of the tentacle following its amputation. Furthermore, using positron emission tomography (PET), for the first time, in invertebrates, we demonstrated how the migration and flow of endosymbionts occur during these processes.

MATERIALS AND METHODS

Sample collection

A. viridis specimens were collected in autumn 2021 on the coastal area of Palermo (Italy). The animals were housed in facilities at the Marine Immunobiology laboratory (University of Palermo, Italy) and maintained in filtered and oxygenated seawater at 18 ± 1 °C for at least one week before initiating the experimental design. The experimental groups (N = 30 in duplicate) consisted of three control organisms (healthy organisms) and twelve injured organisms (removal of 25% of the total tentacles), which were observed for histological analyses at different times: 1 h, 6 h, 24 h, and 7 days after amputation. As regards PET technique (N = 12), were collected other three organisms for each time point and for the controls. The time points at which examination occurred were 1 h, 24 h, and 14 days, in order to observe the event over a longer time period.

Positron Emission Tomography (PET)

Epifluorescence in the *A. viridis* total bodies was monitored at different time points (t = 0, 1 h, 24 h, and 14 days) with PET, a nuclear diagnostic imaging technique, in order to clarify the processes following cutting of the tentacles. PET was performed using an IVIS Spectrum system (Perkin-Elmer, Hopkinton, MA, USA) at the animal facility of the ATeN Center, University of Palermo. The epifluorescence of *A. viridis* was imaged using the absorption and emission spectra of the endosymbiont *Symbiodinium* sp. (chlorophyll a, excitation filter at 495 nm, and emission filter at 595 nm). The fluorescent intensity was normalised to a background signal to follow only the zooxanthellae signal.

Light and Transmission Electron Microscopy (TEM)

Embedding Tissue in Paraffin and Staining

The healthy tentacles and the budding area of the regrowing tissues from three *A. viridis* subjected to amputation of 25% of the total number of tentacles at four time points (0 h, 6 h, 24 h, and 7 days after amputation) were fixed in 4% paraformaldehyde in PBS for 2 h, washed several times in PBS solution, dehydrated in increasing concentrations of ethanol (30%, 50%, 70%, 90%, 96%, and absolute), and paraffin-embedded. Sections (7 mm thick) were obtained with a rotary microtome (Jung multicut 2045, Leica, Wetzlar, Germany) and processed for conventional histological staining with haematoxylin and eosin (HE) and for two specific stains, as suggested by the datasheets: Masson–Fontana staining to visualise the melanotic pigment (Masson Fontana kit, Bio Optica, Milan, Italy) and mucicarmine staining

to highlight acidic mucopolysaccharides (mucins) of epithelial nature (Mucicarmine kit, Bio Optica). Images were recorded with a Nikon Digital Sight DS-SM Light Microscope (Nikon, Tokyo, Japan).

Embedding Tissue in Epoxy Resin for TEM

A. viridis tissues, dissected from healthy tentacles and from regenerating areas, were fixed for 2 h in 4% glutaraldehyde in a cacodylate buffer (pH 7.4). After several washes in the same buffer, the samples were post-fixed for 1 h with 1% osmium tetroxide in a 0.1M cacodylate buffer (pH 7.4). After serial ethanol dehydration (70%, 90%, and 100%), the specimens were embedded in an Epon-Araldite 812 mixture. For the ultrastructural TEM analyses, ultrathin sections (80 nm in thickness), obtained with a Reichert Ultracut S ultratome (Leica), were placed on copper grids (300 mesh, Sigma-Aldrich, Milan, Italy), counterstained with uranyl acetate and lead citrate, and observed with a Jeol 1010 EX transmission electron microscope (Jeol, Tokyo, Japan). Images were recorded with a MORADA digital camera system (Olympus, Tokyo, Japan).

Biometric measures

The colour intensity of the Fontana–Masson-stained sections was measured as integrated density values (the product of the area and mean grey values of pixels within the selection) using an ImageJ software package on 6 fields (45,000 μm^2) for each slide (Schneider et al., 2012). Similarly, on six TEM microphotographs of agranular amoebocytes, granulocytes, mucocytes, gland cells, and zooxanthellae, the length, width, and area of the cell were calculated (see the Supplementary Materials for an example).

Statistical Analyses

The data were tested for ANOVA assumptions, and differences between the groups were shown using a one-way ANOVA as mean ± standard deviation (SD). Differences between the means were considered significant for $p < 0.05$. Tukey's multiple comparison post hoc test was applied in order to establish significant differences between the control and injured tissue at the different time points using GraphPad Prism 8.0.2 (GraphPad Software, La Jolla, CA, USA).

RESULTS

Positron Emission Tomography (PET) analysis

The control organism showed a generally high epi-fluorescence that extended from the body to the tentacles (Figure 2A). On the contrary, 1 h after amputation, the signal disappeared in the area that was cut (Figure 2B). Observations 24 h after the tentacles were cut showed fluorescence re-establishment in the whole animal, likely an index of recovery by the endosymbiont in the injured area (Figure 2C). Total recovery of the signal was observed at 14 days, reaching the same fluorescence levels as the control organism, evidence of the restoration of natural conditions (Figure 2D).

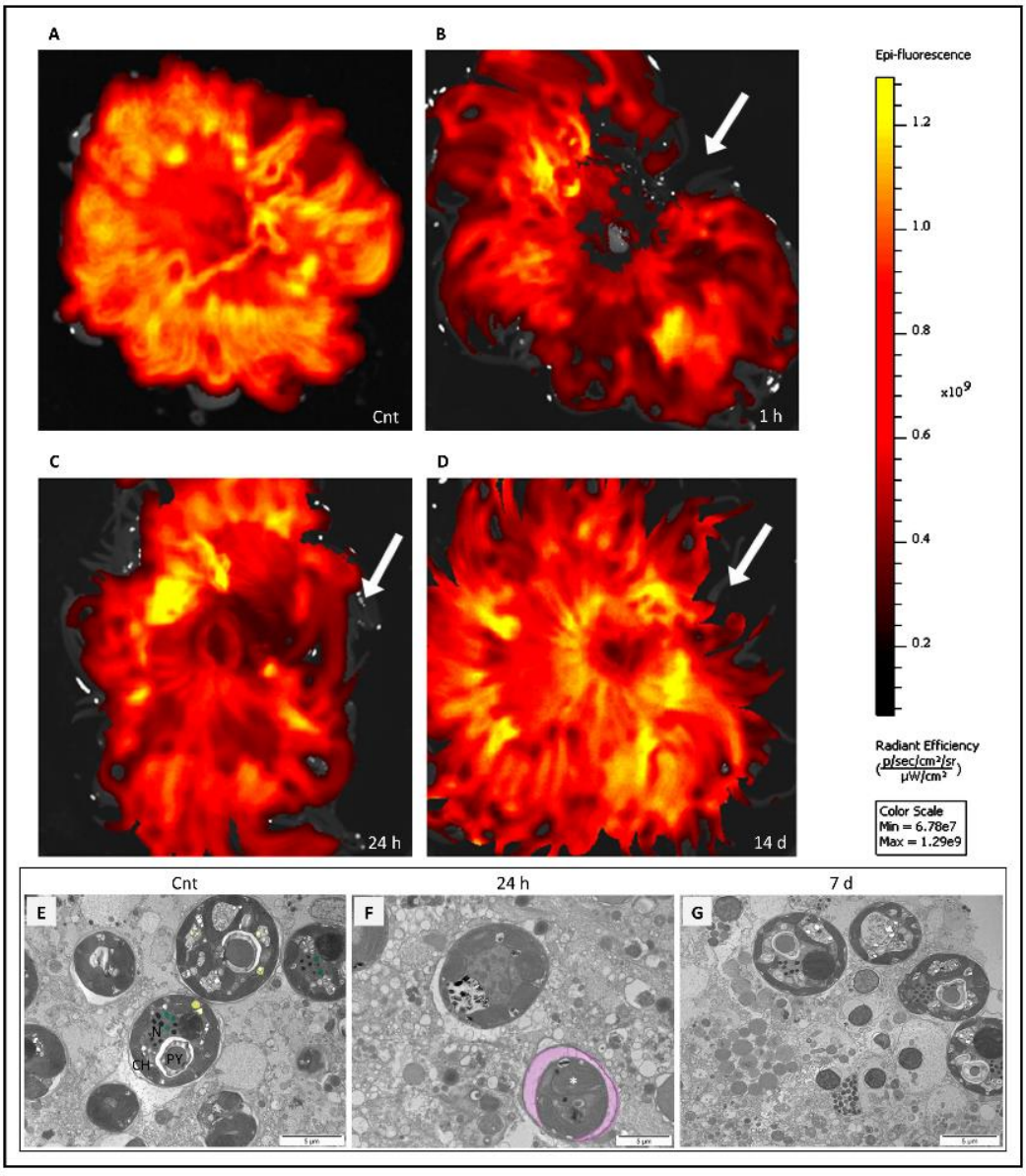

Figure 2 Representative images of in vivo positron emission tomography (PET) of Anemonia viridis samples and TEM observation of Symbiodinium sp. during wound healing and regeneration. ***(A)*** *Cnt = control organism, not injured, high*

epi-fluorescence in the whole body; ***(B)*** *1 h = animal observed one hour after the tentacles were cut, no signal in the wound area (arrow);* ***(C)*** *24 h = A. viridis observed 24 h after the tentacles were cut, re-establishment of the signal (arrow);* ***(D)*** *14 d = organism observed 14 days after tentacle amputation, tentacular regeneration occurred. The signal intensity is comparable with that of the control (arrow).* ***(E)*** *Symbionts in healthy tissues (control organisms), well-defined cell compartments. N = Symbiodinium nucleus; CH = chloroplasts; PY = pyrenoid; in yellow = starch granule; in green = accumulation body.* ***(F)*** *Symbionts at 24 h after injury have a lower electron density compared with the control; organelles are not clearly identifiable. In pink = enlargement of membrane, white asterisk = chloroplast swelling.* ***(G)*** *At 7 days after the tentacles were cut, Symbiodinium sp. appeared to recover their functionalities. Scale bar: 5 µm.Cell measurements.*

Cell Measurements

The agranular amoebocytes from the biometric analysis had a mean area of 19.58 ± 14.42 µm^2. Their mean length was 8.89 ± 3.60 µm. Their nuclei occupied 40.86 ± 16.01% of the cellular space. The zooxanthellae symbionts had a diameter of 8.27 ± 0.26 µm and a mean area of 53.06 ± 1.74 µm^2. The granulocytes had a highly variability in size, a mean length of 10.99 ± 3.53 µm, and a calculated mean area of 42.27 ± 23.49 µm^2. Finally, the mucocytes had an average length equal to 38.67 ± 4.76 µm and a mean area of 282.83 ± 73.44 µm^2.

Morphological Analyses and Characterisation of Cells Involved in Tentacle Regrowth in Injured A. viridis

In order to shed light on the cell types involved in wound healing and tentacle tissue regeneration from injured *A. viridis*, morphological analyses were performed, both via light microscopy and TEM on the just amputated area (T0) and on the regenerating tentacle 6 h, 24 h, and 7 days after cutting. The results were compared with tissue from a healthy tentacle.

Healthy tentacles

In the healthy animal control, the tentacle was about 2.5 up to 3 mm long and its epidermis consisted of a single layer of columnar cells arranged obliquely to the main axis of the tentacle and with the basal part lying on the mesoglea layer (Figure 3A). In the part facing outwards, these cells were ciliated and were joined via obvious junctions (Figure 3B). Proceeding towards the innermost region, the epithelial cells appeared densely compacted and contained numerous symbiotic zoochlorellae algae (Figure 3A,C). The epidermis was also populated in the innermost portion by spirocysts; mucus-cell-containing electron-lucent granules; and gland cells with electron-dense spherical or ovoid granules, with diameters varying from 1 to 2.5 µm (Figure 3C,D). The electron density of the granules was generally homogeneous; however, some granules possessed a small, more electron-dense central core (Figure 3D). Interestingly, these glands containing heterogeneous electron-dense granules observed in *A. viridis* appeared similar to serous gland cells secreting lysozymes described for mammals and was considered a defence system against infections (Bowes and Corrin,

1977). The mesoglea was visible between the epidermis and gastrodermis. It consisted of an amorphous fibrous matrix (Figure 3A) in which a few roundish amoebocytes with large nuclei were detectable (Figure 3E). The monolayered gastrodermis, containing zymogen-type gland cells (Fautin and Mariscal, 1991), was formed by columnar cells, including numerous symbiotic zoochlorellae and larger endosymbiotic dinoflagellate zooxanthellae specific to this epithelial layer (Figure 3A,F).

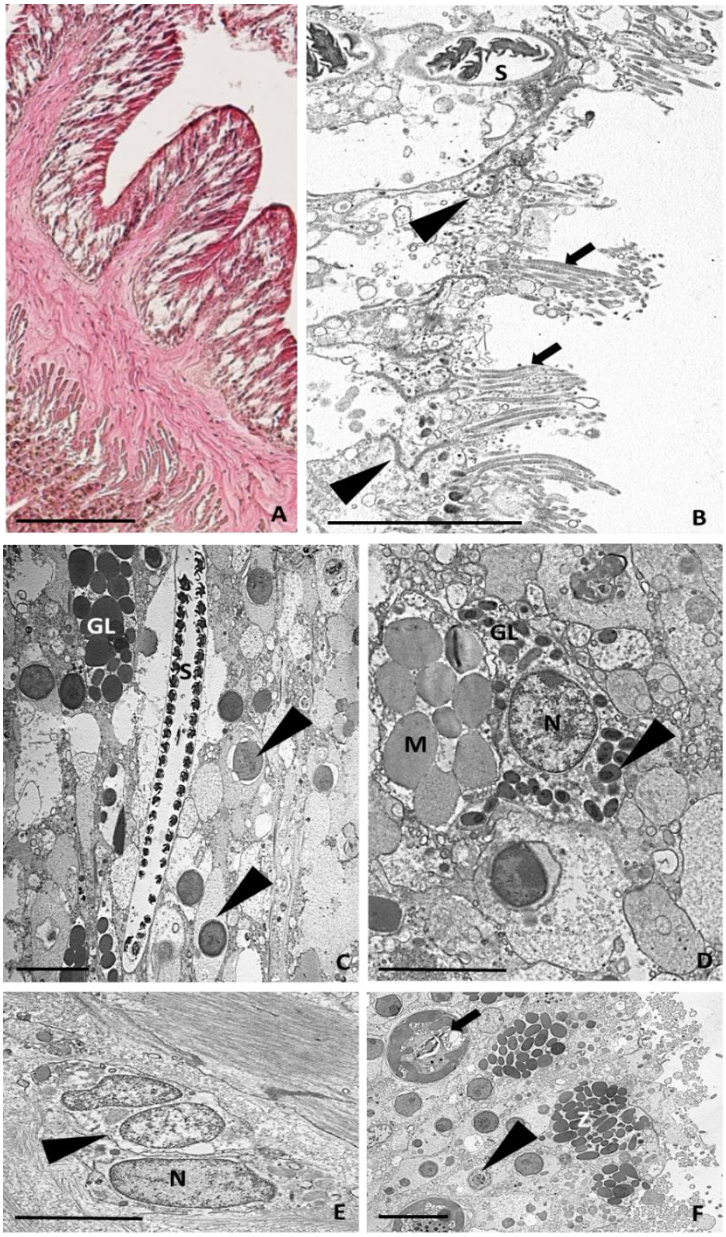

Figure 3 Morphological analyses from light microscope and TEM. ***(A)*** *Image of control tentacle, 2.5 mm long, from light microscope.* ***(B)*** *TEM image of apical side of epidermis. Ciliated cells (arrows) joined by junctions (arrowheads) and spirocysts (S) are visible.* ***(C)*** *TEM image of innermost part showing columnar cells containing symbiotic zoochlorella algae (arrowheads), spirocysts (S), and gland cells (GL) with electron-dense spherical or ovoid granules.* ***(D)*** *Detailed TEM image of mucous cell containing electron-lucent granules (M) and gland cells with large nuclei and containing granules with an electron-dense small central core (arrowheads).* ***(E)*** *Detailed TEM image of amoebocytes (arrowheads) with large nuclei (N) localised in the mesoglea.* ***(F)*** *Detailed TEM image of the gastro- dermal layer. Zymogenic gland cells (Z), zoochlorellae (arrowheads), and zooxanthellae (arrows) are visible. Bar in* ***(A)****, 100 µm; bars in* ***(B–D,F)****, 5 µm; bar in* ***(E)****, 2 µm.*

Tentacle Amputation at Time Zero

Immediately post-injury, the epidermis and the gastrodermis of the severed tentacles were destroyed, the cell outlines were no longer distinguishable, and the symbiotic algae were extruded from the epithelial cells (Figure 4A–C). Gland cells, with empty granules, were observed in the cut region (Figure 4B). Waste material, including spirocysts, gland cells, and symbiotic algae, was abundant in the area adjacent to the cut (Figure 4D).

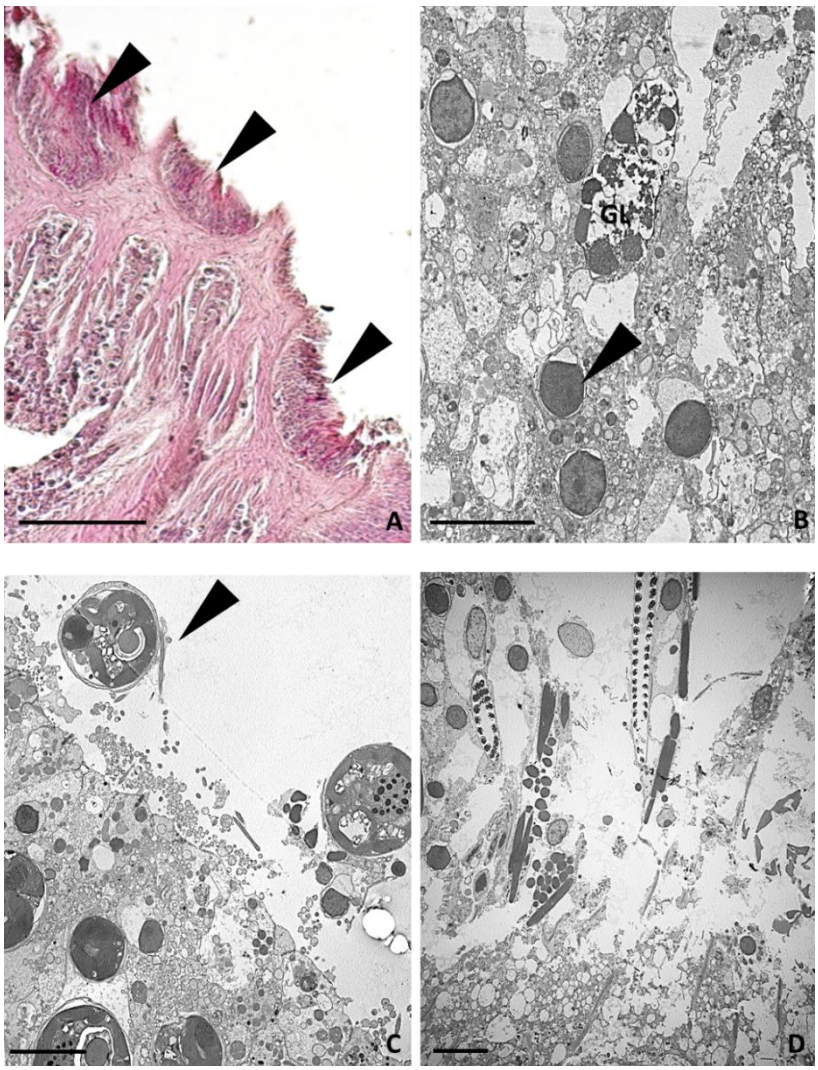

Figure 4 Morphological analysis of the area just amputated (T0) from light and TEM microscopes. ***(A)*** *Overview from light microscope showing the area where the tentacles were cut away. The arrow- heads indicate what remains of the tentacle after its amputation from the animal body.* ***(B,C)*** *TEM images showing the destroyed epidermal* ***(B)*** *and gastrodermal* ***(C)*** *cell layers from which symbiotic algae (arrowheads) were expelled. A gland cell with empty granules is visible (GL).* ***(D)*** *Detailed TEM image of expelled waste material. Bar in* ***(A)****, 100 µm; bars in* ***(B–D)****, 5 µm.*

Six Hours after Tentacles Amputation

Six hours after the injury, the regenerating tentacle buds measured approximately 1.8 mm in length (Figure 5A). The thick layer of a mucous substance deposited on the cut surface (Figure 5B) suggested its important role in forming the first barrier against infection. Indeed, the mucus layer provided a physical shield preventing bacteria and debris from accumulating

on the regrowing tentacle surface. Large degranulating mucus-secreting and gland cells were visible just below the injured area (Figure 5C). The innermost part of the new bud was populated by both granular and agranular amoebocytes, with the latter containing small, electron-dense granules (Figure 5D). Granular (Figure 5E) and agranular (Figure 5F) amoebocytes were visible in the mesoglea and infiltrated the regrowing bud (Parisi et al., 2021), migrating towards the injured area (Figure 5G).

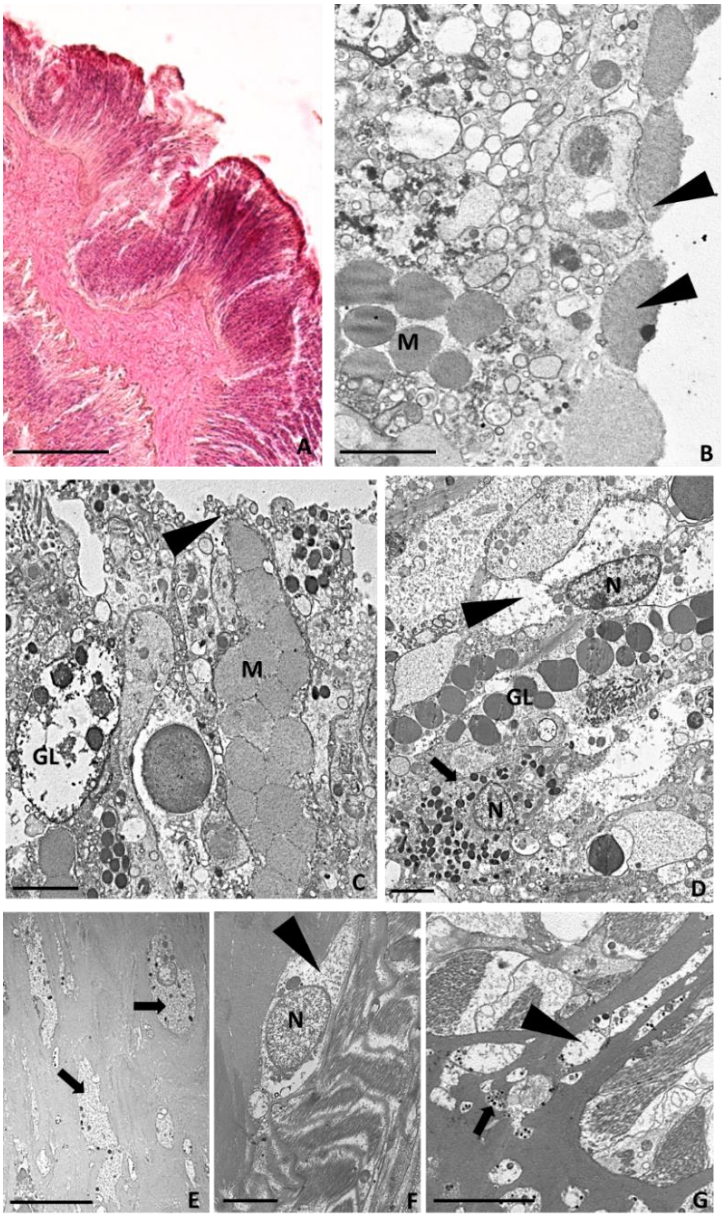

Figure 5 Morphological analysis of the tentacle bud regrown 6 h after cutting from light and TEM microscopes. ***(A)*** *Light microscope overview showing the regrown tentacle bud.* ***(B–G)*** *Ultrastructural TEM analysis showing mucous cells (M) and gland cells (GL), some of which, with empty granules, are visible just below the cut area. A thick mucus layer (arrowheads in* ***(B)****) as product of mucous cells (arrowheads in* ***(C)****) is visible at the edge of the lesion. Agranular (arrowhead in* ***(D)****) and granular amoebocytes (arrows in* ***(D)****) are visible in the regenerating epidermal layer.* ***(E–G)*** *Detailed TEM images of granular (arrows in* ***(E,G)****) and agranular amoebocytes (arrowheads in* ***(F,G)****) present in the mesoglea and migrating towards the wound-healing region. Bar in* ***(A)****, 100 µm; bars in* ***(B–D,F)****, 2 µm; bar in* ***(E,G)****, 5 µm.*

Twenty-Four Hours after Tentacle Amputation

The regrown tentacles measured about 2 mm in length (Figure 6A). Granular amoebocytes migrating from the mesoglea had reached the injured area and formed a thin layer along the lesion edge (Figure 6B), establishing an epithelial front and contributing to the formation of a plug. This clot formation was similar to what was previously observed for other anthozoans (Palmer et al., 2010), where melanin-containing granular cells were reported. Inside this newly formed epithelial-like layer was numerous mucous and secreting gland cells with empty granules (Figure 6B). The presence of both mucous and empty-appearing gland cells confirmed their possible role in secreting many active products, including mucins and lysozymes, as a mechanism of defence against the entrance of foreign organisms. Dense aggregations of agranular amoebocytes were also present throughout the wound-healing site (Figure 6C).

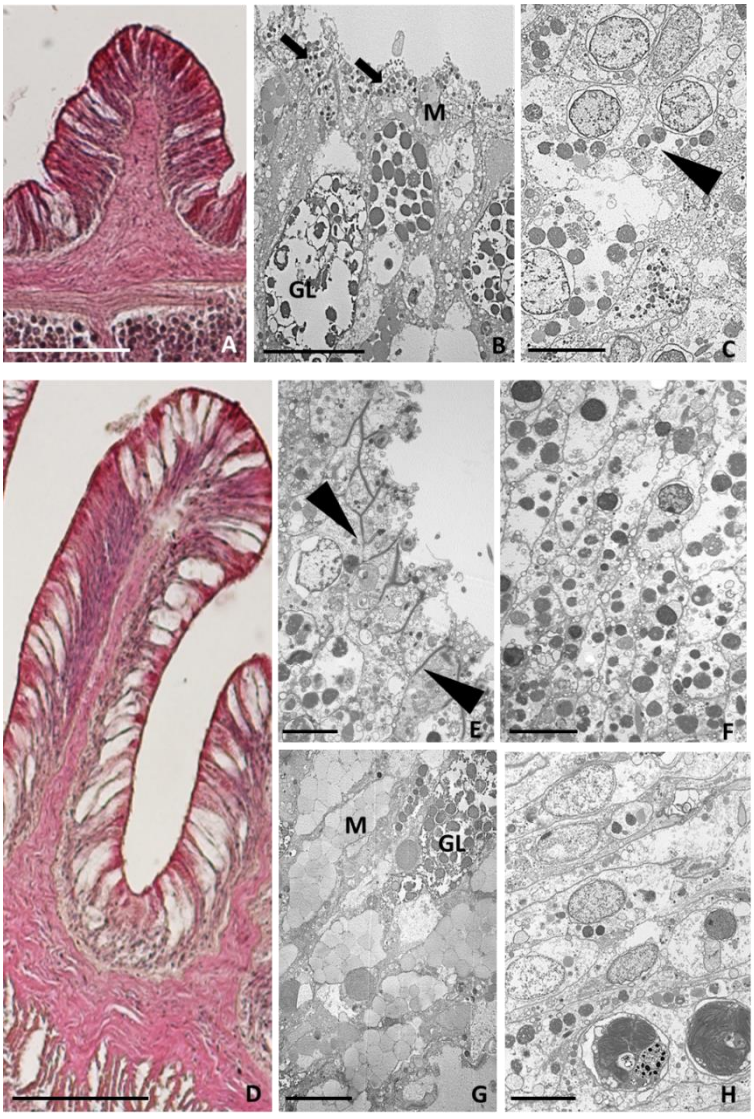

*Figure 6 Morphological analysis of the regrown tentacle 24 h **(A–C)** and 7 days after amputation **(D–H)** via light and TEM microscopes. **(A)** Light microscope overview of 2 mm long regrown tentacle 24 h post-injury. **(B,C)** Detailed TEM images showing a layer of granular amoebocytes (arrows in **(B)**) along the newly forming epithelial layer and agranular*

*amoebocytes (arrowheads in **(C)**) containing symbiotic algae. **(D)** Light microscope overview of 3 mm long regrown tentacle 7 days post-injury. **(E–H)** TEM images showing intercellular junctions (arrowheads in **(E)**), differentiated epithelial cells in epidermis **(F)** and in gastrodermis **(H)**, and gland (GL) and mucous (M) cells **(G)**. Bar in **(A,D)**, 100 µm; bars in **(B,C,E–H)**, 5 µm.*

Seven Days after Tentacle Amputation

Seven days after the cut, the regenerated tentacles were about 2.5–3 mm long, and their shape and morphology were very similar to the control tentacles (Figure 6D). At the superficial level, cellular cilia and intercellular joint points were visible (Figure 6E). The outer layer of granular amoebocytes was no longer present, and the newly formed epidermis mainly consisted of differentiating epithelial cells containing the symbiotic zoochlorella (Figure 6F), and numerous gland and mucous cells (Figure 6G). Well-differentiated columnar cells containing the symbiotic algae formed the gastrodermal layer (Figure 6H).

Colorimetric Analyses of cells involved in wound-healing

Mucicarmine staining (Figure 7A–E), specific for highlighting the presence of epithelial acidic mucopolysaccharides (mucins), and Fontana–Masson staining (Figure 7F–J), specific for highlighting melanin, were carried out on histological sections of both the control and regrown tentacles after different time periods, since their amputation for the regrowth case. The obtained results clearly showed the different roles of the cells involved in wound closure. Indeed, while in the CNT tentacle, positivity for mucicarmine (Figure 7A) and Fontana–Masson (Figure 7B) was very low or absent, after cutting, increasing positivity was observed for both stains, but in reverse order. Immediately after tentacle amputation (T0), a strong, intensely fuchsia-coloured signal was localised in the mucous cells at the edge of the lesion (Figure 7B). After 6 h, the signal was also visible on the external surface, as a result of mucins secretion by the mucous cells (Figure 7C). The mucus secretion decreased after 24 h (Figure 7D) and disappeared completely after 7 days, where the positivity remained confined to only within the mucous cells (Figure 7E). Conversely, melanin positivity was low at times T0 (Figure 7G) and 6 h (Figure 7H). It was mainly confined to the few granular amoebocytes previously described (Figure 6D–G), localised in the basal region of the epidermis bordering the mesoglea and migrating towards the injured area. Twenty-four hours after amputation (Figure 7H), the signal for Fontana–Masson was very dark and localised in the superficial area corresponding to the layer of granular amoebocytes involved in the formation of the plug. At 7 days post-injury, the melanin signal was absent (Figure 7J), in agreement with the absence of granular amoebocytes on the newly formed epithelial layer, similarly to that in the CNT.

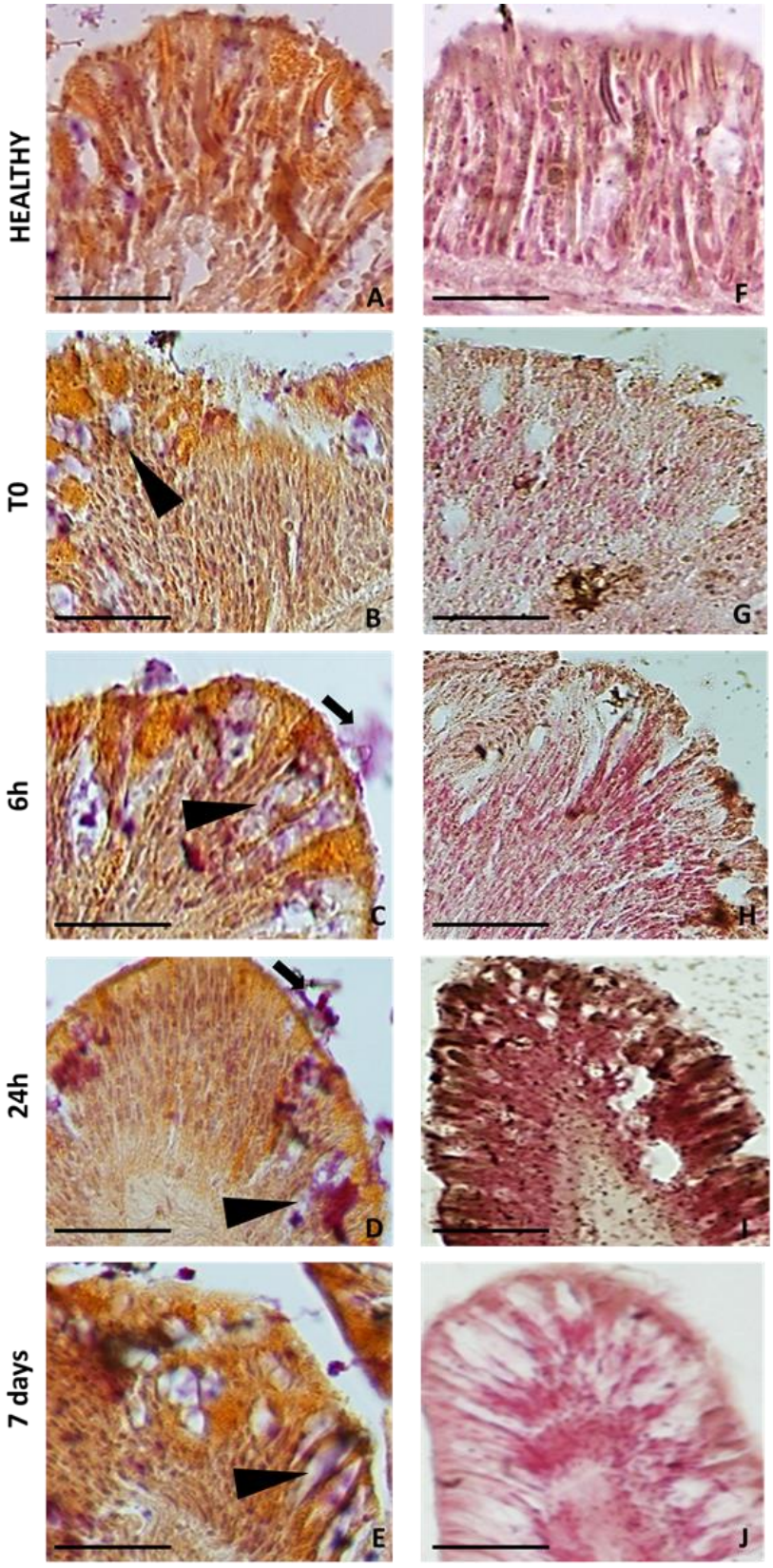

*Figure 7 Tissue sections stained with mucicarmine **(A–E)** and Fontana–Masson stain **(F–J)**. Mucus is stained in fuchsia and is localised in mucous cells (arrowheads) and on the surface (arrow) at the edge of the lesion. Melanin-containing granular cells are stained in black. Bar in **(A–J)**, 25 µm.*

The densitometric analysis (Figure 8) calculated on tentacle sections at various times from amputation and stained with Fontana–Masson was represented in a graph and confirmed the histological data.

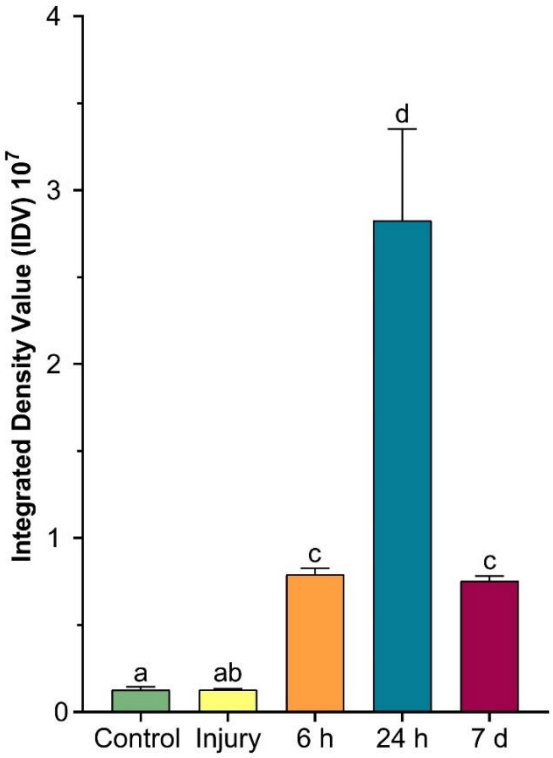

Figure 8 The graph shows the densitometric analysis calculated on A. viridis sections stained with Fontana–Masson. Here, the integrated value of density (IDV) represents the quantification of colour intensity at the different time points. Data were tested for ANOVA assumptions, and differences between groups are shown using a one-way ANOVA as mean ± standard deviation (SD). Differences between means were considered significant for $p < 0.05$. Letters (a–d) indicate differences between treatments.

DISCUSSION

Cnidarians are exposed to physical damage from a variety of sources that injure tissues and result in open wounds. The aim of this research was to explore and characterise, for the first time, the cells present during the wound-healing process and their functions in the soft coral *A. viridis*. As demonstrated in our previous work focused on this anthozoan, lesions are completely healed within 24 h (Parisi et al., 2021), as already observed in other corals such as *Porites cylindrica* (Palmer et al., 2011), and the wound-healing process follows all of the four previously characterised phases. In particular, granulocytes, immune cells already well-described in the literature (Calisi et al., 2008; Mydlarz et al., 2008; Parisi et al., 2014), degranulate and release antimicrobial and cytotoxic molecules, including peroxidase, lysozyme, phenoloxidase, and melanin. These cells have been observed in other cnidarians and are involved in pathogen removal at the lesioned site before plug formation occurs (Coaglio et al., 2018; Di Falco et al., 2017; Krzyszczyk et al., 2018). As shown in Figures 3 and 5, disrupted cells, degranulated granulocytes, and possible pathogens are immediately expelled when an injury arises. Likewise, the endosymbiont algae appear to not be functional at the time when a cut occurs, suggesting that it incurs the same fate. A similar behaviour during regeneration was also observed in *Calliactis parasitica*, where the different roles of the cells and the interactions of the ectodermal and mesoglea layers have been investigated (Young, 1974). In contrast, six hours post-injury (Figure 3), in *A. viridis*, eosinophilic (acidophilic) amoebocytes densely gather, as evidenced by the intense pink colour derived from H&E staining. The high density of these cells in the injured area is explained by their role as effectors of an immune response to infection, contrariwise to the state of healthy tissue, in which they are quite completely absent (de Lima et al., 2023; Vargas-Ángel et al., 2007). A similar result was detected in the study by Mydlarz *et alii* (2008) conducted on *Gorgonia ventalina*, in which animals were exposed to the fungal pathogen *Aspergillus sydowii* (Mydlarz et al., 2008). Indeed, a massive and dense increase in amoebocytes was evident in the infected coral tissues. Moreover, in the Caribbean soft coral *Plexaurella fusifera*, after three weeks of healing, the authors not only observed the four major stages of wound healing but also underlined the key role of these cells in the re-epithelisation of the injured area (Meszaros and Bigger, 1999). In particular, acidophilic granular amoebocytes promptly constituted an epithelial-like layer by aggregating and spreading along the injury's edge. Interestingly, similar findings were also found in other invertebrates (Ferrario et al., 2018; Young, 1974). Moreover, the evidence obtained in this work suggests that the granules of these cells might contain melanin, which could be necessary to strengthen the epidermal

layer during re-epithelialisation, as already described in the literature (Palmer et al., 2011). However, further molecular studies could be necessary to support this hypothesis. At the same time, post-injury, oval hyaline cells, also involved in activation with few or no granules, have been detected migrating to the wound area. Compared with granular amoebocytes, these cells possess a less dense cytoplasm, and both the size and the nucleus are more similar to those of fibroblasts or granulocytes. This may suggest that cells originate from a common cell type that differentiate during various stages of wound healing and regeneration. The differences observed after Masson–Fontana staining, relative to *A. viridis*'s structural organisation, are clearly evident when comparing the tissues after 24 h and 7 days from injury. This could be consistent with the reorganisation activity of fibroblasts induced by collagen deposition, as already demonstrated (see Parisi et al., 2021). Our evidence regarding the high presence of melanin at 24 h after amputation of the tentacles appears to be consistent with what was observed in *P. cylindrica* (Palmer et al., 2011), suggesting structural support during regeneration closely related to the increase in fibroblasts-like cells. In addition, a defensive role could be attributable to mucous and empty-appearing gland cells secreting several active com- pounds, such as mucins and lysozyme (Figure 4). As revealed by the PET observation, in the whole injured area, no signals were registered by the device 1 h post tentacle amputation. These data are consistent with the loss of functionality by symbionts, also visible at the histological level. Moreover, the initial loss of the symbionts, derived from their expulsion from the anemone, could be related to a defence strategy induced by conditions of stress. A similar behaviour was also observed in *P. cylindrica*, in which the effect could be imputed to the cytotoxicity induced by the degranulation of granular cells (Parisi et al., 2022). Consistent with recovering tissue, *Symbiodinium* cells were again visible between 24 h and 7 days (Figure 2E–G) following lesion reorientation of the cells, and reorganisation of their morphology occurred, observed as lining up side-by-side and perpendicularly to the injury site. Such cell organisation is characteristic of a healthy cnidaria epidermis (Cirino et al., 2022; Jahnel et al., 2014; Menzel et al., 2015). However, the presence of cells rich in melanin-like granules evidenced by Masson–Fontana staining suggests that granular eosinophil amoebocytes could include prophenoloxidase, the precursor to melanin synthesis. Interestingly, as shown in mucicarmine-stained tissue sections, mucus plays a fundamental role in sealing the injury and in isolating the lesioned site from external potential pathogens. At 24 h and 7 days after injury, mucus is confined to and accumulated as granules to be subsequently expelled by degranulating mucocytes (Figure 3). It could be argued that the apoptotic mechanism is

activated, and the dead cell material is first accumulated and then eliminated, thus contributing to the healing process and to proper systemic functioning of the organism (Greenhalgh, 1998; Raskin, 1997). Evidence also emphasises the role of mucocytes and mucus secretion under stress, also reporting a change in the density of these cells (Fransolet et al., 2013).

CONCLUSIONS

In the present work, conducted in *A. viridis*, it has been observed, once again, that the wound-healing process is preserved among metazoans. In fact, this work focused on the events that occur during regeneration and tentacle regrowth, describing all of the intercurrent phases, and our results are applicable to different organisms from various taxonomies. Cells of the immune system have been identified and characterised for the first time, including their distribution, contents, and hypothetical role in the regeneration process. Future studies are encouraged to explain the events that occur during wound healing and regeneration using molecular tools and immune markers. Furthermore, at this time, this study represents an interesting point of view in comparative morphological analyses, showing a novel zoological scenario.

REFERENCES

Arenas Gómez, C.M., Sabin, K.Z., Echeverri, K., 2020. Wound healing across the animal kingdom: Crosstalk between the immune system and the extracellular matrix. Dev. Dyn. 249, 834–846. https://doi.org/10.1002/dvdy.178

Baranzini, N., Weiss-Gayet, M., Chazaud, B., Monti, L., de Eguileor, M., Tettamanti, G., Acquati, F., Grimaldi, A., 2020. Recombinant HvRNASET2 protein induces marked connective tissue remodelling in the invertebrate model *Hirudo verbana*. Cell Tissue Res. 380, 565–579. https://doi.org/10.1007/s00441-020-03174-0

Bely, A.E., Nyberg, K.G., 2010. Evolution of animal regeneration: re-emergence of a field. Trends Ecol. Evol. 25, 161–170. https://doi.org/https://doi.org/10.1016/j.tree.2009.08.005

Bisanti, L., de Sabata, E., Visconti, G., Chemello, R., 2022. Towards a local mass mortality of the Mediterranean orange coral *Astroides calycularis* (Pallas, 1766) in the Pelagie Islands Marine Protected Area (Italy). Aquat. Conserv. Mar. Freshw. Ecosyst. 32, 551–557. https://doi.org/10.1002/aqc.3772

Boström-Einarsson, L., Babcock, R.C., Bayraktarov, E., Ceccarelli, D., Cook, N., Ferse, S.C.A., Hancock, B., Harrison, P., Hein, M., Shaver, E., Smith, A., Suggett, D., Stewart-Sinclair, P.J., Vardi, T., McLeod, I.M., 2020. Coral restoration – A systematic review of current methods, successes, failures and future directions. PLoS One 15, 1–24. https://doi.org/10.1371/journal.pone.0226631

Bowes, D., Corrin, B., 1977. Ultrastructural immunocytochemical localisation of lysozyme in human bronchial glands. Thorax 32, 163–170. https://doi.org/10.1136/thx.32.2.163

Calisi, A., Lionetto, M.G., Caricato, R., Giordano, M.E., Schettino, T., 2008. Morphometric Alterations In *Mytilus galloprovincialis* Granulocytes: A New Biomarker. Environ. Toxicol. Chem. 27, 1435–1441. https://doi.org/10.1897/07-396

Cirino, L., Tsai, S., Wang, L.H., Hsieh, W.C., Huang, C.L., Wen, Z.H., Lin, C., 2022. Effects of cryopreservation on the ultrastructure of coral larvae. Coral Reefs 41, 131–147. https://doi.org/10.1007/s00338-021-02209-4

Coaglio, A.L., Ferreira, M.A.N.D., Dos Santos Lima, W., De Jesus Pereira, C.A., 2018. Identification of a phenoloxidase- and melanin-dependent defence mechanism in *Achatina fulica* infected with *Angiostrongylus vasorum*. Parasites and Vectors 11, 1–8. https://doi.org/10.1186/s13071-018-2710-2

de Lima, F.M.R., Abrahão, I., Pentagna, N., Carneiro, K., 2023. Gradual specialization of phagocytic ameboid cells may have impaired regenerative capacities in metazoan lineages. Dev. Dyn. 252, 343–362. https://doi.org/10.1002/dvdy.543

Di Falco, F., Cammarata, M., Vizzini, A., 2017. Molecular characterisation, evolution and

expression analysis of g-type lysozymes in *Ciona intestinalis*. Dev. Comp. Immunol. 67, 457–463. https://doi.org/10.1016/j.dci.2016.09.010

Dinsmore, C.E., 2007. A History of Regeneration Research: Milestones in the Evolution of a Science. Cambridge University Press.

Fautin, D.G., Mariscal, R.N., 1991. Cnidaria: Anthozoa In Harrison F., & Westfall J.(Eds.), Microscopic anatomy of invertebrates: Protozoa (vol. 2, pp. 267–358). New York, NY: Wiley-Liss.[Google Scholar], pp. 267–358.

Ferrario, C., Ben Khadra, Y., Czarkwiani, A., Zakrzewski, A., Martinez, P., Colombo, G., Bonasoro, F., Candia Carnevali, M.D., Oliveri, P., Sugni, M., 2018. Fundamental aspects of arm repair phase in two echinoderm models. Dev. Biol. 433, 297–309. https://doi.org/10.1016/j.ydbio.2017.09.035

Fransolet, D., Roberty, S., Herman, A.C., Tonk, L., Hoegh-Guldberg, O., Plumier, J.C., 2013. Increased Cell Proliferation and Mucocyte Density in the Sea Anemone *Aiptasia pallida* Recovering from Bleaching. PLoS One 8, 1–7. https://doi.org/10.1371/journal.pone.0065015

Greenhalgh, D.G., 1998. The role of apoptosis in wound healing. Int. J. Biochem. Cell Biol. 30, 1019–1030. https://doi.org/10.1016/S1357-2725(98)00058-2

Jahnel, S.M., Walzl, M., Technau, U., 2014. Development and epithelial organisation of muscle cells in the sea anemone *Nematostella vectensis*. Front. Zool. 11, 1–15. https://doi.org/10.1186/1742-9994-11-44

Krzyszczyk, P., Schloss, R., Palmer, A., Berthiaume, F., 2018. The role of macrophages in acute and chronic wound healing and interventions to promote pro-wound healing phenotypes. Front. Physiol. 9, 1–22. https://doi.org/10.3389/fphys.2018.00419

La Corte, C., Baranzini, N., Grimaldi, A., Parisi, M.G., 2022. Invertebrate Models in Innate Immunity and Tissue Remodeling Research. Int. J. Mol. Sci. 23, 6843. https://doi.org/10.3390/ijms23126843

Loof, T.G., Schmidt, O., Herwald, H., Theopold, U., 2011. Coagulation Systems of Invertebrates and Vertebrates and Their Roles in Innate Immunity: The Same Side of Two Coins? J Innate Immun 3, 34–40. https://doi.org/10.1159/000321641

Menzel, L.P., Tondo, C., Stein, B., Bigger, C.H., 2015. Histology and ultrastructure of the coenenchyme of the octocoral Swiftia exserta, a model organism for innate immunity/ graft rejection. HHS Public Access Zool. 118, 115–124. https://doi.org/10.1016/j.zool.2014.09.002

Meszaros, A., Bigger, C., 1999. Qualitative and Quantitative Study of Wound Healing Processes in the Coelenterate, *Plexaurella fusifera*: Spatial, Temporal, and Environmental (Light Attenuation) Influences. J. Invertebr. Pathol. 73, 321–331.

https://doi.org/10.1006/jipa.1999.4851

Mydlarz, L.D., Holthouse, S.F., Peters, E.C., Harvell, C.D., 2008. Cellular responses in sea fan corals: Granular amoebocytes react to pathogen and climate stressors. PLoS One 3. https://doi.org/10.1371/journal.pone.0001811

Palmer, C. V., Bythell, J.C., Willis, B.L., 2010. Levels of immunity parameters underpin bleaching and disease susceptibility of reef corals. FASEB J. 24, 1935–1946. https://doi.org/10.1096/fj.09-152447

Palmer, C. V., Traylor-Knowles, N.G., Willis, B.L., Bythell, J.C., 2011. Corals Use Similar Immune Cells and Wound-Healing Processes as Those of Higher Organisms. PLoS One 6, e23992. https://doi.org/10.1371/journal.pone.0023992

Parisi, M.G., Baranzini, N., Dara, M., Corte, C. La, Vizioli, J., Cammarata, M., 2022. AIF-1 and RNASET2 are involved in the inflammatory response in the Mediterranean mussel *Mytilus galloprovincialis* following *Vibrio* infection. Fish Shellfish Immunol. 127, 109–118. https://doi.org/10.1016/j.fsi.2022.06.010

Parisi, M.G., Grimaldi, A., Baranzini, N., La Corte, C., Dara, M., Parrinello, D., Cammarata, M., 2021. Mesoglea extracellular matrix reorganization during regenerative process in *Anemonia viridis* (Forskål, 1775). Int. J. Mol. Sci. 22. https://doi.org/10.3390/ijms22115971

Parisi, M.G., Trapani, M.R., Cammarata, M., 2014. Granulocytes of sea anemone *Actinia equina* (Linnaeus, 1758) body fluid contain and release cytolysins forming plaques of lysis. Invertebr. Surviv. Journal; Vol 11 No 1.

Raskin, C.A., 1997. Apoptosis and cutaneous biology. J. Am. Acad. Dermatol. 36, 885–896.

Raymundo, L.J., Licuanan, W.L., Kerr, A.M., 2018. Adding insult to injury: Ship groundings are associated with coral disease in a pristine reef. PLoS One 13. https://doi.org/10.1371/journal.pone.0202939

Robson, M.C., Steed, D.L., Franz, M.G., 2001. Wound healing: Biologic features and approaches to maximize healing trajectories. Curr. Probl. Surg. 38, A1. https://doi.org/10.1067/msg.2001.111167

Sánchez Alvarado, A., Tsonis, P.A., 2006. Bridging the regeneration gap: genetic insights from diverse animal models. Nat. Rev. Genet. 7, 873–884. https://doi.org/10.1038/nrg1923

Schneider, C.A., Rasband, W.S., Eliceiri, K.W., 2012. NIH Image to ImageJ: 25 years of image analysis. Nat. Methods 9, 671–675. https://doi.org/10.1038/nmeth.2089

Tettamanti, G., Grimaldi, A., Rinaldi, L., Arnaboldi, F., Congiu, T., Valvassori, R., de Eguileor, M., 2004. The multifunctional role of fibroblasts during wound healing in

Hirudo medicinalis (Annelida, Hirudinea). Biol. Cell. https://doi.org/10.1016/j.biolcel.2004.04.008

Traylor-Knowles, N., 2019. Heat stress compromises epithelial integrity in the coral, *Acropora hyacinthus*. PeerJ 2019. https://doi.org/10.7717/peerj.6510

Van De Water, J.A.J.M., Ainsworth, T.D., Leggat, W., Bourne, D.G., Willis, B.L., Van Oppen, M.J.H., 2015. The coral immune response facilitates protection against microbes during tissue regeneration. Mol. Ecol. 24, 3390–3404. https://doi.org/10.1111/mec.13257

Vargas-Ángel, B., Peters, E.C., Kramarsky-Winter, E., Gilliam, D.S., Dodge, R.E., 2007. Cellular reactions to sedimentation and temperature stress in the Caribbean coral *Montastraea cavernosa*. J. Invertebr. Pathol. 95, 140–145. https://doi.org/10.1016/j.jip.2007.01.003

Work, T.M., Aeby, G.S., 2010. Wound repair in *Montipora capitata*. J. Invertebr. Pathol. 105, 116–119. https://doi.org/10.1016/J.JIP.2010.05.009

Young, J.A., 1974. The nature of tissue regeneration after wounding in the sea anemone *Calliactis parasitica* (couch). J. Mar. Biol. Assoc. United Kingdom 54, 599–617. https://doi.org/10.1017/S0025315400022773

Zhao, R., Liang, H., Clarke, E., Jackson, C., Xue, M., 2016. Inflammation in chronic wounds. Int. J. Mol. Sci. 17, 1–14. https://doi.org/10.3390/ijms17122085

SUPPLEMENTARY MATERIALS

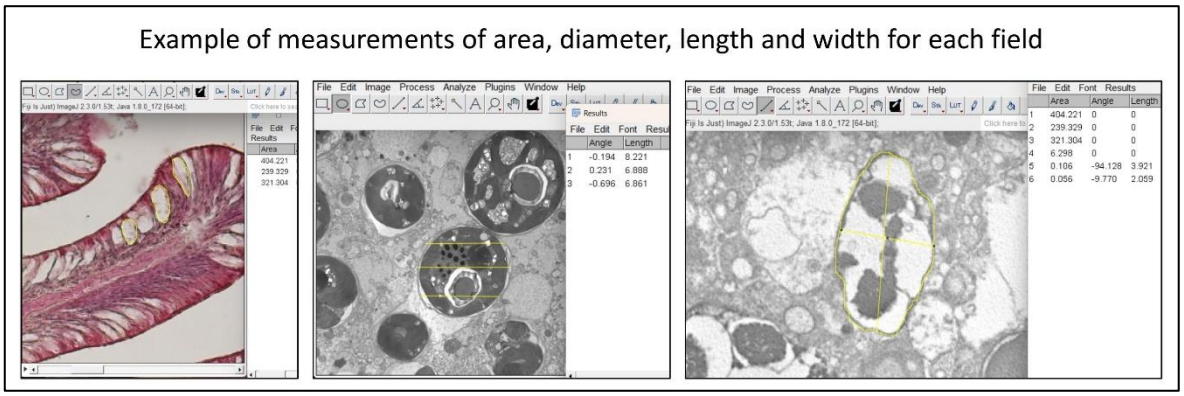

The figure supports the paragraph *Biometric measures.*

The next chapter addresses the topic of regeneration under a thermal stress condition. The main questions attempted to be answered can be summarized as follows: What molecules are expressed during the regenerative event under basal conditions? How much are expressed? Can *A. viridis* regenerate in the same manner after thermic stress?

Chapter 5

Transcriptomic approach to investigate wound healing, regeneration, acclimatization and the role of symbiont in basal conditions and after multiple stressors

ABSTRACT

This chapter is born from the need of a transcriptomic deepening of the regenerative event seen the gap of knowledge for this species that on several occasions has shown to diversify from other organisms of the same class. This approach has been used both to clarify what happens under natural conditions, but above all, by analysing a boundary condition such as that of a multiple stress caused by an increase in temperature, thus also evaluating the thermal effect, plausible condition given the continuous increase in sea temperatures in recent years. In order to have an even wider view of the phenomenon were evaluated markers of oxidative stress (carbonylation and total antioxidant capacity), evaluation of the photosynthetic efficiency of the symbiont through Pulse Amplitude Modulation (PAM) and blotting to investigate the expression and modulation of proteins involved in the regenerative event. Moreover, in order to answer the question: "Does an anthozoan subjected to thermal stress regenerate in the same way as an organism that undergoes the only wound?", the phenotype of organisms was observed for 7 days and the tentacular length of the tentacles in regeneration was measured. Results show a higher antioxidant capacity of the sea anemone higher at 20° C after 6 and 24 hours from the tentacles cut compared to the values at 27° C. Expression and modulation of proteins visualized in blotting and studied through q/RT-PCR suggest the activation and production of compensative molecules in an attempt to restore the internal homeostasis even if biomarkers of oxidative stress show a highly critical situation, further compromised also by the lower photosynthetic efficiency of the symbiont, consistent with what was observed previously also at the histological level.

Keywords: Thermal stress; regeneration; molecules expression; oxidative stress

INTRODUCTION

Physiological and molecular mechanisms in cnidarians are not entirely clear and responses to thermal stress were extremely different although in some studies the species considered were genetically similar (Walsh and Somero, 1981). Marine invertebrates, including anthozoan cnidarians, can "acclimate" to thermal stress by modifying some components of their cellular metabolism to better cope with high water temperatures (O. Hoegh-Guldberg, 1999). An increase in thermal tolerance was evidenced in three coral genera: *Acropora*, *Pocillopora* and *Porites*. Both temperature rises and dips can impair immunity, and seasonal temperature variation makes some invertebrates susceptible to illness at particular periods of the year.

Some invertebrates harbour photosynthetic dinoflagellates, which can alter the oxidative status of host tissues on a daily basis (Regoli et al., 2000; Richier et al., 2005, 2003). As a result, symbiotic organisms have an improved or more efficient antioxidant system, as well as greater resistance to oxidative stress. The crucial role of ROS in defence, as well as their capacity to control the oxidative condition of tissues following infection by pathogens and use reactive oxygen as a respiratory burst, is critical. Phagocytosis and reactive oxygen generation, *e.g.* provided antibacterial efficacy and inhibited *Psychrobacter immobilis* (Gram$^-$ bacterium) growth in amoebocytes isolated from sea anemones. In *Acropora grandis* heat stress stimulates the production of heat shock proteins (Fang et al., 1997). Particularly, some HSPs families (HSP70, HSP90) are expressed and modulated in thermal stress conditions suggesting their potential use as biomarker of exposure to heat stress (Louis et al., 2017; Sharp et al., 1994). Inadequate symbiosis can result in hyperoxia, which can damage the host's tissue even while it may increase tolerance to changes in the oxidative state of tissues and offer immunological protection. In fact, an imbalance in symbiont-host relationships has consequences on the physiology of the animal. An example of this is the phenomenon of coral bleaching, which can lead to mass mortality and leave corals susceptible to disease. Bleaching promotes the discharge of intact endoderm host cells and the symbionts they carry, implying that heat stress causes malfunction in cnidarian host cell adhesion (Mydlarz et al., 2006). Other extrinsic variables besides changes in the environment might also have an impact on immunity. Food supplies, wounds, and physical damage can change immunological characteristics. The implications of wound healing on invertebrates immune responses are discussed in Henry and Hart (2005). They argue that the resources dedicated to allorecognition and cell-mediated immune responses may be reduced during wounds repair. Additionally, cells involved in both wound healing and immunity, may be

reduced in their capacity to fight illness during regeneration (Mydlarz et al., 2006). By exposing the organisms to earlier exposure to thermal stress, the temperature tolerance of acclimatization may be modified and alterations in the symbiotic animals in the "acclimated" organism were also discovered (Maynard et al., 2008). This adaptation could concern both symbiont and host organism and might be influenced by heat shock proteins. Previous studies have indicated a link between the regulation of the activity of antioxidant enzymes and acclimatization from thermal stress in coral reefs (Gates and Eomund, 1999). Indeed, environmental stress can induce an increase in the production of reactive oxygen species (ROS) which damage the symbiosis system (Downs et al., 2002). The cellular response to the formation of oxygen radicals includes many defence mechanisms including the activation of enzymes such as peroxidase (GPx) superoxide dismutase (SOD) and catalase (CAT) which act in concert to inactivate the radicals responsible for major cell damage. ROS production, according to the bleaching paradigm, are to be ascribed to higher temperature and irradiance, and this impact on lipids, proteins, DNA, serving also as signals and mediators of cellular damage cascades like apoptosis and autophagy (Lesser, 2006; Richier et al., 2006). Although it has recently been demonstrated that symbiotic Cnidarians also bleach in reaction to heat stress alone, irrespective of photosynthetic activity, the extra energy created by the high light radiation producing an increase in ROS and cannot be processed by the photosystem II (Tolleter et al., 2013). In research conducted on two symbiotic corals subjected to elevated irradiance was investigated the photochemical efficiency of dinoflagellates using the pulse amplitude modulated (PAM) chlorophyll fluorescence techniques. The study demonstrated that the excess of light affects the symbiont causing also their lost from the hosts and this could happen moreover in elevated irradiance only (Jones and Hoegh-Guldberg, 2001). The phenomenon of bleaching is one of the stress responses and evidence has shown that this can occur as a result of a huge variety of environmental factors, the most investigated of which is the relationship with rising water temperatures. Even a difference of one or two degrees Celsius above normal summer temperatures has shown the occurrence of serious phenomena (Ove Hoegh-Guldberg, 1999).

It is now widely accepted that exposure to temperatures above 32 °C results in the loss of variable chlorophyll fluorescence and photosynthetic oxygen evolution. Analyses conducted on bleaching corals in warm water show a reduction in the D1 reaction centre protein of photosystem II and lower ratios of variable to maximum fluorescence (Iglesias-Prieto, 1997; Jones and Hoegh-Guldberg, 2001; Takahashi and Murata, 2008)

Collagen is a key factor in the regeneration process (Parisi et al., 2021) and also for heat stress responses as shown by previous transcriptome and microarray studies irrespective of collagen type. Masson's trichrome was used on corals under thermal stress to stain collagen and was observed to be present in controls as a component of the mesoglea, but under stress conditions this was also visible in the other epithelial layers. This suggests the importance of its rapid production and deposition indicating a rearrangement of the tissue following thermal stress. Interestingly, it is precisely because of the presence of different types of the molecule that several studies have shown different expression depending on the type of transcriptionally activated collagen even within the same species, thus imposing itself as a fundamental protective system against thermal stress (Traylor-Knowles, 2019).

Crucial protein in regeneration is also the Proliferating Cellular Nuclear Antigen (PCNA). It is a nuclear protein that acts as a cofactor for DNA polymerase δ and is involved in DNA repair. It is also known to play an important role in cell cycle regulation, DNA translesion synthesis, DNA methylation and chromatin remodelling. Genes coding for PCNA and its homologues have been isolated from a wide variety of animals (vertebrates and invertebrates), fungi, and marine phytoplankton. This explains why the presence and expression of this molecule was sought in regenerated tissues of *A. viridis*. Cell proliferation factor is involved in the S-phase of the cell cycle for DNA synthesis, but also during DNA damage before it enters mitosis in order to repair it and prevent the cell from going into apoptosis (Maga and Hübscher, 2003).

The use of *Anemonia viridis* as model organism will make it possible to read the responses to thermal stress to acquire new knowledge on cellular and molecular mechanisms also in the context of the regenerative process operating in invertebrates, and therefore to have immediate information on the state of health of our seas, with the potential possibility of the applicability of the results on different focuses. The knowledge of the immunological effectors thus involved will be important for developing monitoring programs and coordinated management of the coastline.

MATERIAL AND METHODS

Sample collection and preparation

The trial was conducted in two phases (Fig.1-2). At first the study included the investigation of the regenerative event and the modulation of the molecules involved in stress in basal conditions. The trial lasted one week. A total of 16 animals were collected, of which 4 were used as controls, while the other 12, after a period of acclimatisation in the tank, cut 25% of the tentacles at the base of the body. At each observation time (T0 = injury, 6h, 24h, 3d, 7d), 4 animals were recovered and processed in their entirety for protein extraction and RNA.

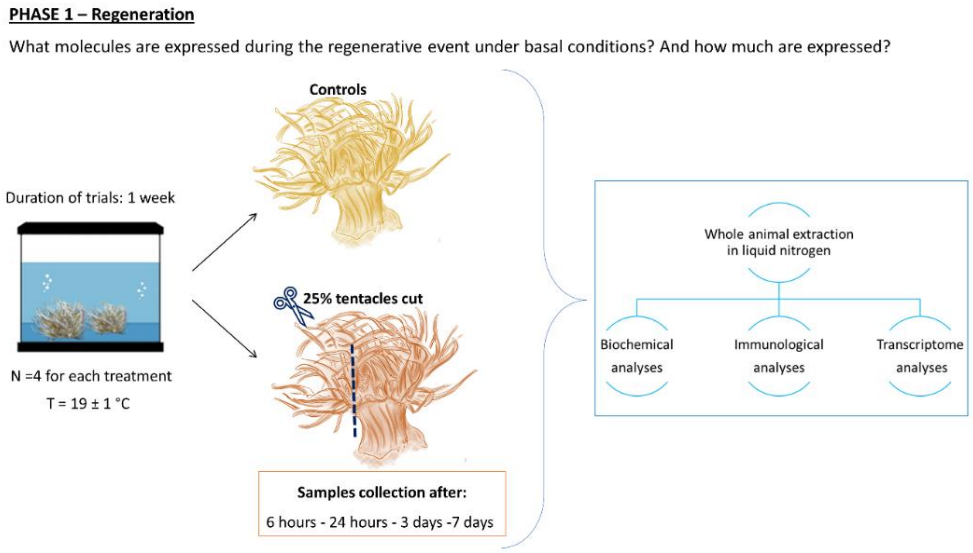

Figure 1 Experimental design of Phase 1: regeneration at T = 19 °C.

In phase two a condition of multiple stresses was foreseen. In fact, following a thermal ramp that allowed the organisms to be conditioned at 27 °C (a daily increase of 1 °C from 19 °C), the animals were then processed as for phase 1. The last time of observation in this case was until 3 days, because animals did not survive after these time point.

Anemonia viridis whole body were flash frozen in liquid nitrogen and homogenised with a tissue lyser (TissueLyser II Qiagen) for 30 seconds 25htz at each experimental time. The powder was divided into two tubes and stored at -80 °C until analyses: dry for protein extraction and with Trizol (Thermo Fisher, cat no. 15596018) added to preserve RNA.

Analysis using PAM included 20 animals. All were acclimated to 19 °C for a week, after which photosynthetic efficiency measurements were conducted on 5 animals for other seven days. One measure each day for each animal. The water temperature was increased until the

achievement of the 27 °C (1 °C every day), after one day at this temperature, the 25% of the tentacles were cut to 5 animals and the remaining 5 were used as controls. Measurements on the cutting area were made at the time of injury, after 6-24h and 3-7 days, bringing the probe closer to the area in regeneration. The measurements were taken for all samples at the base of the tentacle near the body. In order to investigate the growth rate of tentacles after the cutting at the two experimental temperatures, photographs were taken at 24 hours, 3, and 7 days to measure the regrowing tentacles using an image analysis software (Fiji open source software), to avoid further stress to the animals. Nikon D5100 was used and to calibrate the measure was included in each photo a ruler.

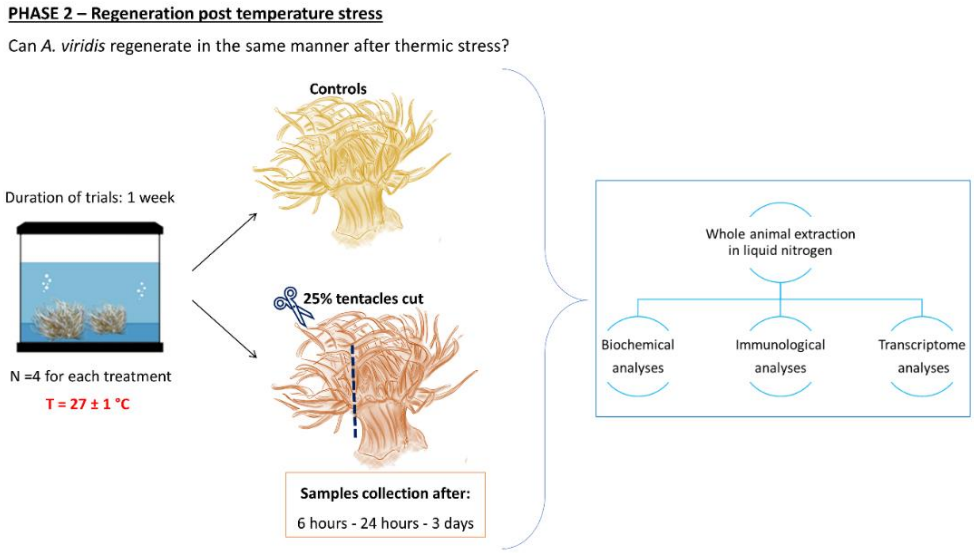

Figure 2 Experimental design of Phase 1: regeneration at T = 27 °C.

Protein extractions

Samples were weighed, defrosted and incubated at 4 °C with lysis extraction buffer (HEPES 25 mM Sigma-Aldrich H-3375, $MgCl_2$ 5 mM Sigma-Aldrich M9272-500G, EDTA 5 mM, Sigma-Aldrich P3803, DTT 5 mM Sigma-Aldrich E-5134, PMSF 2 mM Sigma P-7626, anti-Phosphatase 10 µl/ml, Thermo Scientific 79 78441) in ratio 1:1. Samples were sonicated (10" at 4 °C) and centrifuged (15000rpm for 20 minutes at 4 °C) to recover the cytosoluble protein content. The total protein concentration of each sample was evaluated by a Bradford assay (Bradford reagent; Sigma B6916), using 0-2 µg/µl bovine serum albumin solution as standard curve.

RNA extraction, cDNA retrotranscription RT-PCR and q/RT-PCR

Total RNA was extracted from whole body at selected the time points following manufacturer's protocol. Then, 1 µg of RNA samples was reverse transcribed using iScript cDNA Synthesis Kit™ (BIORAD). A volume of 1 µl of cDNA was used for PCR amplifications with primers specifically designed (Table 1) against transcripts identified *from A. viridis* transcriptome (Pey et al., 2017; Sabourault et al., 2009). COPγ2(to ensure that there was no trace of genomic DNA) was used as house-keeping gene in the PCRs. The primers of the molecules of interest (HSP90, CDC37 a co-chaperon of HSP90, COL24A1, PCNA) were tested for temperature tuning for q/RT-PCR The PCR conditions were as follows: 60°C and 35 cycles (30") for HSP90 and COL24A1; 58 °C 35 cycles (30") for PCNA. 1µl per gene was loaded and positive controls were used in both set-up conditions. Finally, q/RT-PCR was performed as follow: 50° C x 2', 95 °C x 10.15', 58 °C x 30", 95 °C x 15", 58 °C x 1' and 95 °C for 15" using Step One Plus ™ Instrument (Applied Biosystems).

Table 1 Primers sequences used in q/RT-PCR.

Genes	Forward	Reverse
COPγ2	GCCTGTTGGACACCGATGAT	TGCAAGGCTCTCTCCAGTCC
PCNA	CTCCACAGCATCAGACTGGA	GGGAGATTGGCTTAGCATGA
COL24A1	TACCCATGGTGCAAGACGAC	GCGAGGCTTGAAGAGAACCT
CDC37	AATCAAGCACTTTGGGATGC	GCCAGGTAGTTAGCCGTGTC
HSP90	TCATCCGCAAGAACCTGGTC	GACGCTGTCCTCGTGGATAC

Protein carbonylation analysis

Carbonyl content of protein samples was measured using both the ELISA assay and spectrophotometry (490 nm) according to (Buss et al., 1997). Protein derivatization was done by adding a dinitrophenylhydrazine (DNP) solution (10 mM in 6 M guanidine hydrochloride, 0.5 M potassium phosphate buffer) to the protein samples (1 mg/ml). After immobilizing on Nunc-Immuno Maxisorp plate (Dutscher, 055221), derivatized proteins were revealed by ELISA assay using anti-DNP antibody produced in rabbit (1:2000; Sigma-Aldrich D9656) and anti-rabbit IgG secondary antibody (1:3000; Sigma-Aldrich A9169). 0–100% reduced bovine serum albumin (BSA) were used as standard curve. Carbonyl content of

protein samples was expressed in milligram of protein/ml and was then standardized by a control sample of *A. viridis* protein.

Total oxyradical scavenging capacity (TOSC) assay

The TOSC of protein samples were evaluated using fluorometric assay consistent with Naguib (2000), with some modifications to perform it in 96-well microplates. Briefly, the volume corresponding to 0.9 μg of protein samples was incubated with 75 mm phosphate buffer (pH 7.0), 180 nM 6-carboxylfluorescein as fluorescent probe and 36 mM AAPH (2,2′ azobis (2- amidinopropane) dihydrochloride) as the peroxyl radical generator. In the assay, 20 μM Trolox (6-hydroxy-2,5,7,8- tetramethyl-1-chroman-2-carboxylic acid) is used as antioxidant calibrator. The fluorescence recordings were performed in black microplates (96-wells Grener Bio-One), and fluorescence decay was measured by spectrofluorometer (Safas, Monaco) every minute for a total duration of 45 min at an excitation/emission wavelength of 520/495 nm. Relative anti-oxidant activities of protein samples (tested in duplicate) were measured by comparison with Trolox standard and results are expressed in Trolox equivalents (Naguib, 2000).

Pulse-Amplitude-Modulated (PAM) fluorometry

A pulse amplitude modulated (PAM) chlorophyll fluorometer (DIVING-PAM, Walz) was used to assess the maximum potential quantum yield (Fv/Fm) of the symbiotic algae in *A. viridis*, using the procedures and instrumental settings outlined in literature (Jones and Hoegh-Guldberg, 2001). Measurements were taken in the dark after being kept under these conditions for 30 minutes. Measurements were taken on the cut zone and tentacular zone at the base of the body for controls and regenerating organisms, immediately after cutting (T0), at 6-24 h, 3 and 7 days after cutting. Baseline measurements were considered and performed on the same animals to normalise the trial data before proceeding with the experimental plan.

Western blotting

Western blot analysis was performed to determine the antibody specificity against selected target proteins in *A. viridis* whole body extracts (0.3mg/ml) of samples in regeneration under basal and thermal stress condition. A preliminary investigation was conducted on the NCBI (National Center for Biotechnology Information) database to be sure of similarity of the protein sequences present in species phylogenetically close to our model versus the antibodies sequences (see Supplementary material). SDS-PAGE was carried out according to the method of Laemmli (1970) using a 4% (stacking) and a 10% (separating)

poly-acrylamide gel for 30 min at 180 V using a Bio-Rad mini gel kit. Proteins separated by SDS-PAGE were electroblotted onto a nitro-cellulose membrane. The gels were prepared in blotting buffer (20 mM Tris–HCl, 192 mM glycine, 20% methanol, pH 8.8), and a semi-dry blotting bath (Bio-Rad Laboratories) was used (0.8 mA cm^2 for 75 min). The filter membrane was soaked in blocking buffer (TBS containing 3% BSA and 1% Tween-20) and, incubated overnight with the following appropriate primary polyclonal antibodies diluted in blocking solution: Anti-Heat Shock Protein 70 (HSP70) antibody SAB4200714, Anti-Hsc70 (Hsp73) antibody SAB3701436 and Anti-Interleukin-1β (I3642, Sigma-Aldrich). All primary antibodies were diluted 1:1,000. Membranes were then washed with blocking buffer and incubated with anti-mouse IgG (whole molecule) alkaline phosphatase conjugate (1:5,000 in washing buffer, 0.1% BSA; A3562) for 1 h. Antibody binding was detected by chromogen substrate BCIP/NBT. The cross-reactivity of the antibodies was established by the similarity of the epitopes (see supplementary materials) between *A. viridis* phylogenetically closer species proteins and those used for antibody raising (human HSP70, HSC73 and IL-1 β).

Dot-blotting

Dot-blotting were performed in order to investigate the expression of HSP70, HSC73, IL-1β under basal and thermal stress conditions. Samples concentration was 0.3 mg/ml. Also in this case were kept the same dilutions of the antibodies used for the western blot. Bio-Dot Microfiltration Apparatus (Bio-Rad) was used, and nitrocellulose membrane was washed in TBS buffer (pH 7.4; 1.21 g Tris-base; 9 g NaCl) prior to perform the experiment and each well was hydrated before incubate the antigen, which was allowed to filter by gravity for 1h. Blocking solution (TBS containing 0.05% Tween20 + 1% BSA) was added in each well for 1h. After three vacuum washes with 0.1% TBS-Tween 20 solution (TBS-T), the membrane was incubated with primary antibody diluted in TBS-T buffer + 0.1% BSA and left 1h. Again, it was filtered by gravity, three washes were carried out and in each well was added the secondary antibody conjugated with alkaline phosphatase for 1h. Twice washed with TBS-T by vacuum, the membrane was removed from the apparatus and washed twice more with TBS to remove excess Tween 20. It was treated with the BCIP/NBT development solution, and then washed with distilled water to block the reaction.

The densitometric analysis of the membrane was conducted through the processing image software "Fiji".

Statistical analyses

For carbonylation, data were tested for one-way ANOVA. Post-hoc False Discover Rate (Benjamini- Hochberg) was used to evidence differences between groups in single evaluation for each temperature. For the comparison between treatments versus temperature was used Kruskal-Wallis and Dunn's test followed by Benjamini- Hochberg correction. As regards TOSC assay Brown-Forsythe ANOVA test and Two-stage linear step-up procedure of Benjamini, Krieger and Yekutieli was performed. For densitometric analysis one-way ANOVA was conducted and differences between the means were considered significant for $p < 0.05$. Tukey's multiple comparison post hoc test was applied. Also for PAM two-way ANOVA was used to highlight differences between groups. Sidak post-hoc test was used for multiple comparison. All data are presented as mean ± standard deviation (SD) and statistical tests were chosen on the basis of normality and homoschedasticity of the data. R studio and GraphPad Prism 8.0.2 software were used to perform the several analyses.

RESULTS

Growth rate of tentacles

In the experimental conditions, tentacle measurements were taken from the base of the body (Fig. 3). The biometric results processed using Fiji software indicate an average tentacle length at 24 hours post-amputation of 0.391 ± 0.131 cm at a temperature of 20 °C, as opposed to 0.337 ± 0.082 cm at 27 °C. After 3 days, they reach 0.566 ± 0.114 cm and 0.489 ± 0.138 cm, respectively, with a growth increase of 44.57% and 45.14% at the higher temperature. On the seventh day of regeneration, tentacles at 20°C measure 0.899 ± 0.164 cm, while at 27 °C, they measure 0.599 ± 0.143 cm. The percentage increase in regrowth compared to the 24-hour time point was 129.86% for organisms maintained at 20 °C and 77.75% for organisms regenerating at 27 °C. Statistical analyses conducted for the different conditions (Kruskal-Wallis followed by multiple comparisons with Dunn test) revealed significance for individual temperatures (approximate p-value <0.0001) and for the comparison between different time points at 20 °C. At 27 °C, no statistical significance was observed at the 3-day and 7-day time points post-amputation. The Dunn test further revealed statistical significance at 7 days between the two different temperatures (p-value = 0.0360).

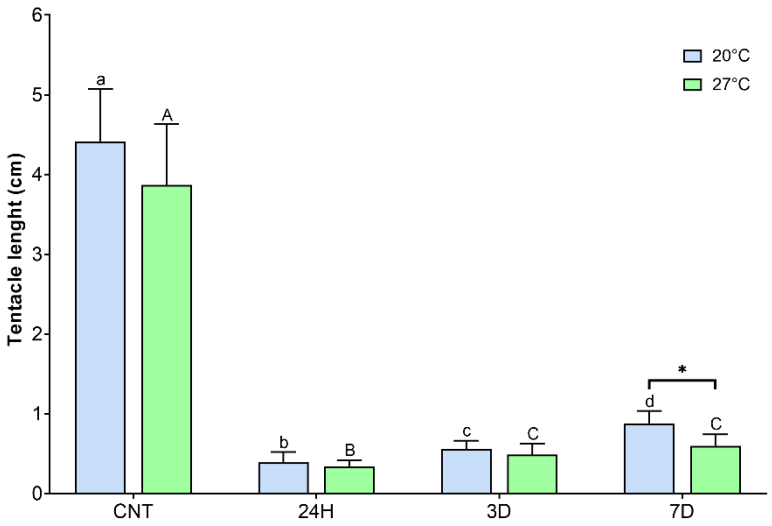

*Figure 3 Tentacular length measured in regenerating A. viridis organisms. Results are presented as mean ± SD. Letters indicate differences between treatments. Differences between means were considered significant for p < 0.05. * Indicates differences between temperature groups at each time. Significant differences were detected by Dunn's test—* p < 0.05, ** p < 0.01, *** p < 0.0001. Upper or lower case to distinguish treatment at 20 °C from 27 °C (intra-group).*

Protein carbonylation

To estimate the damages on protein generated from oxidative stress, carbonylated protein levels were measured. Compared to the control (20 °C), the carbonylation of proteins was

significantly doubled after 6 and 24 hours and returned to basal levels at three days (Fig. 4A). At 27 °C the measured values are already double in the controls and a general statistically significant inhibition is visible in the following times (Fig. 4B).

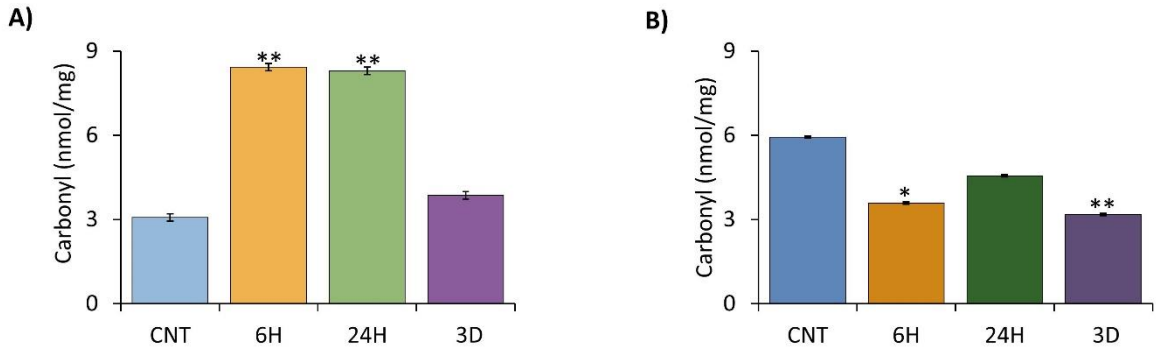

Figure 4 Carbonylation assay. ***(A)*** *T = 20 °C;* ***(B)*** *T = 27 °C. Data were tested for one-way ANOVA. Post-hoc False Discover Rate (Benjamini- Hochberg) was used to evidence differences between treatments. Asterisks indicate differences compared to the control.*

The thermal effect alone causes an increase in the levels of protein carbonylation visible in the controls. Statistically significant differences were found also between temperature treatments at 6h and 24h.

Antioxidant defences: TOSC

TOSC kinetic was performed in order to evaluate the total antioxidant capacity of the organisms under stressed conditions. A statistically significant increase was observed from the control up to 1 day from the cut (four times as much as the control) with a return to normal conditions at 3 days for treatment conducted at 20 °C (Fig. 5A). In contrast, at 27 °C, a general decrease in total antioxidant capacity compared to treatment under basal conditions with statistically significant values higher at 6h respect to the other time points (Fig. 5B).

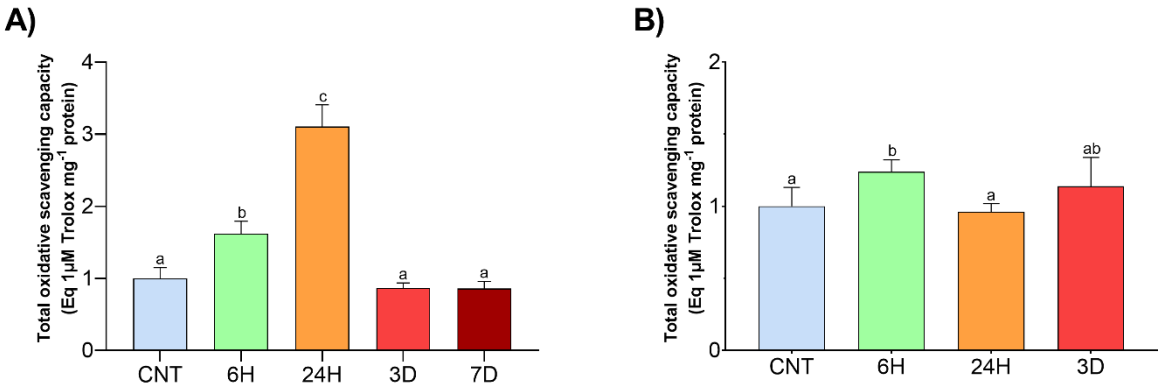

Figure 5 Total oxidative scavenging capacity (TOSC) of Anemonia viridis. TOSC (equivalent to 1 µM Trolox) was measured on whole body extracts. Results are presented as mean ± SD. ***(A)*** *Kinetic at 20 °C.* ***(B)*** *Kinetic at 27 °C. Letters indicate differences between treatments. Brown-Forsythe ANOVA test e Two-stage linear step-up procedure of Benjamini, Krieger and Yekutieli (FDR = 0.05).*

PAM results

Photosynthetic efficiency (Fv/Fm = maximum quantum yield of PSII) was measured via PAM to assess the health status and involvement of the symbiont (Fig. 6). The graph shows the ratio for the controls (in blue) post thermal increase and for the samples in post ramp regeneration (in red). Data have been normalized for basal conditions. Lower values were measured at 1 day after cutting (0.651 ± 0.082). Two-way ANOVA and the post-hoc Sidak test showed significant differences between controls and treated for each experimental time. A preliminary analysis between controls at T = 19 °C versus T = 27 °C did not result in significant differences. The values increase to 3 and 7 days.

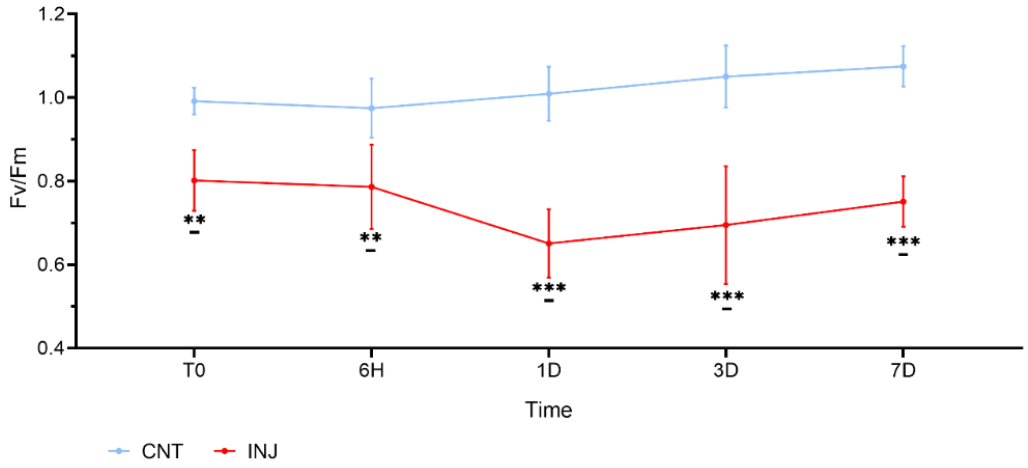

*Figure 6 PAM measurement. In blue controls; in red injured. Fv/Fm = maximum quantum yield of PSII. Data were tested for ANOVA assumptions, and differences between groups are shown using a two-way ANOVA as mean ± standard deviation (SD). Differences between means were considered significant for p < 0.05. * Indicates differences between groups at each time. Significant differences were detected by Sidak post hoc test—* p < 0.05, ** p < 0.01, *** p < 0.0001.*

Immunoblotting: Western & Dot

Western blotting was exploited to ensure the specific cross-reactivity of the antibodies used (Fig. 7) to subsequently investigate their modulation by dot-blot. In the first case, it was decided to test the samples in regeneration after 3 days for the two temperatures under investigation, assuming the expression of the molecules given the stress condition. A densitometric and comparative analysis was conducted between the two temperatures up to 3 days; most of the specimens due to thermal stress at 7 days after cutting could not survive.

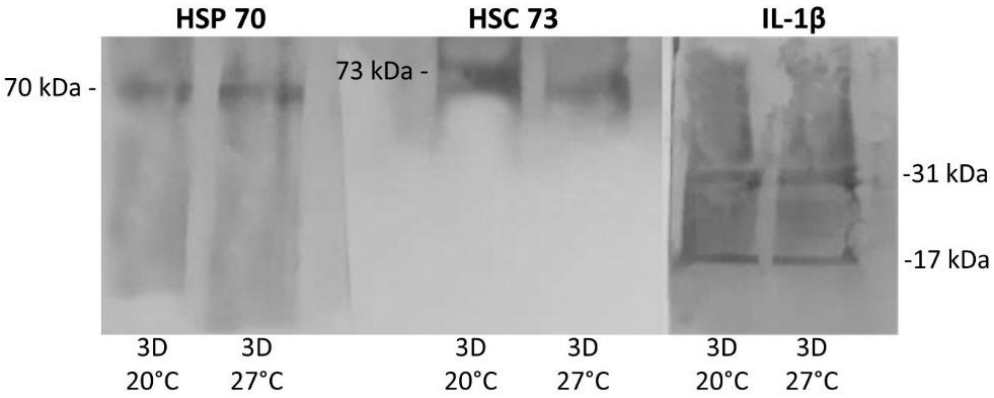

Figure 7 Western blotting for HSP 70, HSC 73 and IL-1 beta.

Densitometric analysis showed a higher expression at 27 °C than the lower temperature treatment for HSP 70. The one-way ANOVA and the post-hoc Tukey test have evidenced statistical significance between 6h 20 °C and 27 °C and between 6h 27 °C and 24h 27 °C (Fig. 8A). As far as HSC 73 is concerned, a general inhibition is observed at 27 °C with statistical significance for control, 24h and 3d considering temperatures. Under basal conditions, there is a statistically significant difference at 6h after cutting compared to the other experimental times. Similarly, at 27 °C the time at 6h is significant compared to the control (Fig. 8B) Densitometry for IL-1β shows lower values at 27 °C. Significance at 20 °C is detected at 6h, 24h and 3d compared to the control. At 27 °C only at 3d compared to control. Comparing temperatures: between the 6h and 3d treatments (Fig. 8C).

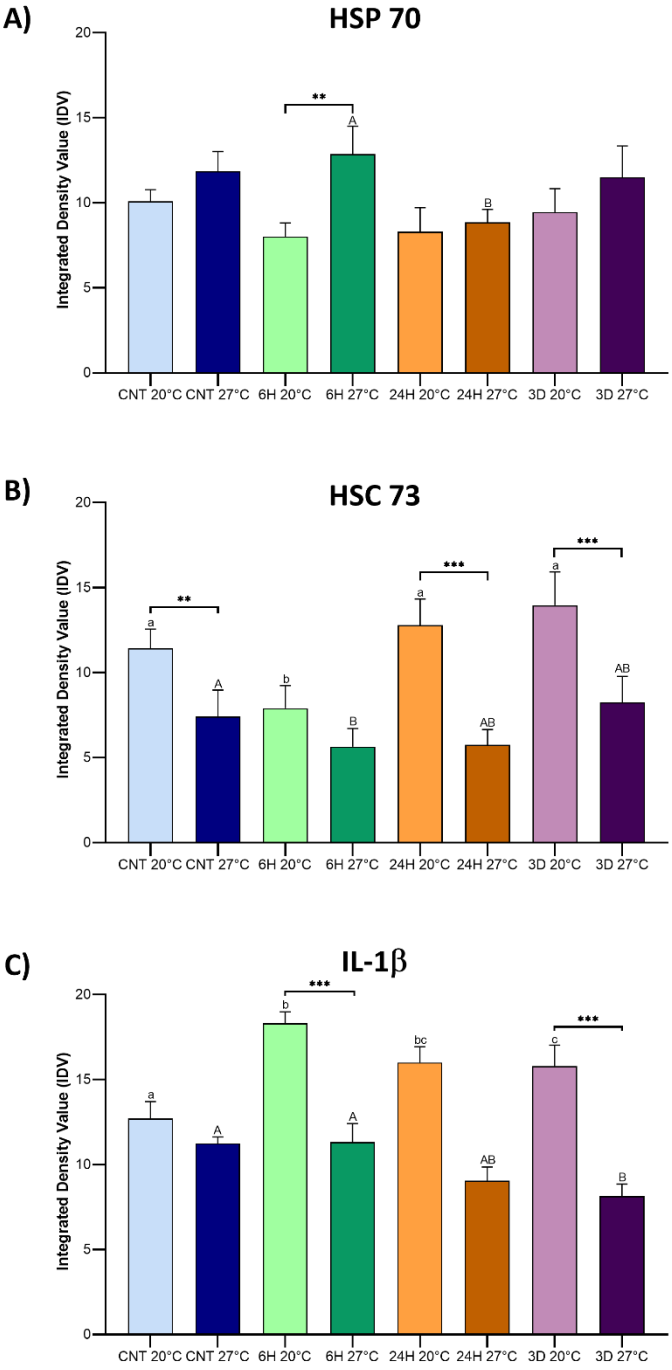

*Figure 8 Densitometric analyses of A. viridis extracts. Plots indicate the integrated density value (IDV) calculated on dot-blot spot for **(A)** HSP 70, **(B)** HSC 73, **(C)** IL - 1β antibodies. Data were tested for ANOVA assumptions, and differences between groups are shown using a one-way ANOVA as mean ± standard deviation (SD). Differences between means were considered significant for p < 0.05. Significant differences were detected by Tukey post hoc test—* p < 0.05, ** p < 0.01, *** p < 0.0001. Letters indicate significance within the same temperature; upper or lower case to distinguish treatment at 20 °C from 27 °C (intra-group). * show significance at the same time but for different temperatures (intergroup).*

Gene expression

Expression of PCNA, HSP90, CDC37 and COL24A1 after 6 and 24 hours, 3 days and 7 days (only for treatment conducted at 20 °C) was measured using q/RT-PCR on regenerating organisms both at basal temperature (Fig. 9A,C,E,G) and under heat stress (Fig. 9B, D, F, H).

Gene expression, normalized to COPγ, is given related to control. Error bars represent standard deviation. Comparing the two temperatures, a lower level of gene expression is observed at 27 °C. As for PCNA, at 20 °C expression increases at 24H and 7 days after cutting. The Tukey post-hoc test conducted following the one-way ANOVA (P value = 0.0004, R square = 0.9311) revealed statistical significance between all experimental times (including control) compared to time 7 days. For the 27 °C treatment, a significant upregulation of the expression is observed compared to the other times and the 6H control. Statistically significant lower levels (Welch-ANOVA test P value = 0.0014 and post-hoc Two-stage linear step-up procedure of Benjamini, Krieger and Yekutieli) were measured at 24H (vs 6H) and 3D (vs CNT and 6H). The HSP90 levels of the two controls were comparable for the two temperatures analysed. At 20 °C, the statistical analysis showed significance only at 24 hours compared to the control, Welch-ANOVA test (P value = 0.0817) and post-hoc Two-stage linear step-up procedure of Benjamini, Krieger and Yekutieli were used for statistical analysis. A gene expression downregulation was measured at three days after cutting. At a temperature of 27 °C, a strong decrease in gene expression was observed at three days, also supported by statistical analysis, which showed a difference between the different experimental times and the control (one-way ANOVA, P value = 0.0014; Tukey's multiple comparisons). For the CDC37, an increase in expression is observed particularly at three and seven days with statistical significance of the two times for the 20 °C temperature. During thermal stress, on the other hand, the opposite behaviour is observed with a decrease in expression at 24 hours and three days with statistical significance of the two times towards the control and at six hours (one-way ANOVA with P value = 0.0006 at 20°C e Welch ANOVA P value = 0.0489 for the heat stress treatment; Tukey test and Two-stage linear step-up procedure of Benjamini, Krieger and Yekutieli for multiple comparisons). Finally, as regards COL24A1, there is an increase in gene expression has basal temperature at six hours and 24 hours after cutting with a subsequent decrease in expression at three days and seven days. Statistical significance was shown at six hours and 7D compared to control and 3D (one-way ANOVA, P value = 0.0004 and Tukey as post-hoc test).

Under thermal stress conditions, control and 3D have comparable expression at basal temperature. An opposite trend is observed at the control temperature with downregulation at 6H (statistically different from the other times) and 24H. Statistical analysis (Welch's ANOVA test with P value 0.0157 and two-stage linear step-up procedure of Benjamini, Krieger and Yekutieli for multiple comparisons) showed statistical significance of all

experimental times with respect to CNT (see supplementary materials for multiple comparison tables).

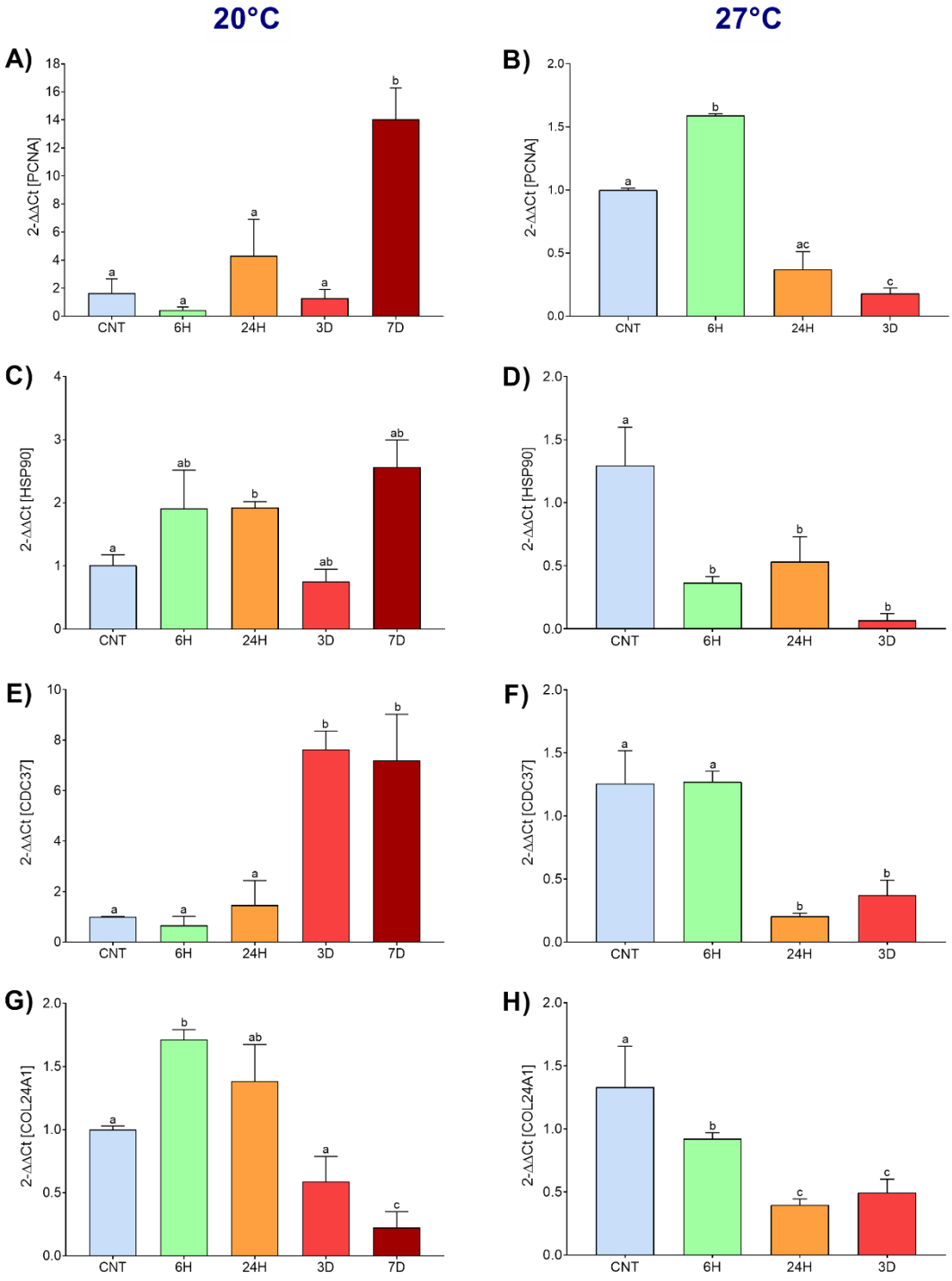

*Figure 9 Real-time quantitative PCR quantifications of gene expression (±SD). The assays were performed on organisms in regeneration at basal conditions **(A, C, E, G)** and under heat stress **(B, D, F, H)**. The considered genes are: PCNA, HSP90, CDC37, COL24A1. Differences between means were considered significant for $p < 0.05$. Letters indicate significant differences between the experimental time points.*

DISCUSSION

In order to assess the immune responses of *Anemonia viridis* to a single stress, such as increased temperature and regeneration caused by tentacular cuts, and their combination, Biometric measurements on tissue regrowth and molecular analyses were performed on total tissue extracts of the animal, exploiting some of the markers known to be involved in these dual conditions. In particular, biometric results show slower growth of the tentacles in organisms subjected to multiple stress. This is interesting as in the literature a decrease in body size and growth rate was observed as adaptation to a temperature rise condition in *Actinia equina* and in *Aurelia aurita* (Chomsky et al., 2004; Hansson, 1997), which also confirms what has been observed in *A. viridis*. Markers related to oxidative stress (carbonylation, total antioxidant capacity, heat shock proteins), inflammation and regeneration (interleukins, collagen, nuclear antigen of cell proliferation) were considered. Oxidative stress occurs when there is an imbalance between the ability of cells to eliminate reactive oxygen species and their production (Singh et al., 2009). They are a normal product of aerobic metabolism, but pose a problem when present at high concentrations, as they contribute to the damage of biomolecules and activate an inflammatory response (Sies, 2017). Several studies have shown that these are compounds with crucial regulatory roles in wound healing processes (Barrera et al., 2018; Butterfield et al., 2007; Cecarini et al., 2007; Dalle-Donne et al., 2003). They are indeed necessary both as mediators of intracellular signals in the defence against potential infections (Barrera et al., 2018; Battisti et al., 2008; Linares et al., 2011). In addition to this, high levels of ROS have been correlated with DNA fragmentation events, lipid peroxidation, protein carbonylation leading to dysfunction or cell death (Battisti et al., 2008). In any case, cells are equipped with enzymes and molecules with antioxidant activity that have the task of coping with and maintaining low levels of reactive oxygen species (Battisti et al., 2008; Fedorova et al., 2014). In order to more specifically assess the effects of free radicals on organisms, more energy is being put into measuring their target products in recent times, and useful methods involve the quantification of lipid peroxidation and protein carbonylation (Ahmad et al., 2010, 2008) which is capable of causing a loss of the functionality and structure of proteins due to their oxidation. In fact, under such conditions, they cannot be easily eliminated as they aggregate, polymerise or change their conformation, which causes cellular dysfunction (Butterfield et al., 2007; Cecarini et al., 2007). Among the protein oxidations that occur most easily is the formation of aldehydes and ketones (Dalle-Donne et al., 2003), which, being stable compounds, are

exploitable for laboratory analysis by immunoblotting or spectrophotometer, thus making them excellent markers of oxidative stress (Levine et al., 1994). By derivatizing the carbonyl group with dinitrophenylhydrazine (DNPH), which produces the stable dinitrophenylhydrazone (DNP) product, one may determine the amount of carbonyls present in proteins (Barrera et al., 2018; Buss et al., 1997; Linares et al., 2011). Finally, protein carbonylation can result from direct events caused by oxidative stress and indirect by secondary metabolites and it has been linked to the aetiology of various illnesses and in humans, less protein carbonylation has been observed in the fluid of acute injuries than in chronic ones (Rodríguez-García et al., 2020). Our results show that the amputation of tentacles of *A. viridis*, when investigating the regenerative process, consistently caused oxidative stress. Indeed, analysis of protein carbonylation shows an increase in this in the early stages of regeneration, accompanied likewise by an increase in total detoxification capacity (TOSC) particularly after 24 h. The increase in temperature in combination with the regenerative event seems to have an inhibitory effect on TOSC, but also on carbonylation, suggesting the activation of other processes probably also linked to the presence of the symbiont. It could be concluded that the organism is able to re-establish basal conditions in the single stress 'regeneration' condition, but the temperature, as already indicated in the literature, has a significant effect on the animal's physiological responses. It should be noted, in confirmation of this, that when comparing the two control organisms at different temperatures, at 27 °C the measured values of carbonylation are twice as high as at 20 °C and the TOSC remains identical. The organisms underwent a gradual increase in temperature that led to their acclimatisation to the stressful condition. It has also been observed that symbiotic sea anemones appear to be much more resistant to thermal stress than non-symbiotic ones (Richier et al., 2006). Overall, this could explain why the total oxyradical scavenging capacity (TOSC) does not change in control individuals at different temperature conditions. The heat shock proteins (HSPs) (Kenkel et al., 2011; Leggat et al., 2011; Meyer et al., 2011; Rodriguez-Lanetty et al., 2009; Rosic et al., 2011), notably hsp70 and hsp90, are among the most researched potential genes in coral and *Symbiodinum sp.* transcriptome reactions to thermal stress. A variety of stresses can cause the production of HSPs, which are conserved proteins (Schmitt et al., 2007).

HSPs are molecular chaperones that play a critical role in cells protection because are able to reestablish proteolytic equilibrium through their functions. They participate in assembly of complex, sorting, transport, and protein folding and unfolding. Additionally, they shield cells from stress and apoptosis (Li and Srivastava, 2003). Occurrences like

protein misfolding, aggregation or disruption of regulation, and disassembly of multiprotein complexes may take place during a stress, like as exposure to increased temperature, and this may trigger the initiation of signalling pathways. During laboratory-induced heat stress tests, HSP70 expression has been shown to be increased in stony coral hosts. On adult colonies of *Acropora aspera* exposed to an increase of 1 °C for six days and then for a further two days at 34 °C, an upregulation of the HSP70 transcript level was observed (Leggat et al., 2011). Similar evidence has been reported on aposymbiotic larvae of *A. millepora* (Rodriguez-Lanetty et al., 2009). Different ramping and sample periods might explain the variations in outcomes. Leggat *et alii* (2011) also showed a considerably more restricted rise in the symbiont's HSP70 gene expression. Similar evidence was also found in this study, particularly at six hours after cutting at 27 °C, with slightly higher values than regeneration at 20 °C at the other experimental times. Other factors also influence hsp70 expression like copper as for *Montastraea* (*Orbicella*) *franksi*, in which an upregulation of ~5 fold after 4 h of exposure to 100 ppb and ~3.5 fold after 8 h of exposure to both 30 and 100 ppb was highlighted. Also, oil dispersant (Corexit TM9527) caused an increase in expression levels of 3-3.5 fold after 8 h considering the three concentrations of 5, 10 and 50 ppm (Venn et al., 2009). Experiments conducted on *M. faveolata* colonies subjected to thermal stress showed a 1.28-fold increase in HSP90 compared to the control situation (Desalvo et al., 2008) and at 5, 7 and 8 days in *Acropora aspera* nubbins (Leggat et al., 2011; Rodriguez-Lanetty et al., 2009). Blotting with HSC73 showed a decrease in expression when comparing the times between the two temperatures. HSC73 is a constitutively expressed chaperonin crucial in regulating the cell cycle and this explains why there are almost comparable values between the different step points at 20 °C (with the lowest value always measured after 6h). At 27 °C, a decrease in activity is observed, probably due to the increase in temperature. As already mentioned, heat shock proteins are not only expressed and modulated in relation to heat stress, high levels of HSP90 in the early stages of regeneration also seem to regulate the folding of evolutionarily conserved client proteins (Echeverría et al., 2011). Also, in the case of the expression of HSP90 in *A. viridis* evidenced by q/RT-PCR, an upregulation with respect to the control organism at T = 20 °C and an opposite trend in the combined effect with a collapse in activity was found. CDC37 chaperonin was found to be upregulated at 3 days and 7 days at 20 °C, suggesting a combined action of HSP90 and chaperonin. This is most visible in the expression of the two molecules at 27 °C where one appears to supplant the other at the time points studied.

Additional help for the internal defence system is provided by the cytokine network, which is involved in immunosurveillance, development and growth, and repair processes. Among these, a central role is played by interleukin-1beta (IL-1β) (Beck and Habicht, 1991). The IL-1 family comprises more than 80 sequences in amphibians, fish, birds and mammals, and some of the members of this family in mammals are of recent origin (Boraschi, 2022; Huising et al., 2004; Scapigliati et al., 2007). It is characterised by a b-trefoil barrel structure, common to molecules with different defence and recognition activities found throughout the living kingdom (Hatakeyama et al., 2007; Heuck et al., 2001; Kaus and Olson, 2014; Murzin et al., 1992; Varki et al., 2022).

Immunocytochemistry with antibodies against mammalian interleukin-1 gave positive responses with lymphocyte-like cells, granular amoebocytes of ascidians and fractionated coelomic fluid, as well as cell extracts of starfish and molluscs (Beck et al., 1993a; Ottaviani et al., 1995; Ottaviani and Franceschi, 1998). IL-1β also stimulated haemocyte proliferation in ascidians and molluscs under *in vitro* conditions (Ottaviani et al., 1995). But it has also been shown that in echinoderms IL-1 is responsible for the production of fibroblasts, stimulates protein synthesis and the production of Prostaglandin E_2 characteristic of vertebrate interleukin-1 (Beck and Habicht, 1991; Habicht et al., 1985). In addition to showing cytotoxic activity towards human melanoma cell line A375, also common in vertebrates (Nakai et al., 1988). This is in line with what has been observed in this work if one observes the interleukin trend studied by dot-blot and the expression of collagen evidenced by q/RT-PCR, which at 20 °C mirrors what has already been observed by histological analysis in previous studies (La Corte et al., 2023; Parisi et al., 2021). Interestingly, the IL-1β trend remains more or less constant at 27 °C except at 3 days, with a lower measured IDV compared to the control temperature, but also collagen production is inhibited as a result of the temperature increase.

The results therefore show that molecules attributable to the interleukin-1 family and the Toll receptor family conservation (O'Neill and Dinarello, 2000; Parisi et al., 2022) are present in invertebrates. In any case, phylogenetic analyses of these two superfamilies suggest independent evolution between vertebrates and invertebrates (Beschin et al., 2001, 1999).

From the considerations found in the literature, it is clear that due to the lack of molecular information and orthologous IL-1- like genes in clades close to vertebrates, it would appear that in the first ones, its functions are performed by different molecules (Beck, 1998; Beck

et al., 1993b; Beschin et al., 2001; Raftos, 1996). Nevertheless, several IL-1R-like orthologous genes have been characterised in *Cnidaria*, *Protostomia* and *Deuterostomia*, implying important functions not yet identified (Watkins and Maier, 2002; Weigent and Blalock, 1995). As far as PCNA is concerned, molecular analysis showed an increase in cell proliferation at 24 hours and at 7 days at 20° C, which can be correlated with the production of gland cells and granulocytes at 24 hours with the task of eliminating dead cells and remaining pathogens, and at 7 days a new increase could be attributable to the final maturation of the reformed epithelial tissue (La Corte et al., 2023). The 6-hour increase in PCNA expression at 27 °C could indicate an attempt to produce useful cells to close the wound and begin the restoration of lost tissue, but the markedly lower expression levels at 20 °C and the downregulation at 24h and 3d could be indicative of a shift in metabolic energies towards the production of other molecules that might first ensure the animal's survival, considering that the regenerative event is a metabolically intensive process.

Cnidarians are among the most striking examples of symbiosis in the aquatic environment. Symbiosis allows these and other organisms to have a greater availability of nutrients and carbon in oligotrophic waters and also protection from UV radiation. At the same time, however, they make them susceptible to photosynthetic stress, and the symbiosis is the first to suffer under other stressful conditions (Brown, 1997; O. Hoegh-Guldberg, 1999). This represents an opportunity in the rapid assessment of the health status of these organisms by exploiting fluorescence techniques that investigate chlorophyll *a*. Zooxanthallae photosynthetic state may be utilised as a proxy for the overall health of the holobiont.

Photosynthetic stresses include abiotic factors such as high irradiance, changes in temperature and salinity, pollution (Brown, B. E., et al., 2000; Hill et al., 2004; Hill and Ralph, 2006; Hoegh-Guldberg and Smith, 1989; Jones and Kerswell, 2003; Saxby et al., 2003; Warner et al., 1996). For this reason, pulse amplitude modulated (PAM) fluorometry is a valuable tool even under conditions of multiple stressors for early monitoring and assessment of the health status of the symbiont and holobiont in a non-invasive manner, even before other status indicators are evident (e.g. reduced reproductive capacity, symbiont or tissue loss) (Bruckner, 2015; Roff et al., 2008). Chlorophyll *a*, *c2*, and a variety of accessory pigments are found in *Symbiodinium* cells. The chlorophyll a pigment complex in *Symbiodinium* absorbs light at 440 and 678 nm. Carotenoids and other accessory pigments broaden the wavelength range that may be absorbed. Several studies have reinforced the idea

that acclimatisation can increase thermal tolerance in Cnidarians. Indeed, it has been shown that organisms in natural conditions when subjected to a thermal increase have a higher tolerance than conspecifics living in more stable conditions (Castillo and Helmuth, 2005; Oliver and Palumbi, 2011) and further, that under such conditions, bleaching also occurs less severely when exposed to thermal stress (Bay and Palumbi, 2015; Middlebrook et al., 2008). Here, consistent with this, by means of PAM we investigated the health of sea anemones under multiple stress conditions (temperature - regeneration) by exploiting the presence of the symbiont. In accordance with histological evidence (La Corte et al., 2023), a decrease in photosynthetic efficiency was measured at 6h and 1 day after cutting with values reaching the time of cutting (T0), this could be correlated with the expulsion of the zooxanthellae, the loss of functionality due to the dual stressogenic effect and the occurrence of oxidative stress clearly evidenced by the other markers examined.

CONCLUSIONS

In this work, biometric measures and a molecular approach were used to investigate the regenerative event under constitutive conditions and following thermal stress in the Mediterranean anemone *A. viridis*. The results showed a significant difference between the treatments at different temperatures, indicating two critical moments during the process, i.e. 6 hours and one day after cutting. The analyses also showed changes in the functionality of the symbiont as well as the activation of pathways and an up/down regulation of molecules to counteract the imposed stress. The subject is extremely complex and further investigations, such as an in-depth analysis of the transcriptome at these experimental times, a study of the resilience capacity might be desirable in order to have a clear map of the whole event and provide information on the breakdown point of the animal also in relation to populations belonging to different areas.

REFERENCES

Ahmad, R., Tripathi, A.K., Tripathi, P., Singh, R., Singh, S., Singh, R.K., 2010. Studies on lipid peroxidation and non-enzymatic antioxidant status as indices of oxidative stress in patients with chronic myeloid leukaemia. Singapore Med. J. 51, 110–115.

Ahmad, R., Tripathi, A.K., Tripathi, P., Singh, S., Singh, R., Singh, R.K., 2008. Malondialdehyde and protein carbonyl as biomarkers for oxidative stress and disease progression in patients with chronic myeloid leukemia. In Vivo 22, 525–528.

Barrera, G., Pizzimenti, S., Daga, M., Dianzani, C., Arcaro, A., Cetrangolo, G.P., Giordano, G., Cucci, M.A., Graf, M., Gentile, F., 2018. Lipid Peroxidation-Derived Aldehydes, 4-Hydroxynonenal and Malondialdehyde in Aging-Related Disorders. Antioxidants. https://doi.org/10.3390/antiox7080102

Battisti, V., Maders, L.D.K., Bagatini, M.D., Santos, K.F., Spanevello, R.M., Maldonado, P.A., Brulé, A.O., do Carmo Araújo, M., Schetinger, M.R.C., Morsch, V.M., 2008. Measurement of oxidative stress and antioxidant status in acute lymphoblastic leukemia patients. Clin. Biochem. 41, 511–518.

Bay, R.A., Palumbi, S.R., 2015. Rapid Acclimation Ability Mediated by Transcriptome Changes in Reef-Building Corals. Genome Biol. Evol. 7, 1602–1612. https://doi.org/10.1093/gbe/evv085

Beck, G., 1998. Macrokines:invertebrate cytokine-like molecules? Front. Biosci. 3, 559–569. https://doi.org/10.2741/A303/PDF

Beck, G., Habicht, G.S., 1991. Purification and Biochemical of an Invertebrate. Mol. Immunol. 28, 577–584.

Beck, G., O'Brien, R.F., Habicht, G.S., Stillman, D.L., Cooper, E.L., Raftos, D.A., 1993a. Invertebrate cytokines. III: Invertebrate interleukin-1-like molecules stimulate phagocytosis by tunicate and echinoderm cells. Cell. Immunol. 146, 284–299. https://doi.org/10.1006/CIMM.1993.1027

Beck, G., O'Brien, R.F., Habicht, G.S., Stillman, D.L., Cooper, E.L., Raftos, D.A., 1993b. Invertebrate Cytokines III: Invertebrate Interleukin-1-like Molecules Stimulate Phagocytosis by Tunicate and Echinoderm Cells. Cell. Immunol. 146, 284–299. https://doi.org/10.1006/CIMM.1993.1027

Beschin, A., Bilej, M., Brys, L., Torreele, E., Lucas, R., Magez, S., De Baetselier, P., 1999. Convergent evolution of cytokines. Nature 400, 627–628. https://doi.org/10.1038/23164

Beschin, A., Bilej, M., Torreele, E., De Baetselier, P., 2001. On the existence of cytokines in invertebrates. Cell. Mol. Life Sci. 58, 801–814. https://doi.org/10.1007/PL00000901

Boraschi, D., 2022. What Is IL-1 for? The Functions of Interleukin-1 Across Evolution. Front. Immunol. 13, 1–12. https://doi.org/10.3389/fimmu.2022.872155

Brown, B. E., Dunne, R. P., Warner, M. E., Ambarsari, I., Fitt, W. K., Gibb, S. W., & Cummings, D.G., 2000. Damage and recovery of Photosystem II during a manipulative field experiment on solar bleaching in the coral *Goniastrea aspera*. arine Ecol. Prog. Ser. 195, 117–124.

Brown, B.E., 1997. Coral bleaching: Causes and consequences. Coral Reefs 16, S129–S138. https://doi.org/10.1007/S003380050249/METRICS

Bruckner, A.W., 2015. History of Coral Disease Research, Diseases of Coral. https://doi.org/10.1002/9781118828502.ch5

Buss, H., Chan, T.P., Sluis, K.B., Domigan, N.M., Winterbourn, C.C., 1997. Protein carbonyl measurement by a sensitive ELISA method. Free Radic. Biol. Med. 23, 361–366. https://doi.org/10.1016/S0891-5849(97)00104-4

Butterfield, D.A., Reed, T., Newman, S.F., Sultana, R., 2007. Roles of amyloid β-peptide-associated oxidative stress and brain protein modifications in the pathogenesis of Alzheimer's disease and mild cognitive impairment. Free Radic. Biol. Med. 43, 658–677. https://doi.org/https://doi.org/10.1016/j.freeradbiomed.2007.05.037

Castillo, K.D., Helmuth, B.S.T., 2005. Influence of thermal history on the response of Montastraea annularis to short-term temperature exposure. Mar. Biol. 148, 261–270. https://doi.org/10.1007/S00227-005-0046-X

Cecarini, V., Gee, J., Fioretti, E., Amici, M., Angeletti, M., Eleuteri, A.M., Keller, J.N., 2007. Protein oxidation and cellular homeostasis: Emphasis on metabolism. Biochim. Biophys. Acta - Mol. Cell Res. 1773, 93–104. https://doi.org/https://doi.org/10.1016/j.bbamcr.2006.08.039

Chomsky, O., Kamenir, Y., Hyams, M., Dubinsky, Z., Chadwick-Furman, N.E., 2004.

Effects of temperature on growth rate and body size in the Mediterranean Sea anemone *Actinia equina*. J. Exp. Mar. Bio. Ecol. 313, 63–73. https://doi.org/10.1016/j.jembe.2004.07.017

Dalle-Donne, I., Giustarini, D., Colombo, R., Rossi, R., Milzani, A., 2003. Protein carbonylation in human diseases. Trends Mol. Med. 9, 169–176.

Desalvo, M.K., Voolstra, C.R., Sunagawa, S., Schwarz, J.A., Stillman, J.H., Coffroth, M.A., Szmant, A.M., Medina, M., 2008. Differential gene expression during thermal stress and bleaching in the Caribbean coral *Montastraea faveolata*. Mol. Ecol. 17, 3952–3971. https://doi.org/10.1111/J.1365-294X.2008.03879.X

Downs, C.A., Fauth, J.E., Halas, J.C., Dustam, P., Bemiss, J., Woodley, C.M., 2002. Oxidative Stress and Seasonal Coral Bleaching. Free Radic. Biol. Med. 33, 533–543.

Echeverría, P.C., Bernthaler, A., Dupuis, P., Mayer, B., Picard, D., 2011. An interaction network predicted from public data as a discovery tool: Application to the Hsp90 molecular chaperone machine. PLoS One 6. https://doi.org/10.1371/journal.pone.0026044

Fang, L., Huang, S., Lin, K., 1997. High temperature induces the synthesis of heat-shock proteins and the elevation of intracellular calcium in the coral *Acropora grandis*. Coral Reefs 16, 127–131. https://doi.org/10.1007/s003380050066

Fedorova, M., Bollineni, R.C., Hoffmann, R., 2014. Protein carbonylation as a major hallmark of oxidative damage: Update of analytical strategies. Mass Spectrom. Rev. 33, 79–97. https://doi.org/10.1002/MAS.21381

Gates, R.D., Eomund, P.J., 1999. The physiological mechanisms of acclimatization in tropical reef corals. Am. Zool. 39, 30–43. https://doi.org/10.1093/icb/39.1.30

Habicht, G.S., Beck, G., Benach, J.L., Coleman, J.L., Leichtling, K.D., 1985. Lyme disease spirochetes induce human and murine interleukin 1 production. J. Immunol. (Baltimore, Md. 1950) 134, 3147–3154.

Hansson, L.J., 1997. Effect of temperature on growth rate of *Aurelia aurita* (Cnidaria, Scyphozoa) from Gullmarsfjorden, Sweden. Mar. Ecol. Prog. Ser. Mar Ecol Prog Ser 161, 145–153.

Hatakeyama, T., Unno, H., Kouzuma, Y., Uchida, T., Eto, S., Hidemura, H., Kato, N.,

Yonekura, M., Kusunoki, M., 2007. C-type lectin-like carbohydrate recognition of the hemolytic lectin CEL-III containing ricin-type β-trefoil folds. J. Biol. Chem. 282, 37826–37835. https://doi.org/10.1074/jbc.M705604200

Henry, L.-A., Hart, M., 2005. Regeneration from injury and resource allocation in sponges and corals - A review. Int. Rev. Hydrobiol. 90, 125–158. https://doi.org/10.1002/iroh.200410759

Heuck, A.P., Tweten, R.K., Johnson, A.E., 2001. β-Barrel pore-forming toxins: Intriguing dimorphic proteins. Biochemistry 40, 9065–9073. https://doi.org/10.1021/BI0155394/ASSET/BI0155394.FP.PNG_V03

Hill, R., Larkum, A.W.D., Frankart, C., Kühl, M., Ralph, P.J., 2004. Loss of Functional Photosystem II Reaction Centres in Zooxanthellae of Corals Exposed to Bleaching Conditions: Using Fluorescence Rise Kinetics. Photosynth. Res. 82, 59–72. https://doi.org/10.1023/B:PRES.0000040444.41179.09

Hill, R., Ralph, P.J., 2006. Photosystem II heterogeneity of in hospite zooxanthellae in scleractinian corals exposed to bleaching conditions. Photochem. Photobiol. 82, 1577. https://doi.org/10.1562/2006-04-13-RA-871

Hoegh-Guldberg, O., 1999. Climate Change, coral bleaching and the future of the world' s coral reefs. Ove Hoegh-Guldberg. Mar. Freshw. Res. 50, 839–866.

Hoegh-Guldberg, Ove, 1999. Climate change, coral bleaching and the future of the world's coral reefs. Mar. Freshw. Res. 50, 839–866. https://doi.org/10.1071/MF99078

Hoegh-Guldberg, O., Smith, G.J., 1989. The effect of sudden changes in temperature, light and salinity on the population density and export of zooxanthellae from the reef corals *Stylophora pistillata* Esper and Seriatopora hystrix Dana. J. Exp. Mar. Bio. Ecol. 129, 279–303. https://doi.org/10.1016/0022-0981(89)90109-3

Huising, M.O., Stet, R.J.M., Savelkoul, H.F.J., Verburg-Van Kemenade, B.M.L., 2004. The molecular evolution of the Interleukin-1 family of cytokines; IL-18 in teleost fish. Dev. Comp. Immunol. 28, 395–413. https://doi.org/10.1016/J.DCI.2003.09.005

Iglesias-Prieto, R., 1997. Temperature-dependent inactivation of photosystem II in symbiotic dinoflagellates, in: Proc 8th Int Coral Reef Symp. pp. 1313–1318.

Jones, R.J., Hoegh-Guldberg, O., 2001. Diurnal changes in the photochemical efficiency of

the symbiotic dinoflagellates (Dinophyceae) of corals: Photoprotection, photoinactivation and the relationship to coral bleaching. Plant, Cell Environ. 24, 89–99. https://doi.org/10.1046/j.1365-3040.2001.00648.x

Jones, R.J., Kerswell, A.P., 2003. Phytotoxicity of Photosystem II (PSII) herbicides to coral. Mar. Ecol. Prog. Ser. 261, 149–159. https://doi.org/10.3354/MEPS261149

Kaus, K., Olson, R., 2014. Structure and Glycan-Binding Properties of the *Vibrio vulnificus* Hemolysin B-Trefoil Lectin. Biophys. J. 106, 87a. https://doi.org/10.1016/j.bpj.2013.11.555

Kenkel, C.D., Aglyamova, G., Alamaru, A., Bhagooli, R., Capper, R., Cunning, R., deVillers, A., Haslun, J.A., Hédouin, L., Keshavmurthy, S., Kuehl, K.A., Mahmoud, H., McGinty, E.S., Montoya-Maya, P.H., Palmer, C. V., Pantile, R., Sánchez, J.A., Schils, T., Silverstein, R.N., Squiers, L.B., Tang, P.C., Goulet, T.L., Matz, M. V., 2011. Development of Gene Expression Markers of Acute Heat-Light Stress in Reef-Building Corals of the Genus Porites. PLoS One 6, e26914. https://doi.org/10.1371/JOURNAL.PONE.0026914

La Corte, C., Baranzini, N., Dara, M., Bon, C., Grimaldi, A., Parisi, M.G., Zizzo, M.G., Cammarata, M., 2023. Step-by-Step Regeneration of Tentacles after Injury in *Anemonia viridis*—Morphological and Structural Cell Analyses. Int. J. Mol. Sci. 24, 8860. https://doi.org/10.3390/ijms24108860

Laemmli, U.K., 1970. Cleavage of Structural Proteins during the Assembly of the Head of Bacteriophage T4. Nature 227, 680–685. https://doi.org/10.1038/227680a0

Leggat, W., Seneca, F., Wasmund, K., Ukani, L., Yellowlees, D., Ainsworth, T.D., 2011. Differential Responses of the Coral Host and Their Algal Symbiont to Thermal Stress. PLoS One 6, e26687. https://doi.org/10.1371/JOURNAL.PONE.0026687

Lesser, M.P., 2006. Oxidative stress in marine environments: biochemistry and physiological ecology. Annu. Rev. Physiol. 68, 253–278. https://doi.org/10.1146/annurev.physiol.68.040104.110001

Levine, R.L., Williams, J.A., Stadtman, E.P., Shacter, E., 1994. Carbonyl assays for determination of oxidatively modified proteins. Methods Enzymol. 233, 346–357. https://doi.org/10.1016/S0076-6879(94)33040-9

Li, Z., Srivastava, P., 2003. Heat-Shock Proteins. Curr. Protoc. Immunol. 58, A.1T.1-

A.1T.6. https://doi.org/10.1002/0471142735.IMA01TS58

Linares, M., Marín-García, P., Méndez, D., Puyet, A., Diez, A., Bautista, J.M., 2011. Proteomic approaches to identifying carbonylated proteins in brain tissue. J. Proteome Res. 10, 1719–1727. https://doi.org/10.1021/PR101014E/ASSET/IMAGES/MEDIUM/PR-2010-01014E_0004.GIF

Louis, Y.D., Bhagooli, R., Kenkel, C.D., Baker, A.C., Dyall, S.D., 2017. Gene expression biomarkers of heat stress in scleractinian corals: Promises and limitations. Comp. Biochem. Physiol. Part - C Toxicol. Pharmacol. 191, 63–77. https://doi.org/10.1016/j.cbpc.2016.08.007

Maga, G., Hübscher, U., 2003. Proliferating cell nuclear antigen (PCNA): A dancer with many partners. J. Cell Sci. 116, 3051–3060. https://doi.org/10.1242/jcs.00653

Maynard, J.A., Anthony, K.R.N., Marshall, P.A., Masiri, I., 2008. Major bleaching events can lead to increased thermal tolerance in corals. Mar. Biol. 155, 173–182. https://doi.org/10.1007/s00227-008-1015-y

Meyer, E., Aglyamova, G. V., Matz, M. V., 2011. Profiling gene expression responses of coral larvae (*Acropora millepora*) to elevated temperature and settlement inducers using a novel RNA-Seq procedure. Mol. Ecol. 20, 3599–3616. https://doi.org/10.1111/J.1365-294X.2011.05205.X

Middlebrook, R., Hoegh-Guldberg, O., Leggat, W., 2008. The effect of thermal history on the susceptibility of reef-building corals to thermal stress. J. Exp. Biol. 211, 1050–1056. https://doi.org/10.1242/JEB.013284

Murzin, A.G., Lesk, A.M., Chothia, C., 1992. beta-Trefoil fold. Patterns of structure and sequence in the Kunitz inhibitors interleukins-1 beta and 1 alpha and fibroblast growth factors. J. Mol. Biol. 223, 531–543. https://doi.org/10.1016/0022-2836(92)90668-A

Mydlarz, L.D., Jones, L.E., Harvell, C.D., 2006. Innate Immunity, Environmental Drivers, and Disease Ecology of Marine and Freshwater Invertebrates. Annu. Rev. Ecol. Evol. Syst. 37, 251–288. https://doi.org/10.1146/annurev.ecolsys.37.091305.110103

Naguib, Y.M.A., 2000. A fluorometric method for measurement of oxygen radical-scavenging activity of water-soluble antioxidants. Anal. Biochem. 284, 93–98. https://doi.org/10.1006/abio.2000.4691

Nakai, S., Mizuno, K., Kaneta, M., Hirai, Y., 1988. A simple, sensitive bioassay for the detection of interleukin-1 using human melanoma A375 cell line. Biochem. Biophys. Res. Commun. 154, 1189–1196. https://doi.org/10.1016/0006-291X(88)90266-5

O'Neill, L.A.J., Dinarello, C.A., 2000. The IL-1 receptor/toll-like receptor superfamily: crucial receptors for inflammation and host defense. Immunol. Today 21, 206–209. https://doi.org/10.1016/S0167-5699(00)01611-X

Oliver, T.A., Palumbi, S.R., 2011. Do fluctuating temperature environments elevate coral thermal tolerance? Coral Reefs 30, 429–440. https://doi.org/10.1007/S00338-011-0721-Y/FIGURES/5

Ottaviani, E., Caselgrandi, E., Franceschi, C., 1995. Cytokines and evolution: in vitro effects of IL-1 alpha, IL-1 beta, TNF-alpha and TNF-beta on an ancestral type of stress response. Biochem. Biophys. Res. Commun. 207, 288–292. https://doi.org/10.1006/BBRC.1995.1185

Ottaviani, E., Franceschi, C., 1998. A new theory on the common evolutionary origin of natural immunity, inflammation and stress response: the invertebrate phagocytic immunocyte as an eye-witness. Domest. Anim. Endocrinol. 15, 291–296. https://doi.org/10.1016/S0739-7240(98)00021-6

Parisi, M.G., Baranzini, N., Dara, M., Corte, C. La, Vizioli, J., Cammarata, M., 2022. AIF-1 and RNASET2 are involved in the inflammatory response in the Mediterranean mussel *Mytilus galloprovincialis* following *Vibrio* infection. Fish Shellfish Immunol. 127, 109–118. https://doi.org/10.1016/j.fsi.2022.06.010

Parisi, M.G., Grimaldi, A., Baranzini, N., La Corte, C., Dara, M., Parrinello, D., Cammarata, M., 2021. Mesoglea extracellular matrix reorganization during regenerative process in *Anemonia viridis* (Forskål, 1775). Int. J. Mol. Sci. 22. https://doi.org/10.3390/ijms22115971

Pey, A., Zamoum, T., Christen, R., Merle, P.L., Furla, P., 2017. Characterization of glutathione peroxidase diversity in the symbiotic sea anemone *Anemonia viridis*. Biochimie 132, 94–101. https://doi.org/10.1016/j.biochi.2016.10.016

Raftos, D., 1996. Interactions of tunicate immunomodulatory proteins with mammalian cells. Immunol. Cell Biol. 74, 26–31. https://doi.org/10.1038/ICB.1996.3

Regoli, F., Cerrano, C., Chierici, E., Bompadre, S., Bavestrello, G., 2000. Susceptibility to

oxidative stress of the Mediterranean demosponge *Petrosia ficiformis*: role of endosymbionts and solar irradiance. Mar. Biol. 137, 453–461.

Richier, S., Furla, P., Plantivaux, A., Merle, P.-L., Allemand, D., 2005. Symbiosis-induced adaptation to oxidative stress. J. Exp. Biol. 208, 277–285. https://doi.org/10.1242/jeb.01368

Richier, S., Merle, P.-L., Furla, P., Pigozzi, D., Sola, F., Allemand, D., 2003. Characterization of superoxide dismutases in anoxia-and hyperoxia-tolerant symbiotic cnidarians. Biochim. Biophys. Acta (BBA)-General Subj. 1621, 84–91.

Richier, S., Sabourault, C., Courtiade, J., Zucchini, N., Allemand, D., Furla, P., 2006. Oxidative stress and apoptotic events during thermal stress in the symbiotic sea anemone, *Anemonia viridis*. FEBS J. 273, 4186–4198. https://doi.org/10.1111/j.1742-4658.2006.05414.x

Rodríguez-García, A., García-Vicente, R., Morales, M.L., Ortiz-Ruiz, A., Martínez-López, J., Linares, M., 2020. Protein carbonylation and lipid peroxidation in hematological malignancies. Antioxidants 9, 1–30. https://doi.org/10.3390/antiox9121212

Rodriguez-Lanetty, M., Harii, S., Hoegh-Guldberg, O., 2009. Early molecular responses of coral larvae to hyperthermal stress. Mol. Ecol. 18, 5101–5114. https://doi.org/10.1111/J.1365-294X.2009.04419.X

Roff, G., Ulstrup, K.E., Fine, M., Ralph, P.J., Hoegh-Guldberg, O., 2008. Spatial heterogeneity of photosynthetic activity within diseased corals from the Great Barrier Reef. J. Phycol. 44, 526–538. https://doi.org/10.1111/J.1529-8817.2008.00480.X

Rosic, N.N., Pernice, M., Dove, S., Dunn, S., Hoegh-Guldberg, O., 2011. Gene expression profiles of cytosolic heat shock proteins Hsp70 and Hsp90 from symbiotic dinoflagellates in response to thermal stress: Possible implications for coral bleaching. Cell Stress Chaperones 16, 69–80. https://doi.org/10.1007/s12192-010-0222-x

Sabourault, C., Ganot, P., Deleury, E., Allemand, D., Furla, P., 2009. Comprehensive EST analysis of the symbiotic sea anemone, *Anemonia viridis*. BMC Genomics 10, 333. https://doi.org/10.1186/1471-2164-10-333

Saxby, T., Dennison, W.C., Hoegh-Guldberg, O., 2003. Photosynthetic responses of the coral *Montipora digitata* to cold temperature stress. Mar. Ecol. Prog. Ser. 248, 85–97. https://doi.org/10.3354/MEPS248085

Scapigliati, G., Buonocore, F., Mazzini, M., 2007. Biological Activity of Cytokines: An Evolutionary Perspective. Curr. Pharm. Des. 12, 3071–3081. https://doi.org/10.2174/138161206777947489

Schmitt, E., Gehrmann, M., Brunet, M., Multhoff, G., Garrido, C., 2007. Intracellular and extracellular functions of heat shock proteins: repercussions in cancer therapy. J. Leukoc. Biol. 81, 15–27. https://doi.org/10.1189/JLB.0306167

Sharp, V.A.A., Miller, D., Bythell, J.C.C., Brown, B.E.E., 1994. Expression of low molecular weight HSP 70 related polypeptides from the symbiotic sea anemone *Anemonia viridis* Forskall in response to heat shock. J. Exp. Mar. Bio. Ecol. 179, 179–193. https://doi.org/10.1016/0022-0981(94)90113-9

Sies, H., 2017. Hydrogen peroxide as a central redox signaling molecule in physiological oxidative stress: Oxidative eustress. Redox Biol. 11, 613–619.

Singh, R.K., Tripathi, A.K., Tripathi, P., Singh, S., Singh, R., Ahmad, R., 2009. Studies on biomarkers for oxidative stress in patients with chronic myeloid leukemia. Hematol. Oncol. Stem Cell Ther. 2, 285–288.

Takahashi, S., Murata, N., 2008. How do environmental stresses accelerate photoinhibition? Trends Plant Sci. 13, 178–182. https://doi.org/10.1016/j.tplants.2008.01.005

Tolleter, D., Seneca, F.O., Denofrio, J.C., Krediet, C.J., Palumbi, S.R., Pringle, J.R., Grossman, A.R., 2013. Coral bleaching independent of photosynthetic activity. Curr. Biol. 23, 1782–1786. https://doi.org/10.1016/j.cub.2013.07.041

Traylor-Knowles, N., 2019. Heat stress compromises epithelial integrity in the coral, *Acropora hyacinthus*. PeerJ 2019. https://doi.org/10.7717/peerj.6510

Varki, A., Cummings, R.D., Esko, J.D., Stanley, P., Hart, G.W., Aebi, M., Mohnen, D., Kinoshita, T., Packer, N.H., Prestegard, J.H., Schnaar, R.L., Seeberger, P.H., 2022. Essentials of Glycobiology. Cold Spring Harb. 823. https://doi.org/10.1101/9781621824213

Venn, A.A., Quinn, J., Jones, R., Bodnar, A., 2009. P-glycoprotein (multi-xenobiotic resistance) and heat shock protein gene expression in the reef coral *Montastraea franksi* in response to environmental toxicants. Aquat. Toxicol. 93, 188–195. https://doi.org/10.1016/J.AQUATOX.2009.05.003

Walsh, P.J., Somero, G.N., 1981. Temperature adaptation in sea anemones: Physiological and biochemical variability in geographically separate populations of *Metridium senile*. Mar. Biol. 62, 25–34. https://doi.org/10.1007/BF00396948

Warner, M.E., Fitt, W.K., Schmidt, G.W., 1996. The effects of elevated temperature on the photosynthetic efficiency of zooxanthellae in hospite from four different species of reef coral: a novel approach. Plant. Cell Environ. 19, 291–299. https://doi.org/10.1111/J.1365-3040.1996.TB00251.X

Watkins, L.R., Maier, S.F., 2002. Beyond neurons: evidence that immune and glial cells contribute to pathological pain states. Physiol. Rev. 82, 981–1011. https://doi.org/10.1152/PHYSREV.00011.2002

Weigent, D.A., Blalock, J.E., 1995. Associations between the neuroendocrine and immune systems. J. Leukoc. Biol. 58, 137–150. https://doi.org/10.1002/JLB.58.2.137

SUPPLEMENTARY MATERIALS

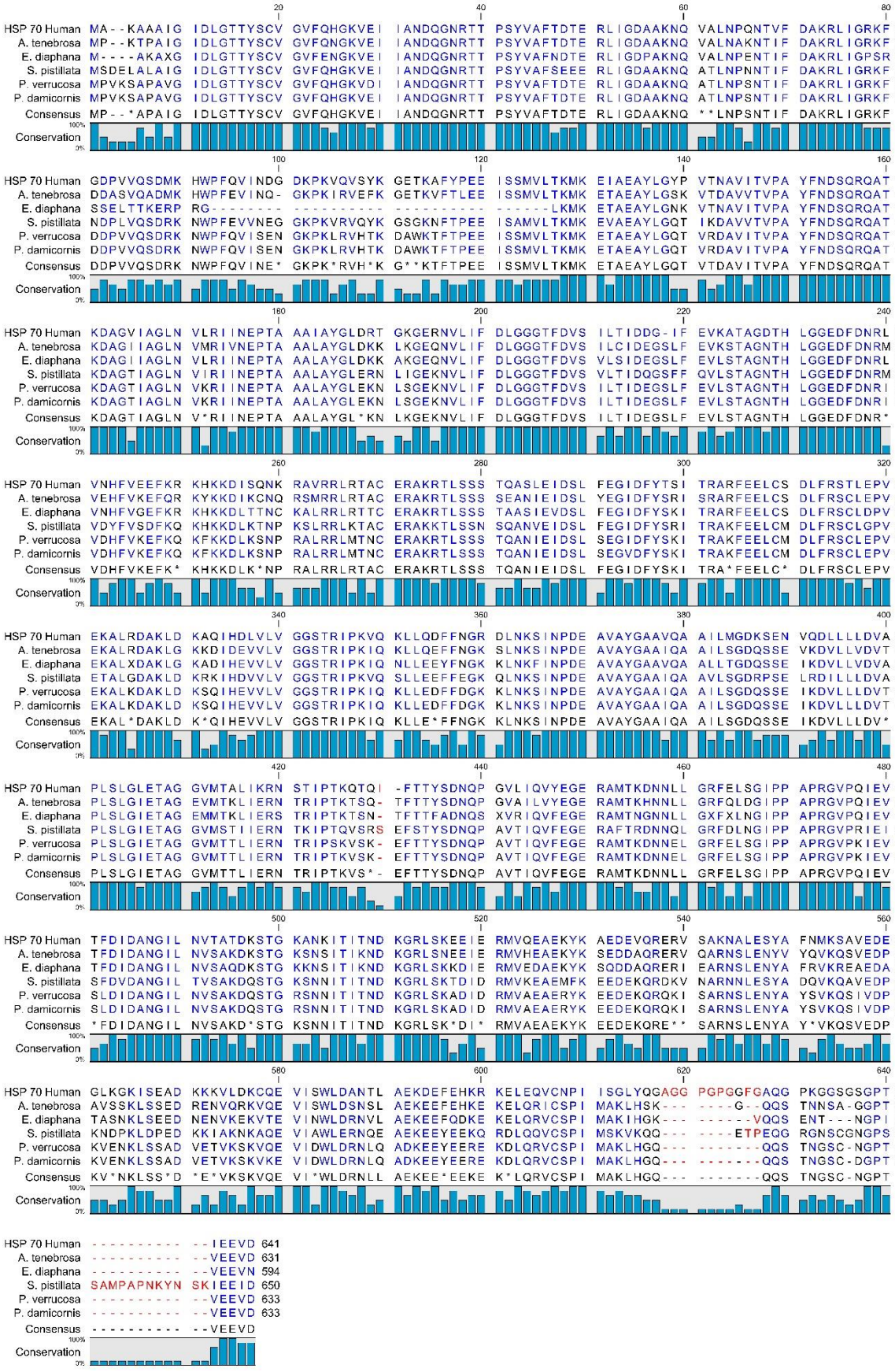

Figure A. HSP70 Multiple alignment.

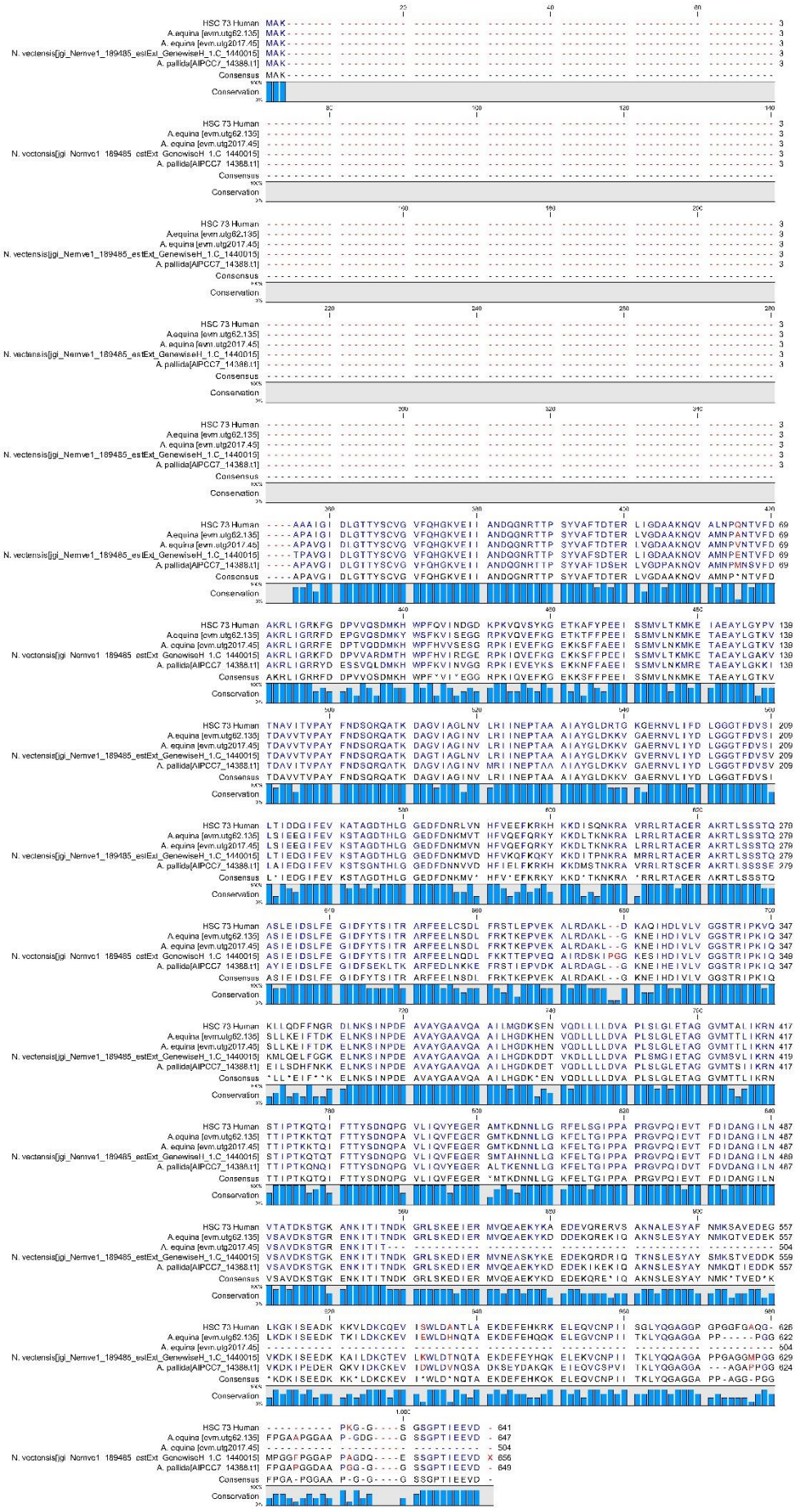

Figure B. HSC73 Multiple alignment.

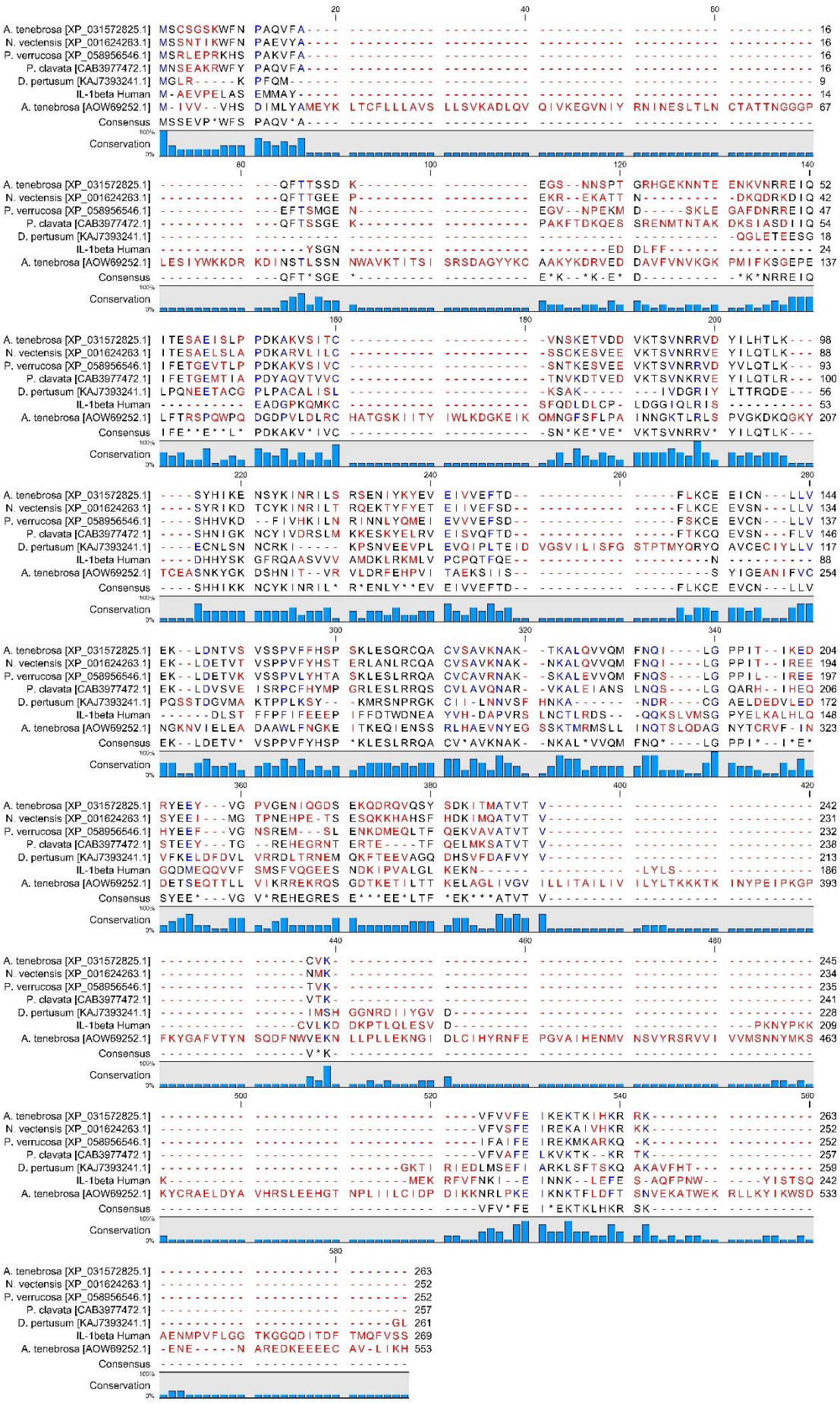

Figure C. IL-1β Multiple alignment.

```
#  Percent Identity  Matrix - created by Clustal2.1 HSP70
#
#

     1: HSP 70 Human     100.00   70.35   73.33   73.33   76.35   72.01
     2: AAF12746.1        70.35  100.00   78.20   78.20   71.95   68.69
     3: XP_027037242.1    73.33   78.20  100.00   99.21   79.05   75.72
     4: XP_058956776.1    73.33   78.20   99.21  100.00   79.05   75.72
     5: XP_031569577.1    76.35   71.95   79.05   79.05  100.00   79.46
     6: KXJ16950.1        72.01   68.69   75.72   75.72   79.46  100.00


2. S. pistillata
3. P. damicornis
4. P. verrucosa
5. A. tenebrosa
6. E. diaphana



#  Percent Identity  Matrix - created by Clustal2.1 IL-1B
#
#
1: sp|P01584|IL1B_HUMAN  100.00   15.52   16.67   20.61   20.77   21.37   16.03
2: KAJ7393241.1           15.52  100.00   18.18   17.86   19.88   20.83   16.07
3: AOW69252.1             16.67   18.18  100.00   15.28   17.43   16.96   15.32
4: CAB3977472.1           20.61   17.86   15.28  100.00   46.15   44.71   44.49
5: XP_058956546.1         20.77   19.88   17.43   46.15  100.00   57.54   55.47
6: XP_031572825.1         21.37   20.83   16.96   44.71   57.54  100.00   64.29
7: XP_001624263.1         16.03   16.07   15.32   44.49   55.47   64.29  100.00


2. D. pertusum
3. A. tenebrosa
4. P. clavata
5. P. verrucosa
6. A. tenebrosa
7. N. vectensis



# Percent Identity  Matrix - created by Clustal2.1 HSC73
#
#
1: HSC_73_Human          100.00   76.56   76.65   83.93   79.56
2: adi_v1.04788           76.56  100.00   77.15   84.13   77.76
3: AIPCC7_14388.t1        76.65   77.15  100.00   84.33   77.97
4: evm.utg2017.45         83.93   84.13   84.33  100.00   87.50
5: jgi_Nemve1_189485_     79.56   77.76   77.97   87.50  100.00
estExt_GenewiseH_1.C_1440015

2. N._vectensis
3. A._pallida
4. A. equina
5. N. vectensis
```

Figure D. Percent Identity Matrix of aligned sequences.

PCNA	Summary	Adjusted P Value
CNT vs. 6H	ns	0.9637
CNT vs. 24H	ns	0.5723
CNT vs. 3D	ns	0.9996
CNT vs. 7D	**	0.0012
6H vs. 24H	ns	0.2681
6H vs. 3D	ns	0.9903
6H vs. 7D	***	0.0006
24H vs. 3D	ns	0.4634
24H vs. 7D	**	0.0025
3D vs. 7D	***	0.0010

HSP90	q Value	Individual P Value
CNT vs. 6H	0.3206	0.2714
CNT vs. 24H	0.0442	0.0047
CNT vs. 3D	0.3206	0.2630
CNT vs. 7D	0.2314	0.0979
6H vs. 24H	0.9311	0.9852
6H vs. 3D	0.3206	0.2027
6H vs. 7D	0.3690	0.3515
24H vs. 3D	0.1654	0.0350
24H vs. 7D	0.3206	0.2685
3D vs. 7D	0.2144	0.0680

Figure E. Statistical analyses on PCNA and HSP90 expression levels. The ANOVA tables are related to the 20 °C treatment. Differences between means were considered significant for $p < 0.05$. Significant differences detected by Tukey post hoc test— $p < 0.05$, ** $p < 0.01$, *** $p < 0.0001$.*

CDC37	Summary	Adjusted P Value
CNT vs. 6H	ns	0.9966
CNT vs. 24H	ns	0.9825
CNT vs. 3D	**	0.0032
CNT vs. 7D	**	0.0045
6H vs. 24H	ns	0.8946
6H vs. 3D	**	0.0025
6H vs. 7D	**	0.0035
24H vs. 3D	**	0.0029
24H vs. 7D	**	0.0043
3D vs. 7D	ns	0.9899

COL24A1	Summary	Adjusted P Value
CNT vs. 6H	*	0.0266
CNT vs. 24H	ns	0.2509
CNT vs. 3D	ns	0.2109
CNT vs. 7D	*	0.0118
6H vs. 24H	ns	0.3634
6H vs. 3D	**	0.0028
6H vs. 7D	***	0.0004
24H vs. 3D	*	0.0163
24H vs. 7D	**	0.0015
3D vs. 7D	ns	0.2236

Figure F. Statistical analyses on CDC37 and COL24A1 expression levels. The ANOVA tables are related to the 20 °C treatment. Differences between means were considered significant for $p < 0.05$. Significant differences detected by Tukey post hoc test— $p < 0.05$, ** $p < 0.01$, *** $p < 0.0001$.*

PCNA	q Value	Adjusted P Value
CNT vs. 6H	0.0018	0.0006
CNT vs. 24H	0.0614	0.0974
CNT vs. 3D	0.0134	0.0127
6H vs. 24H	0.0394	0.0500
6H vs. 3D	0.0103	0.0066
24H vs. 3D	0.1523	0.2900

HSP90	Summary	Adjusted P Value
CNT vs. 6H	**	0.0068
CNT vs. 24H	*	0.0115
CNT vs. 3D	***	0.0010
6H vs. 24H	ns	0.7196
6H vs. 3D	ns	0.3222
24H vs. 3D	ns	0.0596

CDC37	q Value	Individual P Value
CNT vs. 6H	0.3198	0.9137
CNT vs. 24H	0.0001	0.0001
CNT vs. 3D	0.0002	0.0003
6H vs. 24H	0.0001	0.0001
6H vs. 3D	0.0002	0.0003
24H vs. 3D	0.0735	0.1750

COL24A1	q Value	Individual P Value
CNT vs. 6H	0.0045	0.0213
CNT vs. 24H	0.0004	0.0004
CNT vs. 3D	0.0006	0.0012
6H vs. 24H	0.0016	0.0045
6H vs. 3D	0.0045	0.0185
24H vs. 3D	0.0851	0.4862

*Figure G. Statistical analyses on PCNA, HSP90, CDC37 and COL24A1 expression levels. The ANOVA tables are related to the 27 °C treatment. Differences between means were considered significant for $p < 0.05$. Significant differences detected by Tukey post hoc test— * $p < 0.05$, ** $p < 0.01$, *** $p < 0.0001$.*

The following chapter presents the first tissue, cellular, and transcriptomic investigation of the Antarctic anemone *Urticinopsis antarctica*. Finally, an attempt was made to answer the questions: Can the knowledge gained on *Anemonia viridis* be applied to other species of the same class adapted to other environments and subject to other pressures? Can they be validated as bioindicators and compare responses?

Chapter 6

Urticinopsis antarctica: Animal model for Antarctic studies on adaptation capabilities

ABSTRACT

Sea anemones are fundamental components of benthic communities in the Antarctic continent. They represent one of the largest predators in this region and can consume a broad range of prey. To date, very little is known about these organisms in the extreme habitat and in literature there are only few studies about distribution, abundance and feeding behaviour. We focus our study on the sea Antarctic anemone *Urticinopsis antarctica*. A first histological, cell and trascriptomic *de novo* analyses are here showed. The histological and histochemical approach allowed to compare the species on a structural level with other better known anthozoans. The collected data suggest that it is a non-symbiotic species, with the characteristic distinction in two body layers, i. e. the gastrodermis and the epidermis, divided by the mesoglea, the amorphous connective layer. Moreover, some cell types commonly present in the phylum have been found.

RNA-seq data was generated using *Illumina* paired-end sequencing, obtaining ~32 Gbp of sequence data, which were assembled following the Oyster River Protocol into 71920 contigs and annotated with the AnnotaM pipeline. Studies on anemones biology in Antarctic coastal regions can contribute to the baseline knowledge of their adaptation capability to extreme conditions and provide an improved understanding of responses to anthropogenic and environmental disturbances. Besides that, the sequence collection could be used as a strategic reference for future studies on this species.

Keywords: Antarctic species; sea anemone; histology; transcriptome *de novo* assembly

INTRODUCTION

The world's harshest, driest, and most remote region is Antarctic. Its current position in the South Pole is the outcome of a protracted geologic and geological past that began with the disintegration of the supercontinent Gondwana. The emergence of two important deep ocean passageways—one between Tasmania and Antarctica and the other between South America and Antarctica—marked the Cenozoic as a time of significant change (Crame, 1999).

The first began 64 Ma and resulted in complete separation of continental masses by the start of the Eocene 50 Ma, whereas the second generated the disruption of the Weddellian Isthmus and aperture of the Drake Passage (Crame, 1999; Reguero et al., 2014), which is thought to have occurred around 40 Ma, with some dispute about the precise dating of the various geologic phases that followed between 6 and 41 Ma (Barker and Thomas, 2004; Lyle et al., 2007; Scher and Martin, 2004; Thatje, 2012). These last two occurrences, especially the opening of the Drake Passage, enabled deep circum-Antarctic waters to circulate and the Antarctic Circumpolar Current to form. The primary factors that keep the Southern Ocean physically and thermally isolated from other water bodies are these current systems (Reguero et al., 2014; Thatje, 2012). The formation of the Antarctic Circumpolar Current and associated climatic changes are the cause of the distribution and evolution of life in the Southern Ocean.

The Southern Ocean's mean seawater surface temperatures are modest in comparison to other seas. Temperatures in the sub-Antarctic vary from 4 to 8°C in the summer and 1 to 3°C in the winter. In addition south, north of the Antarctic area, they vary from 1 to 2°C in winter to 3 to 5°C in summer, with temperatures as low as -1.9°C near the mainland (David and Saucède, 2015; Knox, 2007).

The rise in greenhouse gases released into the atmosphere since the industrial period has resulted in significant environmental changes. Global oceans mitigate human climate change at the expense of deep changes in their properties, ecology, and ecosystem services (Gattuso et al., 2015). Indeed, the modification induced by anthropogenic activities have no confines with a huge impact also on the Southern Ocean habitats (Convey, 2001; Summerson and Bishop, 2012). Global temperature will continue to increase as described also in the IPCC Sixth Assessment Report (Constable et al., 2022).

This is affecting and will continue to impact Southern Ocean ecosystems and species more quickly than ever before due to changes in water temperature, salinity, pH (ocean acidification), current or glacial cycles (Halanych and Mahon, 2018).

The expected effects are several, prominently an increase in air and ocean temperature of + 0.9 to + 3°C and + 0.7 to + 1.9°C, respectively, which will have a significant impact on ice shelf volume and, consequently, on global sea level. The effects of ocean acidification on calcification, a rise in non-native species, or significant shifts in habitats also affect the biological communities.

In this scenario we develop the first zoological research with a focus on the immune response of *Urticinopsis antarctica*, a sea Antarctic anemone, in order to deepen the basic knowledge of this species and investigate its ability to respond to ongoing environmental changes. *U. antarctica* is a soft coral with a cylindric massive sandy-coloured body column up to fifteen centimetres high and eleven centimetres in diameter (Arntz and Rauschert, 2015).

U. antarctica is among the largest and most conspicuous benthic invertebrates in the Antarctic community and was found from 6 to 223 meters depth (Carlgren, 1949; Gutt and Starmans, 1998). It is one of the most prevalent and abundant sea anemones on the Antarctic shore; prior research has shown that the species is frequent in both Antarctic and Subantarctic waters. It has been observed in the Weddell Sea, South Shetland Islands, Prudz Bay, Cosmonauts Sea, and Haswell Archipelago (Fig. 1).

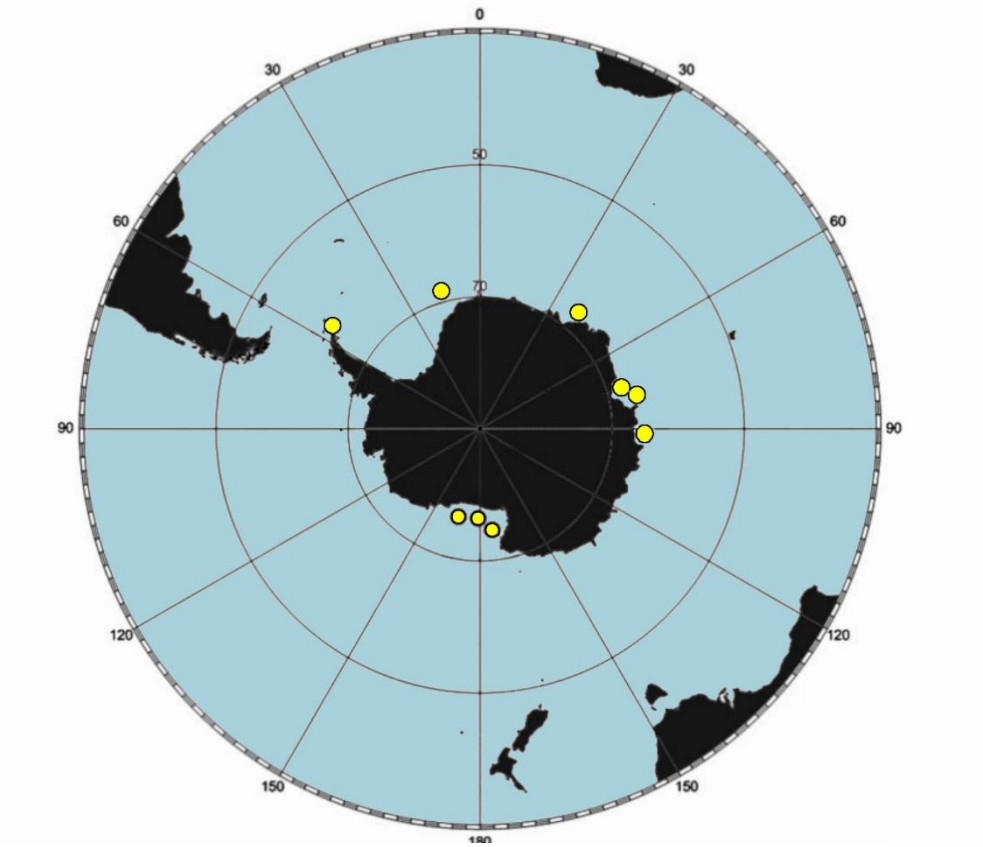

Figure 1 Distribution of Urticinopsis antarctica. Yellow circles: localities from literature data.

Its tentacles and the oral disk are dirty white (Arntz and Rauschert, 2015). An anemone with a diameter of 1.2 cm presents 120 tentacles and a range between 600 to 800 tentacles was measured in specimens with a diameter of 10 cm (Fig. 2). Contracted tentacles are short, conical, with faint lengthwise furrows, and occasionally have rounder ends (Carlgren, 1949, 1927).

Figure 2 Urticinopsis antarctica in its habitat.

77% of the food of *U. antarctica* is made up of seastars and sea urchins (Dayton et al., 1970). One research discovered molluscs, crinoids, sea urchins, ophiuroids, and fish *Trematomus sp.* in the gastrovascular canal of this generalist anemone. In addition, undigested *Conicostoma sp.* amphipods have been discovered, and they may be commensal animals (Ivanova and Grebelnyi, 2017). The newest findings are consistent with those of American experts, who estimated that medusas account for 21% the anemone diet (Dayton et al., 1970) according also that cannibalism is possible in this species.

MATERIAL AND METHODS

Sample collection and data preparation

Specimen of *Urticinopsis antarctica* were collected during divers's immersions in the Gerlache Inlet, Ross sea (74° 41' 42" S 164° 7' 23" E) in the 37° Campaign of Italian PNRA ("Programma Nazionale di Ricerche in Antartide", Project PNRA18_00077) in 2022, and maintained in acquaria in running sea water. Tentacles (30 g) were dissected from a single animal that was left to recovery in aquaria and released in the sea after 20 days. Cells were obtained by tentacles by teasing the tentacles tissue over a stainless-steel mesh (100 mm) employing iso-osmotic PBS (550 mOsm/kg), the homogenized tissue was then washed twice in PBS by centrifuging at 450 x g, and obtained cells counted for viability in trypan blue and immediately employed for analyses. A fraction of tentacles was fixed in ice-cold Bouin's solution in order to preserve tissues for histological staining. After dehydration with increasing series of ethanol, and two steps in toluene (10 min each), tissues were embedded in paraffin. Sections (7 µm in thickness) have been cut in series with a rotary microtome (Microm HM 350S, GMBH,Walldorf, Germany) and processed for Gomori's Trichrome. A $2x10^7$ fraction of tentacle cells of *U. antarctica* were dissolved by gentle pipetting in 1 ml of RNAzol RT (Sigma-Aldrich) for total RNA isolation and immediately frozen at -80 °C for transport. In Italy (University of Tuscia, Viterbo), frozen samples were processed according to the technical procedures of producer nucleic acid extraction. Quality and RNA concentrations were verified using the spectrophotometer Biotech Epoch 2, agarose gel and the Agilent bioanalyzer 2100 system previous to de novo transcriptome assembly (Fig. 3).

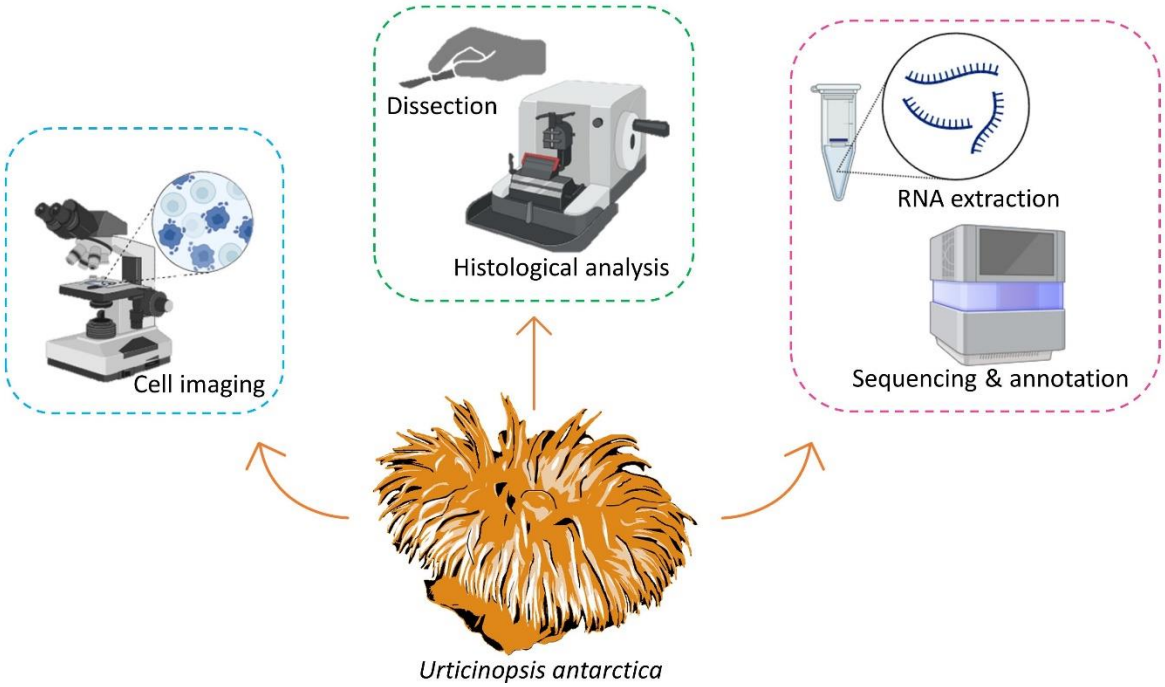

Figure 3 Illustration clarifies the experimental approach.

The extracted total RNA from two cells samples of *U. antarctica* was subjected to poly-A selection and a mRNA library was constructed and sequenced. RNA-seq was performed by BMR Genomics (Padova, Italy) on an Illumina NovaSeq 6000 platform with a 2x100bp paired-end sequencing strategy (aiming at obtaining 60 million of reads/sample). Upon quality control and trimming, performed with fastqc and multiqc, RNA-seq data were assembled following the Oyster River Protocol (MacManes, 2018), which combined the output of two independent assembly algorithms (i.e. Trinity and SPAdes) to improve the quality and completeness of the final set of assembled contigs. Both assembled transcriptomes were evaluated for completeness with BUSCO using the Metazoa OrthoDB v.10 reference and combined, reducing sequence redundancy by (i) collapsing nearly-identical contigs with cd-hit, using a similarity threshold of 98%, and (ii) further clustering redundant sequences using the orthofuser program (Kriventseva et al., 2019; Manni et al., 2021; Simão et al., 2015; Waterhouse et al., 2013). The expression level of all contigs was measured with salmon and for each cluster identified by orthofuser (https://github.com/macmanes-lab/Oyster_River_Protocol/blob/master/orthofuser-README.md) only the sequence showing the highest Transcripts Per Million (TPM) value was selected (Patro et al., 2017).

The resulting sequences were blasted against the uniprot-swissprot database (using blastx, with a default e-value threshold equal to $1x10^{-5}$), and hits were used to create a collection of unique proteins found in the new transcriptome.

A second salmon run was performed to filter the sequences based on a threshold of TPM=1. Sequences passing this threshold were retained in the final transcriptome, whereas those with lower expression values were retained only if they had a hit with the unique proteins found in the previous step. The quantitative evaluation the merged assembly was performed using TrinityStats plugin (Fig. 4).

Subsequently, assembled contigs were annotated with the AnnotaM pipeline (https://gitlab.com/54mu/annotaM/-/tree/master), which assigned each contig to one or more Gene Ontology terms and conserved protein domains.

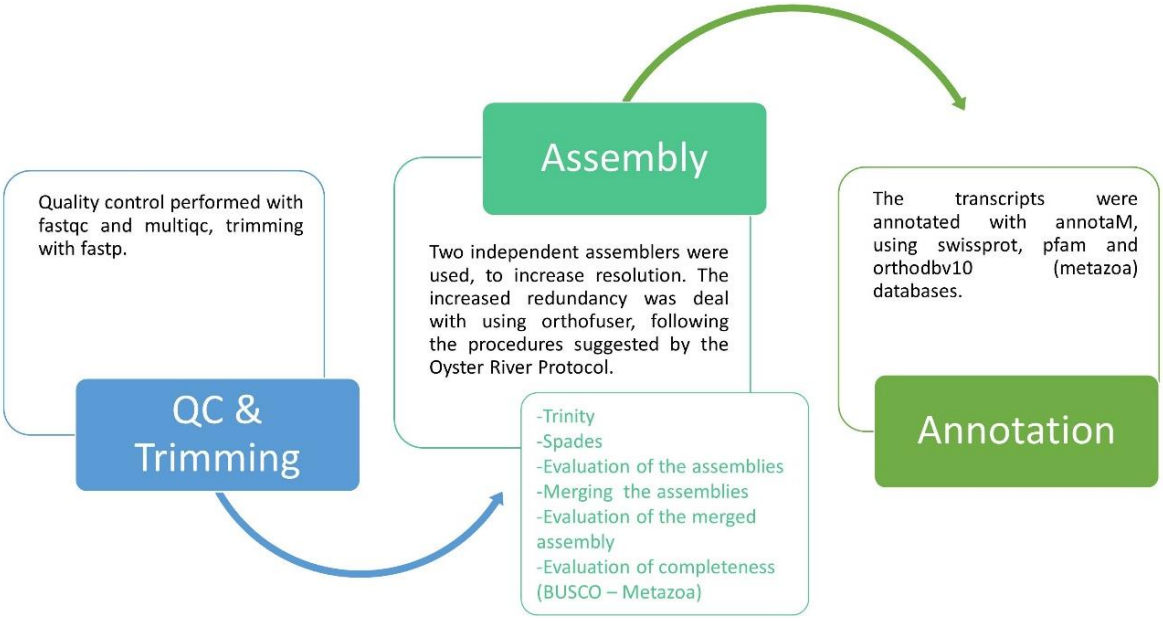

Figure 4 Pipeline of de novo assembled transcriptome used in this study.

Histology & Histochemistry

Tentacles were fixed in Bouin's solution until complete sinking. Subsequently, samples were dehydrated in an increasing scale of ethanol (30%, 50%, 70%, 90%, 96%, 100%) and paraffin-embedded. Histological longitudinal sections (7 μm thick) were cut with a rotary automatic microtome (Microm HM 350S, GMBH,Walldorf, Germany), and processed for the Trichrome stains.

Gomori's Trichrome sections were stained with Carazzi's emalume (200 mL—10 g $KAl(SO_4)$, 0.2 g hematoxylin, 0.04 g KIO_3, 40 mL glycerol) for 10 min at room temperature, washed in distilled water for 15 min, and been left in Gomori's trichrome solution (100 m—

0.6 g chromotropium 2R, 0.3 g fast green FCF, 0.6 g of phosphotungstic acid, 1 mL acetic acid, pH 3.4) and finally washed in acidified water (0.2% acetic acid).

Extracted cell were fixed in paraformaldehyde 4% with osmoconforme sea water. Cells were then stained in May Grünwald-Giemsa for subsequent morphological analysis.

RESULTS

Data description

The raw sequencing output consisted of 113472968 reads for the first sample and 116786307 reads for the second sample (Table 1).

Table 1 Sequencing, de novo assembly statistics.

Number of paired-end reads sample 1	113472968
Number of paired-end reads sample 2	116786307
Total sequencing output	33.2 Gb
Number of assembled contigs	124184
Median contig lenght	1139
Average contig length	1775.11
N50 (nt)	3098

A quality control and a trimming were performed before the assembly and the merging of the two transcriptome datasets (Table 2). The overall quality of the raw reads was very high and no particular issues were detected. The assembly process generated 124184 contigs with a median contig length of 1139 nt and a N50 value 3059. The evaluation of the quality of the transcriptome assembly revealed excellent metrics in terms of completeness. Indeed, 938 out of 954 searched metazoan BUSCOs (denoting single-copy genes expected to be highly conserved and shared by all animals) were detected and found to be complete, indicating a 98.3% recovery rate. Nevertheless, 681 of these BUSCOs were duplicated, suggesting the high prevalence of alternatively spliced isoforms or uncollapsed allelic variants that could not be removed by the redundancy removal efforts outlined above. Only 6 BUSCOs (0,6% of the total) were fragmented, further supporting the high quality of the transcriptome assembly. Finally, 10 BUSCOs (1,1% of the total) were not detected, most likely due to their highly controlled expression, either restricted to early developmental stages, or to other tissues. The BUSCO metrics of the merged assembly were significantly higher than those associated with the two independent assemblies (Trinity and SPAdes), further supporting the reliability of the use of the Oyster River Protocol in this case.

Table 2 Control quality and trimming.

	Sample 1	Sample 2
Duplication %	28.3%	32.5%
% > Q30	92.3%	92.3%
Mb Q30 bases	24312	25385.9
M Reads After Filtering	215.7	221.9
GC content	42.7%	43.5%
% PF	95%	95%
Adapter %	37.2%	28.2%

There was no sign of symbionts, since no genetic traces of molecular markers (rRNA and COI) of suspected organisms, which should certainly be easily identifiable if the symbiont were present, have been found. Were found instead a series of signals of many other organisms present in the Antarctic environment, which certainly correspond to environmental contamination such as: *Trematomus bernacchii*, *Chionodraco hamatus* and *Pleuragramma antarctica* for bony fishes, *Sterechinus neumayeri* and *Ophiosparte sp*. for echinoderms, *Adamussium colbecki* and *Limacina* for molluscs. In addition, additional contaminations were found from human genome, unidentified species of copepods and sponges. The only signal that could not be attributed to metazoa was due to the presence of *Porisira glacialis*, a diatom.

The total annotated transcripts are 71920. In particular, were used swissprot, pfam and orthodb v10 (metazoa) databases. 61772 transcripts had at least one hit on UniProt-SwissProt, 63302 transcripts had at least one Pfam annotation, 32860 transcripts had at least one orthodb hit (Fig. 5).

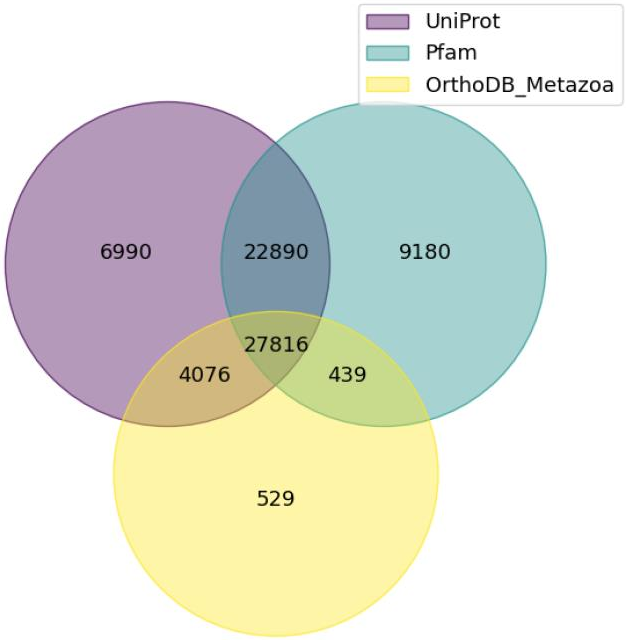

Figure 5 Venn diagram shows the intersection between the annotation sets.

In order to investigate and summarize functional and gene ontology categories (GO terms) in *U. antarctica* transcripts, due to their large number, we sought in particular all those attributable to the internal defence system (Table 3). Within this sub-division, the major representatives are the GO terms related to: the innate immune and the inflammatory responses (GO: 0045087 – 0006954), defence responses to virus and bacteria (GO: 0051607 – 0042742), interleukins (GO: 0070102 – 0032755 – 0032743); NF-kB cascade (GO: 0051092 – 0032088 – 0038061 – 0019221 –0032722) and finally, the Toll-like receptors pathway (GO: 0002224 – 0035666 – 0002755 – 0034138 – 0034142).

Table 3 List of the major Gene Ontology biological processes relevant for immunity and number of corresponding annotated contigs in the U. antarctica transcriptome.

GO category	Description	Annotated contigs
GO: 0045087	Innate immune response	1809
GO: 0006954	Inflammatory response	659
GO: 0006955	Immune response	264
GO: 0051607	Defense response to virus	664
GO: 0051092	Positive regulation of NF-kappaB transcription factor activity	297
GO: 0019221	Cytokine-mediated signaling pathway	44
GO: 0006950	Response to stress	8
GO: 0007179	Transforming growth factor beta receptor signaling pathway	137
GO: 0002376	Immune system process	2080
GO: 0032088	Negative regulation of NF-kappaB transcription factor activity	142
GO: 0002224	Toll-like receptor signaling pathway	90
GO: 0050727	Regulation of inflammatory response	172
GO: 0042742	Defense response to bacterium	654
GO: 0034138	Toll-like receptor 3 signaling pathway	7
GO: 0034142	Toll-like receptor 4 signaling pathway	20
GO: 0050728	Negative regulation of inflammatory response	153
GO: 0035666	TRIF-dependent toll-like receptor signaling pathway	7
GO: 0034097	Response to cytokine	55
GO: 0032722	Positive regulation of chemokine production	28
GO: 0070102	Interleukin-6-mediated signaling pathway	10
GO: 0002755	MyD88-dependent toll-like receptor signaling pathway	16
GO: 0032755	Positive regulation of interleukin-6 production	93
GO: 0032743	Positive regulation of interleukin-2 production	39
GO: 0045088	Regulation of innate immune response	27
GO: 0002474	Antigen processing and presentation of peptide antigen via MHC class I	4
GO: 0007259	JAK-STAT cascade	28
GO: 0038061	NIK/NF-kappaB signaling	69

Histological analysis

In order to shed light on the morphological structure of *U. antarctica*, histological analysis was conducted on tentacles paraffin-embedded and stained with Gomori's Trichrome. Tentacle tissues uncovered an intact epithelium containing cells characteristic for each epithelium (epidermis, gastrodermis) and separated by a loose mesoglea (Fig. 6).

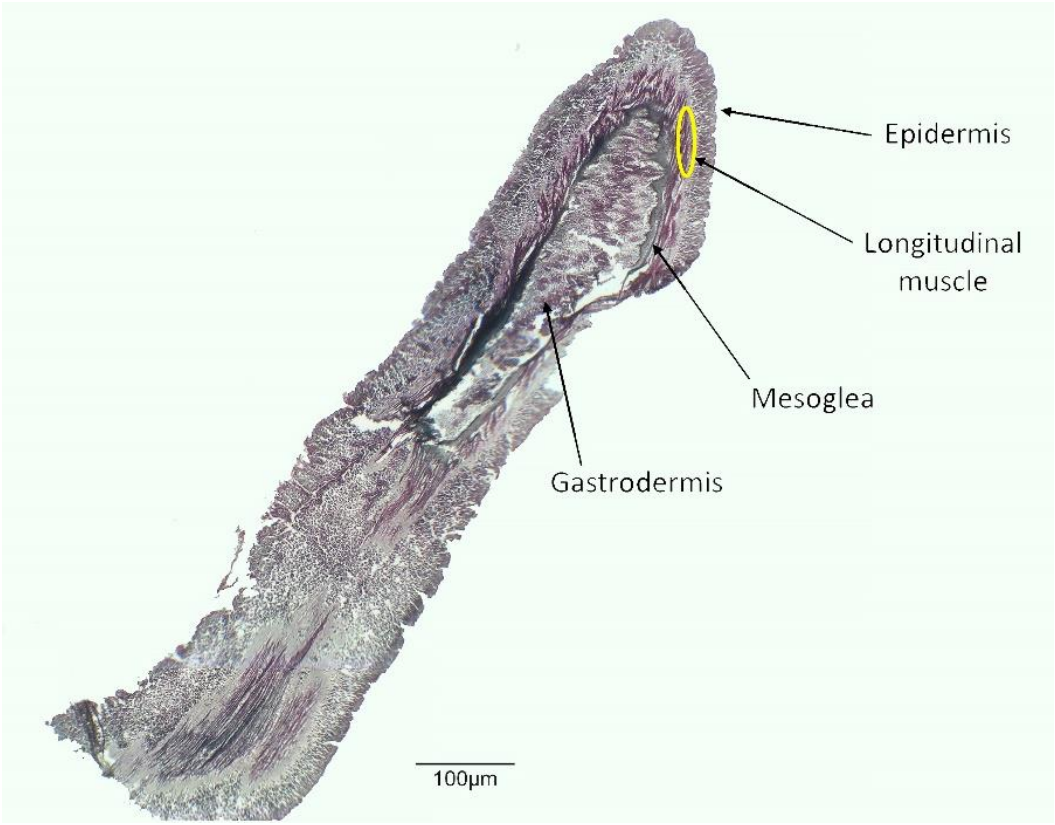

Figure 6 Microphotograph of the epithelial layers of Urticinopsis antarctica tentacle. The outermost layer is the epidermis and the innermost layer is the gastrodermis, both rich in cells. The mesoglea is the central amorphous gelatinous thin layer in blue-green. Scale bar: 100µm.

The thickness of the three body layers were measured and the mesoglea (11.276 ± 5.47 µm) represent the thinner layer in all sections studied (Fig. 7). Finally, epidermis (57.713 ± 15.45 µm) and gastrodermis (60.207 ± 21.48 µm) did not show a significant difference in their size. Data were tested for ANOVA assumptions and ANOVA one-way was performed (F = 36.40; R square = 0.7222; P value = < 0.0001). Mesoglea showed a P value < 0.0001 compared to epidermis and gastrodermis layers.

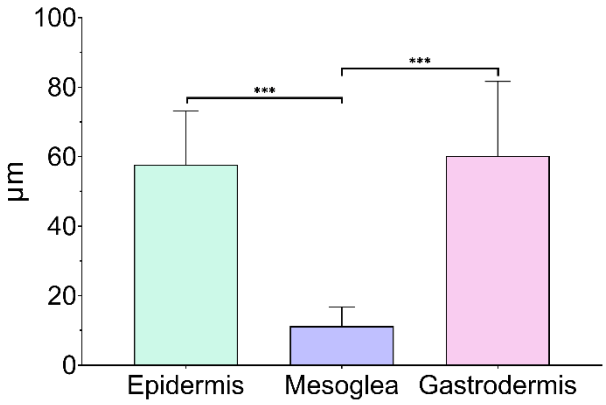

Figure 7 Plot reports the thickness of the three body layers (epidermis, mesoglea and gastrodermis). Data are presented as mean ± standard deviations. Differences between means were considered significant for p < 0.05. Significant differences were detected by Tukey post hoc test— p < 0.05, ** p < 0.01, *** p < 0.0001. Letters indicate significance within the same temperature.*

Epidermis is formed by a single layer of densely packed columnar cells and among them spirocysts have been identified (Fig. 8a). The basal part mounted on the mesoglea and the two layers are bounded by a longitudinal muscle. The mesoglea appeared as an amorphous fibrous matrix containing a large number of rounded and linear cells that migrate within it (Fig. 8b).

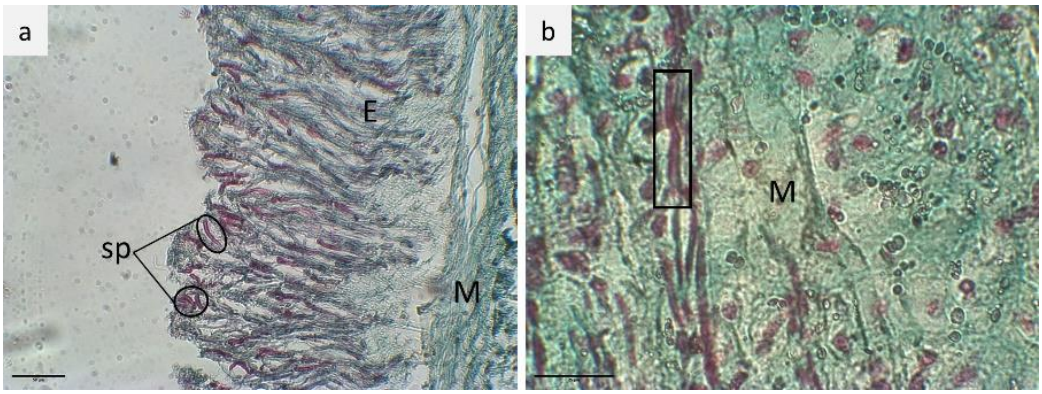

*Figure 8 U. antarctica longitudinal sections of **(a)** epidermis and **(b)** mesoglea layers. E = epidermis, M = mesoglea, sp = spyrocists, black boxes = linear cells. Scale bar: 50µm (a) and 25µm (b).*

On the opposite side, the gastrodermis layer with only some cells clearly distinguishable and in differentiation, like some nematoblasts (Fig. 9a), some oblong (Fig. 9b) and fibroblasts-like cells (Fig. 9c). Observing each layer, there is no sign of endosymbionts.

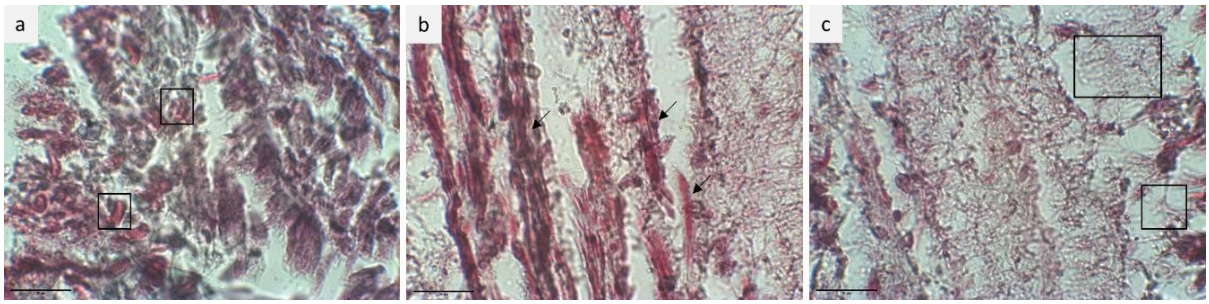

*Figure 9 U. antarctica longitudinal sections of **(a-c)** gastrodermis layer. Black boxes in **(a)** highlight spyrocist cells in differentiation. In **(b)** arrows indicate linear cells, like fibers. In **(c)** boxes evidenced a network of fibroblasts-like cells. Scale bar: 25µm.*

Cells characteristics

May Grünwald-Giemsa cells stained were observed under optical microscope and measured. Spyrocists length is 43.60 ±20.43 µm, amoebocytes length 27.02 ± 0.35 µm and width 12.14 ± 4 µm. The amoebocyte nucleus occupies the 29.6% of the total cell size. Granulocytes area 20.41 ± 0.19µm^2 (Fig. 10a-c).

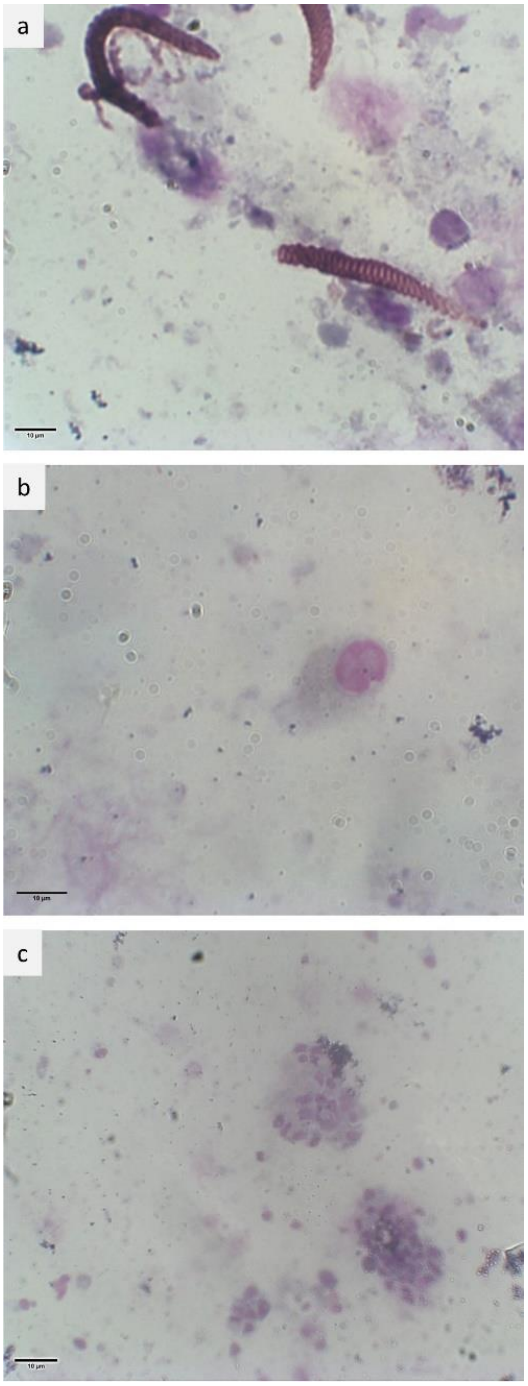

Figure 10 U. antarctica cells stained in May Grünwald-Giemsa. ***(a)*** *spyrocists;* ***(b)*** *amoebocyte;* ***(c)*** *granulocytes. Scale bar: 10 µm.*

Live cells, extracted from the sea anemone tentacles were directly observed under the light microscope. Most of the cells were rounded and isolated, the presence of granules in some of them may indicate that there are more cell populations. The occurrence of some clotted cells allowed to highlight yellowish granules, which could represent a storage area of carotenoids (Fig. 11a,b). Cells were cultured for 24 hours; during this time, they were able to aggregate (Fig. 11c) and differentiate as it is visible also in Fig. 11d, where a black arrow indicate a nematoblast cell.

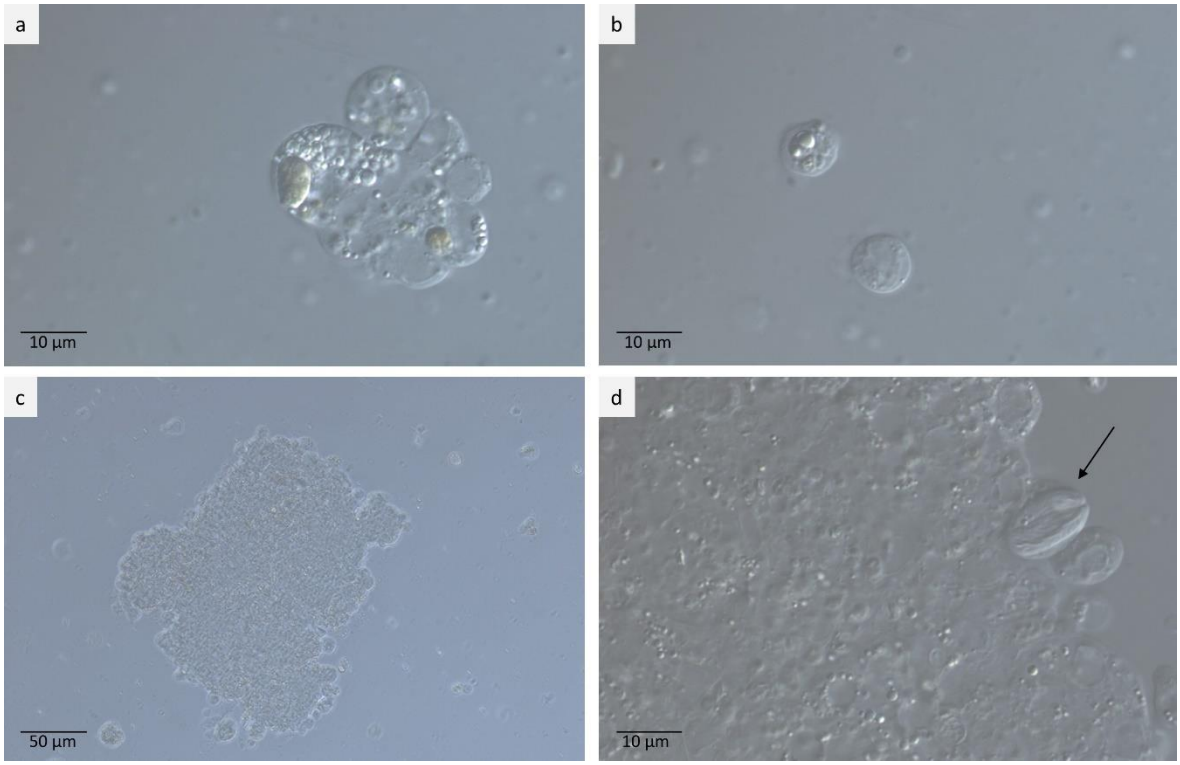

Figure 11 Panel shows live cells of U. antarctica. In (a) aggregate cells containing yellowish granules suggesting a carotenoid storage in some cells. In (b) isolated rounded cells. (c) shows the aggregation of isolated cells cultured for 24h hours and some cells after this time start differentiation (d). Arrow highlights a nematoblast cell.

DISCUSSION

Here, a first Zoological exploratory study based on histological and molecular analysis of *U. antarctica* was conducted. This could lay the basis for further investigation into the potential adaptive capabilities of this species to extreme conditions. Therefore, it would implement the knowledge on the habitat and on the anemone itself and create an opportunity for research on multiple aspects of scientific interests and on many species, considering also the NGS (Next generation sequencing) analysis novelty. Through it, several studies have exploited, for example, developmental strategies, cell trans-differentiation in response to physical damage, adverse environmental conditions and aging, like in *Turritopsis dohrnii* taking into account also the different stages of its life cycle (Matsumoto et al., 2019).

Phenomena such as climate change have repercussions on every aspect of Cnidarian communities, in fact they exhibit complex responses to climatic conditions.

It has been shown that in the Mediterranean, global warming causes marked changes in species composition, in bathymetric distribution, also affecting sexual reproduction and larval dispersion (Rossi et al., 2019).

Cold-water corals are well recognised for their habitat-provision capability, particularly in deep-sea ecosystems and they are frequently documented in association with other species (Angiolillo et al., 2021; Neves et al., 2020; Soetaert et al., 2016).

To date, it is known that the anthozoans have evolved symbiotic relationships with dinoflagellates such as zooxanthellae, but also with fish and marine macroinvertebrates, despite having a varied arsenal of poisons scattered on their bodies that they use as a weapon of predation and defence (Parisi et al., 2020; Trapani et al., 2016). Delgado *et alii* (2022), using transcriptomic data identified differences and similarities in venom profiles of six sea anemone species of three clades of clownfish-hosting and have found 1121 transcript that match with haemolytic and haemorrhagic toxins across all species.

In *U. antarctica* we have found 314 transcripts inherent to toxins (GO: 0090729), of which 111 strictly linked to Cnidarians, the rest are mainly related to reptiles and arthropods toxins.

Moreover, in *Nematostella vectensis*, it has been observed that the toxin Nv1 (the most abundant) under thermal stress conditions was downregulated in the populations studied, suggesting a differential modulation of the production of venom linked to the geographical

position and highlighting also, how downregulation can be an advantageous adaptation given the high metabolic cost that the production of venom involves (Sachkova et al., 2020).

From the transcriptome data of *U. antarctica*, it is evident that many transcripts are highly conserved and among them, 7571 concern immune system responses and 173 transcripts correspond to Heat shock proteins (HSPs), molecules not strictly linked to heat and cold stress, involved also in regeneration or detoxification from metals, which are also expressed in a differential way when the survival of the individual is at stake, cutting the investment of energy in physiological processes at high cost (Goldstone, 2008; Sachkova et al., 2020).

Histological analyses highlighted that *U. antarctica* does not seem to have any symbiosis with zooxanthellae. This may suggest that the presence of a symbiont may not be beneficial in such an extreme environment as the Antarctic. At the same time, however, the sea anemone will have adopted systems to overcome environmental pressures.

These may include the use of pigments such as carotenoids, which are widely distributed among different hard and soft coral species (Czeczuga, 1972). These play disparate roles such as UV protection and ROS scavenging but are also documented in relation to lesions caused by bacterial infections, as for *Gorgonia ventalina* (Leverette et al., 2008). The pigment could in fact be stored inside the cells of the animal, and it may also be the determining factor of the orange colour of the organism, but the certainty can be obtained with further investigation.

Gomori staining, as expected, showed a subdivision of the tissue layers equal to those highlighted in other anthozoans such as *Anemonia viridis*. Unlike it, it has been noted a lower thickness of the connective layer, and an elevated amount of migrant cells within the mesoglea (Parisi et al., 2021). At the tissue level it has not been easy to characterize all the different cell populations, but there are clearly spirocysts in the epidermis layer, nematoblasts in the gastrodermis and fibroblast-like cells in the areas of conjunction between the two epithelial layers and the mesoglea. Elongated and rounded cells are visible, but electron transmission microscopy investigations could help in the detection of additional cell types and help in the characterization of their functions. In addition, from the extracted cells it was possible to detect and measure spirocysts, granulocytes and amoebocytes as was done in a study conducted on *A. viridis* regeneration with results in line with the observed (La Corte et al., 2023). The differences between *A. viridis* and *U. antarctica* related to the biometric measurements, could be attributed to the intrinsic characteristics of the two

specimens, but also to the different experimental conditions to which they have been subject. The obtained outputs can be of considerable support for future investigations that take into account tissue, cellular and molecular markers.

CONCLUSIONS

This work represents a first investigation on *Urticinopsis antarctica*. Here, were used an histochemistry and histological approach in order to study the tissue organization and cells populations in the species and conduct comparative morphological analyses versus other anthozoans. RNA-sequencing, de novo assembly, and functional annotation were performed to characterize the transcriptome profile of the Antarctic anemone. These interesting results encourage further research and insights in order to deal with future environmental challenges, to better understand the adaptation capabilities of this organism or phylogenetically closer species, in extreme habitats.

REFERENCES

Angiolillo, M., La Mesa, G., Giusti, M., Salvati, E., Di Lorenzo, B., Rossi, L., Canese, S., Tunesi, L., 2021. New records of scleractinian cold-water coral (CWC) assemblages in the southern Tyrrhenian Sea (western Mediterranean Sea): Human impacts and conservation prospects. Prog. Oceanogr. 197, 102656.

Arntz, W.E., Rauschert, M., 2015. Antarctic macrobenthos: a field guide of the invertebrates living at the Antarctic seafloor. Arntz & Rauschert Selbstverlag.

Barker, P.F., Thomas, E., 2004. Origin, signature and palaeoclimatic influence of the Antarctic Circumpolar Current. Earth-Science Rev. 66, 143–162.

Carlgren, O., 1949. A survey of the Ptychodactiaria, Corallimorpharia and Actiniaria. K. Sven. Vetenskapsakademiens Handl. 1–121.

Carlgren, O., 1927. Actiniaria and Zoantharia. Furth. Zool. Results Swedish Antarct. Exped. 1901-1903 2.

Constable, A.J., Harper, S., Dawson, J., Holsman, K., Mustonen, T., Piepenburg, D., Rost, B., 2022. Cross-Chapter Paper 6: Polar Regions, Climate Change 2022: Impacts, Adaptation and Vulnerability. Contribution of Working Group II to the Sixth Assessment Report of the Intergovernmental Panel on Climate Change. Cambridge University Press, Cambridge, UK and New York, NY, USA. https://doi.org/10.1017/9781009325844.023

Convey, P., 2001. Terrestrial ecosystem responses to climate changes in the Antarctic. “Fingerprints” Clim. Chang. Adapt. Behav. shifting species ranges.

Crame, J.A., 1999. An evolutionary perspective on marine faunal connections between southernmost South America and Antarctica. Sci. Mar. 63, 1–14. https://doi.org/10.3989/scimar.1999.63s11

Czeczuga, B., 1972. Investigations of carotenoids in some fauna of the Adriatic Sea. II. Anemonia sulcata and *Actinia equina* (Coelenterata: Anthozoa). Mar. Biol. 13, 124–126. https://doi.org/10.1007/BF00366562

David, B., Saucède, T., 2015. Biodiversity of the Southern Ocean.

Dayton, P.K., Robilliard, G., Paine, R., 1970. Benthic faunal zonation as a result of anchor ice at McMurdo Sound, Antarctica. Antarct. Ecol. 244–258.

Delgado, A., Benedict, C., Macrander, J., Daly, M., 2022. Never, Ever Make an Enemy… Out of an Anemone: Transcriptomic Comparison of Clownfish Hosting Sea Anemone Venoms. Mar. Drugs 20. https://doi.org/10.3390/md20120730

Gattuso, J.-P., Magnan, A., Billé, R., Cheung, W.W.L., Howes, E.L., Joos, F., Allemand, D., Bopp, L., Cooley, S.R., Eakin, C.M., 2015. Contrasting futures for ocean and society

from different anthropogenic CO_2 emissions scenarios. Science (80-.). 349, aac4722.

Goldstone, J. V., 2008. Environmental sensing and response genes in cnidaria: The chemical defensome in the sea anemone *Nematostella vectensis*. Cell Biol. Toxicol. 24, 483–502. https://doi.org/10.1007/s10565-008-9107-5

Gutt, J., Starmans, A., 1998. Structure and biodiversity of megabenthos in the Weddell and Lazarev Seas (Antarctica): ecological role of physical parameters and biological interactions. Polar Biol. 20, 229–247.

Halanych, K.M., Mahon, A.R., 2018. Challenging dogma concerning biogeographic patterns of Antarctica and the Southern Ocean. Annu. Rev. Ecol. Evol. Syst. 49, 355–378.

Ivanova, N.Y., Grebelnyi, S.D., 2017. On the food of the Antarctic sea anemone *Urticinopsis antarctica* Carlgren, 1927 (Actiniidae, Actiniaria, Anthozoa). J. Mar. Biol. Assoc. United Kingdom 97, 29–34. https://doi.org/10.1017/S0025315415002131

Knox, G.A., 2007. Biology of the Southern Ocean, 2nd edn. ed. Taylor & Francis, Boca Raton, FL, Boca Raton.

Kriventseva, E. V, Kuznetsov, D., Tegenfeldt, F., Manni, M., Dias, R., Simão, F.A., Zdobnov, E.M., 2019. OrthoDB v10: sampling the diversity of animal, plant, fungal, protist, bacterial and viral genomes for evolutionary and functional annotations of orthologs. Nucleic Acids Res. 47, D807–D811. https://doi.org/10.1093/nar/gky1053

La Corte, C., Baranzini, N., Dara, M., Bon, C., Grimaldi, A., Parisi, M.G., Zizzo, M.G., Cammarata, M., 2023. Step-by-Step Regeneration of Tentacles after Injury in *Anemonia viridis*—Morphological and Structural Cell Analyses. Int. J. Mol. Sci. 24, 8860. https://doi.org/10.3390/ijms24108860

Leverette, C.L., Warren, M., Smith, M.A., Smith, G.W., 2008. Determination of carotenoid as the purple pigment in *Gorgonia ventalina* sclerites using Raman microscopy. Spectrochim. Acta - Part A Mol. Biomol. Spectrosc. 69, 1058–1061. https://doi.org/10.1016/j.saa.2007.07.018

Lyle, M., Gibbs, S., Moore, T.C., Rea, D.K., 2007. Late Oligocene initiation of the Antarctic circumpolar current: evidence from the South Pacific. Geology 35, 691–694.

MacManes, M.D., 2018. The Oyster River Protocol: a multi-assembler and kmer approach for de novo transcriptome assembly. PeerJ 6, e5428. https://doi.org/10.7717/peerj.5428

Manni, M., Berkeley, M.R., Seppey, M., Simão, F.A., Zdobnov, E.M., 2021. BUSCO Update: Novel and Streamlined Workflows along with Broader and Deeper Phylogenetic Coverage for Scoring of Eukaryotic, Prokaryotic, and Viral Genomes. Mol. Biol. Evol. 38, 4647–4654. https://doi.org/10.1093/molbev/msab199

Matsumoto, Y., Piraino, S., Miglietta, M.P., 2019. Transcriptome characterization of reverse

development in *Turritopsis dohrnii* (Hydrozoa, Cnidaria). G3 Genes, Genomes, Genet. 9, 4127–4138. https://doi.org/10.1534/g3.119.400487

Neves, B. de M., Wareham Hayes, V., Herder, E., Hedges, K., Grant, C., Archambault, P., 2020. Cold-Water Soft Corals (Cnidaria: Nephtheidae) as Habitat for Juvenile Basket Stars (Echinodermata: Gorgonocephalidae). Front. Mar. Sci. 7, 1–21. https://doi.org/10.3389/fmars.2020.547896

Parisi, M.G., Grimaldi, A., Baranzini, N., La Corte, C., Dara, M., Parrinello, D., Cammarata, M., 2021. Mesoglea extracellular matrix reorganization during regenerative process in *Anemonia viridis* (Forskål, 1775). Int. J. Mol. Sci. 22. https://doi.org/10.3390/ijms22115971

Parisi, M.G., Parrinello, D., Stabili, L., Cammarata, M., 2020. Cnidarian immunity and the repertoire of defense mechanisms in anthozoans. Biology (Basel). 9, 1–26. https://doi.org/10.3390/biology9090283

Patro, R., Duggal, G., Love, M.I., Irizarry, R.A., Kingsford, C., 2017. Salmon provides fast and bias-aware quantification of transcript expression. Nat. Methods 14, 417–419.

Reguero, M.A., Gelfo, J.N., López, G.M., Bond, M., Abello, A., Santillana, S.N., Marenssi, S.A., 2014. Final Gondwana breakup: the Paleogene South American native ungulates and the demise of the South America–Antarctica land connection. Glob. Planet. Change 123, 400–413.

Rossi, S., Gravili, C., Milisenda, G., Bosch-Belmar, M., De Vito, D., Piraino, S., 2019. Effects of global warming on reproduction and potential dispersal of Mediterranean Cnidarians. Eur. Zool. J. 86, 255–271. https://doi.org/10.1080/24750263.2019.1631893

Sachkova, M.Y., Macrander, J., Surm, J.M., Aharoni, R., Menard-Harvey, S.S., Klock, A., Leach, W.B., Reitzel, A.M., Moran, Y., 2020. Some like it hot: Population-specific adaptations in venom production to abiotic stressors in a widely distributed cnidarian. BMC Biol. 18, 1–13. https://doi.org/10.1186/s12915-020-00855-8

Scher, H.D., Martin, E.E., 2004. Circulation in the Southern Ocean during the Paleogene inferred from neodymium isotopes. Earth Planet. Sci. Lett. 228, 391–405.

Simão, F.A., Waterhouse, R.M., Ioannidis, P., Kriventseva, E. V, Zdobnov, E.M., 2015. BUSCO: assessing genome assembly and annotation completeness with single-copy orthologs. Bioinformatics 31, 3210–3212. https://doi.org/10.1093/bioinformatics/btv351

Soetaert, K., Mohn, C., Rengstorf, A., Grehan, A., van Oevelen, D., 2016. Ecosystem engineering creates a direct nutritional link between 600-m deep cold-water coral mounds and surface productivity. Sci. Rep. 6, 35057.

Summerson, R., Bishop, I., 2012. The impact of human activities on wilderness and aesthetic values in Antarctica. Polar Res. 31, 10858. https://doi.org/10.3402/polar.v31i0.10858

Thatje, S., 2012. Effects of Capability for Dispersal on the Evolution of Diversity in Antarctic Benthos. Integr. Comp. Biol. 52, 470–482. https://doi.org/10.1093/icb/ics105

Trapani, M.R., Parisi, M.G., Maisano, M., Mauceri, A., Cammarata, M., 2016. Old Weapons for New Wars: Bioactive Molecules From Cnidarian Internal Defense Systems. Cent. Nerv. Syst. Agents Med. Chem. 16, 183–196. https://doi.org/10.2174/1871524915666150710120650

Waterhouse, R.M., Tegenfeldt, F., Li, J., Zdobnov, E.M., Kriventseva, E. V, 2013. OrthoDB: a hierarchical catalog of animal, fungal and bacterial orthologs. Nucleic Acids Res. 41, D358-65. https://doi.org/10.1093/nar/gks1116

Chapter 7

Final considerations

In this thesis, to improve the field of general zoology knowledge, immunological and physiological responses to multiple stress conditions were investigated in *Anemonia viridis*. Stress induced by acute exposure to a pollutant with immunomodulatory capacity (such as methylmercury) and bacterial infection were taken into account. Since the peculiarity of *A. viridis* to regenerate lost tissues, effects of heat stress in relation to a regenerative event have been focused. Through the analyses conducted on the constitutive regenerative capacities of the anemone, it was indeed possible to implement basic knowledge about the event itself useful for the purpose of inter-species comparisons. Moreover, ensuring a greater understanding of the process itself following the imposed thermal stress. All of this made it possible to contribute at the validation the Mediterranean anemone as an excellent bioindicator in the proposed cases. More importantly as a result of the analyses performed in an integrated manner at different levels of biological organization, from transcriptome and protein activities, to cells, tissue to macroscopic analysis of the organisms subjected to the different conditions. Overall, the relevant recorded responses may be used as biomarkers in future research, also considering the global climate change we are witnessing.

This PhD thesis can make a great contribution in understanding complex phenomena related to environmental pressures in the class notable in the context of biodiversity. An immunological approach allows to obtain results quickly, sensitively, and specifically to the issue under investigation; therefore, it is argued that they can be easily used as a methodology for studying biodiversity and exposure to multiple stresses.

The basic knowledge gained from the studies presented here, opens up potential innovative applications, both in transferability to other scientific fields and in the comparison between taxonomic groups. Hoping for the exploration of new methodologies, considering what has been achieved by positron emission tomography in studying the involvement of symbionts in the regenerative process. The main results obtained from the different studies presented and the techniques used in the chapters of this dissertation are summarized in Figure 1.

	Topic	Analyses	Results
Chapter 2	Multiple stress caused by methylmercury exposure and bacterial infection	Macroscopic observations; enzymatic activity	MeHg modulate the immunological responses, particularly after bacterial injection. Stressogenic effects are detectable on different levels of biological organization. *Anemonia viridis* could be validated as bioindicator for pollutant exposure.
Chapter 3	Regeneration in constitutive conditions: The role of mesoglea	Macroscopic observations; morphometric measures; enzymatic activity; histology; TEM; immunolocalizations	The mesoglea ECM provides a mechanical support to maintain the shape and integrity of tissues, but also plays a fundamental role in tissue morphogenesis, cell migration and differentiation during tentacle regeneration. The change of mesoglea stiffness, obtained through metalloprotease activity, plays the role of a barrier against the entry of pathogens into the lesion site. The production of new collagen ECM by fibroblast-like cells, differentiated from amoebocytes, acts as a scaffold to guide the correct regrowth of the tentacle.
Chapter 4	Regeneration in constitutive conditions: cellular components and their functions	PET; histology; TEM	Wound-healing process is preserved among metazoans. Results are applicable to different organisms from various taxa. Cells of the immune system have been identified and characterised for the first time, including their distribution, contents, and hypothetical role in the regeneration process.
Chapter 5	Regeneration under thermal stress conditions	Macroscopic observations; enzymatic activity; western blot; dot blot; q/RT-PCR; PAM	A molecular approach was used to investigate the regenerative event under constitutive conditions and following thermal stress in the Mediterranean anemone *Anemonia viridis*. Showed a significant difference between the treatments at different temperatures, indicating two critical moments during the process, i.e. 6 hours and one day after cutting. The analyses also showed changes in the functionality of the symbiont as well as the activation of pathways and an up/down regulation of molecules to counteract the imposed stress.
Chapter 6	First investigation on *Urticinopsis antarctica*	Histology; histochemistry; morphometric measures; trascriptome *de novo* sequencing	First investigation on *Urticinopsis antarctica* tissues, cells and trascriptome. The interesting results encourage further research and insights in order to deal with future environmental challenges, to better understand the adaptation capabilities of this organism or phylogenetically closer species, in extreme habitats.

Figure 1 Table shows the major results obtained in each chapter of the thesis.

Specifically, **in chapter two**, the results of the study with the objective of investigating the effects on the immune response of *A. viridis* in the presence of methylmercury and bacterial infection emphasize how methylmercury has an immunomodulatory effect and also affects the activation of pathways related to the bacterial response. Stressogenic effects were indeed detected macroscopically following bacterial inoculation, with swelling of the animal's pedal area also evidenced by Trapani *et alii* (2016) in the same species and as also highlighted in the polychaete *Sabella spallanzanii* (La Corte et al., 2023), and the appearance of yellowish parts near the point of inoculation. Alteration of enzyme activities with a detoxifying role and that of lysozyme, a key molecule of the internal defence system, have highlighted the single and combined effects of stressors on the ability to maintain homeostasis. Thus, it can be concluded that the use of *A. viridis* is excellent bioindicator in marine-coastal monitoring projects, especially where the assessment of the state of marine ecosystems is still a great challenge, because in general there are no established ecosystem monitoring programs based on the use of physiological responses. **In chapter three**, the regeneration capacity of the sea anemone under basal conditions was investigated. The results showed that the mesoglea plays a key role in tissue morphogenesis, cell migration and differentiation during tentacles regeneration. It was also shown that the change in its consistency by metalloproteases acts as a barrier toward pathogen entry and that the production of new collagen turns as a scaffold for proper tentacle formation. By observing the phenomenon of wound healing from a cellular perspective **in chapter 4**, it was possible to conclude how this process is conserved among metazoans and that this approach is

applicable to other taxa as well. It was possible to characterize cells of the immune system involved in regeneration, emphasizing their distribution and role at different moments of the event itself. This study may be useful for comparative analyses among species of Cnidarians, thus enriching knowledge in the zoological panorama.

Here, was presented a remarkably captivating model for delving into the realms of stem cell biology, cellular reprogramming, and regeneration. The diverse mechanisms and regenerative capabilities found in invertebrates, coupled with the emergence of advanced molecular tools for gene function inhibition and the exploration of genome-wide alterations in gene expression linked to tissue repair, present exceptional prospects for scientists to elucidate the foundational cellular and molecular aspects of regeneration. **Chapter 5** opens to an investigation of the regenerative event in relation to a thermal stress. The integrated approach ensured that the same regenerative event could also be used as a biomarker in a stress condition, such as that of temperature increase, which is useful in the current reality of climate change (IPCC report 2023). A significant difference between experimental times and temperatures was noted, highlighting two critical moments during the process, at six hours and one day after tentacle cutting. The tests also showed a change in symbiont functionality, and in concert, molecular analyses revealed how the organism modulates the expression of the analysed molecules specific indicators of stress, inflammation, and regeneration in order to ensure survival, even at the expense of regeneration itself.

Continuing regeneration research is crucial in contemporary times to enhance our comprehension of animal development. These research findings undeniably drive additional inquiries into the trade-offs associated with regenerative processes. What has received less attention in this course of study is an exploration of the morphological and ecological consequences of regeneration on the organisms themselves. The questions arise as to why certain species maintain the ability to shed and regrow body parts while the majority do not, and what the implications of this phenomenon are for these individuals in terms of advantages and disadvantages (Elchaninov et al., 2021; Fernández-Rodríguez and Braña, 2022). Despite being one of the most ancient and extensively studied aspects of development, regeneration is often overlooked in the broader context of natural selection and evolution. Building on previous research experiences aimed at studying the mechanisms of evolutionary adaptation of organisms to selection pressures in extreme environments, it was decided to conduct a preliminary investigation on tentacular sections and extracted cells were carried out on *Urticinopsis antarctica*, anemone typical of the Antarctic continent, of

which only its distribution and feeding habits and some morphological features are known in the literature (Arntz and Rauschert, 2015; Ivanova and Grebelnyi, 2017; Rodríguez et al., 2007). **In chapter 6**, initial analyses report the characterization of tissue structure, the identification of some cells also typical of the immune system and the early differences with *A. viridis* as well.

In accordance with established biological principles in the post-genomic age, examining the transcriptome not only supports in elucidating the gap between the quantity of coding genes and the number of proteins generated but also serves as the initial stage for exploring translational control. Indeed, transcriptomics enables the detection of genes and pathways that react to and mitigate biotic and abiotic environmental pressures.

A very important achievement is the *de novo* sequencing of the animal's transcriptome. All this encourages further research and investigation of this organism with regard to its ability to adapt to such an extreme environment as the Antarctic, both for comparisons with species phylogenetically similar to it, and because it may prove to be a good bioindicator of such ecosystem. Whereas unfortunately, the latest scientific evidence shows that even such remote environments are being affected by climate change, shifts in species distribution, increases in primary production, mortality events are evident (Jones et al., 2019; Piatt et al., 2020; Siddon et al., 2020). A net decrease in krill habitat and growth potential are predicted as a result of physical and biological changes in Antarctic seas. It's equally conceivable that a decrease in the Antarctic ice pack may lengthen the whole season in regions close to terrestrial predators. (Melbourne-Thomas et al., 2016; Rogers et al., 2019; Swadling et al., 2023).

Based on the experimental plans presented here for regeneration under thermal stress conditions, investigation of the event on already collected samples to evaluate the entire transcriptome at the different observation times is in progress. It would be interesting to further investigate the topics in organisms by evaluating the effect in populations belonging to different ranges, taking into account the distribution and role of different cellular components. Given the huge amount of obtained data, comparison between species adapted to different environments would be desirable, with particular focus on the resilience of sea anemones in order to be able to predict and manage stressogenic effects on them. These are stimulating perspectives capable of explaining the cellular mechanisms and molecular signalling pathways involved in the regulation of internal defence system responses in

marine invertebrates, that represent an important implication in achieving goals for proper natural resource management.

This scientific research has the potential to offer valuable insights for developing strategies to protect the biodiversity in the Mediterranean region. Recent emphasis has been placed on recognizing the connections and scientific evidence that relate nature and biodiversity to human health. This approach, known as "One Health," aims to control global planetary health through a multidisciplinary framework, combining knowledge from various disciplines to ensure the well-being of our planet and a sustainable future for all.

REFERENCES

[Core Writing Team, H.L. and J.R. (eds.)]., 2023. IPCC, 2023: Climate Change 2023: Synthesis Report. Contribution of Working Groups I, II and III to the Sixth Assessment Report of the Intergovernmental Panel on Climate Change. Geneva, Switzerland. https://doi.org/10.59327/IPCC/AR6-9789291691647

Arntz, W.E., Rauschert, M., 2015. Antarctic macrobenthos: a field guide of the invertebrates living at the Antarctic seafloor. Arntz & Rauschert Selbstverlag.

Elchaninov, A., Sukhikh, G., Fatkhudinov, T., 2021. Evolution of Regeneration in Animals: A Tangled Story. Front. Ecol. Evol. 9, 621686. https://doi.org/10.3389/FEVO.2021.621686/BIBTEX

Fernández-Rodríguez, I., Braña, F., 2022. Allocation costs of regeneration: tail regeneration constrains body growth under low food availability in juvenile lizards. Oecologia 198, 853–864. https://doi.org/10.1007/S00442-021-05084-6/FIGURES/4

Ivanova, N.Y., Grebelnyi, S.D., 2017. On the food of the Antarctic sea anemone *Urticinopsis antarctica* Carlgren, 1927 (Actiniidae, Actiniaria, Anthozoa). J. Mar. Biol. Assoc. United Kingdom 97, 29–34. https://doi.org/10.1017/S0025315415002131

Jones, T., Divine, L.M., Renner, H., Knowles, S., Lefebvre, K.A., Burgess, H.K., Wright, C., Parrish, J.K., 2019. Unusual mortality of Tufted puffins (*Fratercula cirrhata*) in the eastern Bering Sea. PLoS One 14, e0216532. https://doi.org/10.1371/journal.pone.0216532

La Corte, C., Dara, M., Bertini, F., Parrinello, D., Piazzese, D., Parisi, M.G., 2023. Response of *Sabella spallanzanii* to multiple stressors. The combined effect of infection and copper sulphate. Comp. Biochem. Physiol. Part C Toxicol. Pharmacol. 263, 109475. https://doi.org/10.1016/j.cbpc.2022.109475

Melbourne-Thomas, J., Corney, S.P., Trebilco, R., Meiners, K.M., Stevens, R.P., Kawaguchi, S., Sumner, M.D., Constable, A.J., 2016. Under ice habitats for Antarctic krill larvae: Could less mean more under climate warming? Geophys. Res. Lett. 43, 10,322-10,327. https://doi.org/10.1002/2016GL070846

Piatt, J.F., Parrish, J.K., Renner, H.M., Schoen, S.K., Jones, T.T., Arimitsu, M.L., Kuletz, K.J., Bodenstein, B., García-Reyes, M., Duerr, R.S., Corcoran, R.M., Kaler, R.S.A., McChesney, G.J., Golightly, R.T., Coletti, H.A., Suryan, R.M., Burgess, H.K., Lindsey, J., Lindquist, K., Warzybok, P.M., Jahncke, J., Roletto, J., Sydeman, W.J., 2020. Extreme mortality and reproductive failure of common murres resulting from the northeast Pacific marine heatwave of 2014-2016. PLoS One 15, e0226087. https://doi.org/10.1371/JOURNAL.PONE.0226087

Rodríguez, E., López-González, P.J., Gili, J.M., 2007. Biogeography of Antarctic sea anemones (Anthozoa, Actiniaria): What do they tell us about the origin of the Antarctic

benthic fauna? Deep Sea Res. Part II Top. Stud. Oceanogr. 54, 1876–1904. https://doi.org/10.1016/j.dsr2.2007.07.013

Rogers, A.D., Frinault, B.A. V, Barnes, D.K.A., Bindoff, N.L., Downie, R., Ducklow, H.W., Friedlaender, A.S., Hart, T., Hill, S.L., Hofmann, E.E., Linse, K., Mcmahon, C.R., Murphy, E.J., Pakhomov, E.A., Reygondeau, G., Staniland, I.J., Wolf-Gladrow, D.A., Wright, R.M., 2019. Antarctic Futures: An Assessment of Climate-Driven Changes in Ecosystem Structure, Function, and Service Provisioning in the Southern Ocean. https://doi.org/10.1146/annurev-marine-010419

Siddon, E.C., Zador, S.G., Hunt, G.L., 2020. Ecological responses to climate perturbations and minimal sea ice in the northern Bering Sea. Deep Sea Res. Part II Top. Stud. Oceanogr. 181–182, 104914. https://doi.org/10.1016/J.DSR2.2020.104914

Swadling, K.M., Constable, A.J., Fraser, A.D., Massom, R.A., Borup, M.D., Ghigliotti, L., Granata, A., Guglielmo, L., Johnston, N.M., Kawaguchi, S., Kennedy, F., Kiko, R., Koubbi, P., Makabe, R., Martin, A., McMinn, A., Moteki, M., Pakhomov, E.A., Peeken, I., Reimer, J., Reid, P., Ryan, K.G., Vacchi, M., Virtue, P., Weldrick, C.K., Wongpan, P., Wotherspoon, S.J., 2023. Biological responses to change in Antarctic sea ice habitats. Front. Ecol. Evol. 10, 1073823. https://doi.org/10.3389/FEVO.2022.1073823/BIBTEX

Trapani, M.R., Parisi, M.G., Parrinello, D., Sanfratello, M.A., Benenati, G., Palla, F., Cammarata, M., 2016. Specific inflammatory response of *Anemonia sulcata* (Cnidaria) after bacterial injection causes tissue reaction and enzymatic activity alteration. J. Invertebr. Pathol. 135, 15–21. https://doi.org/10.1016/j.jip.2016.01.010

Aknowledgements

First thanks to my tutors. Thanks to Prof. Matteo Cammarata for having shared with me his enormous knowledge and for having transmitted me the love for zoology and marine immunobiology, all always with immense fatherly love and support, wonderful teacher and man. Thank you immensely Prof. Parisi (it is almost strange not to write Giovanna), for having believed and believing in me from the first glance in class, which with determination pushes me every day to overcome my limits. As a great and professional woman told me: "Meeting is a coincidence, choosing is a will". Thank you both, because with patience and your safe guidance, you trained me and raised me as a woman in science. Thank you, Prof. Parrinello, silent and always ready to help me. I cannot wait to see what awaits us in the near future and has already said a few years ago during the Master's thesis, wishing you bring good again:

"I really hope to associate my name with yours in future works"

Thank you Prof. Annalisa Grimaldi and Dr. Nicolò Baranzini from University of Insubria, it is great to work with you (scientifically and humanely) and I am happy that we have shed some light on regeneration research, ready for the next step…

Thanks to Prof. Scapigliati and his research group of the University of Tuscia, for their welcome, which together with Prof. Gerdol, from the University of Trieste, allowed me to learn new techniques and for the fruitful collaboration that allowed also to improve this thesis.

Prof. Paola Furla and Dr. Stephanie Barnay-Verdier, from Université Côte d'Azur. Women and unique researchers, attentive, prepared, purposeful and human, who transmit their great passion for science. Absolutely fundamental. Thank you for the scientific baggage you have given me. I hope to collaborate soon again together. To the ALL Eric Röttinger (wonderful) team "Réponse au stress, régénération et longévité", for the availability, hospitality and for making me feel at home.

Thanks to the Centre Scientifique de Monaco and in particular to Dr. Dorota Czerucka and her group "Écosystèmes et Immunité" for providing experimental animals and support during the training period abroad.

I would also like to thank Prof. Jacopo Vizioli from Université de Lille for the opportunity to collaborate in smart-working and for valuable revisions to this thesis, thanks also extended to Prof. Maria Maisano from the University of Messina.

An important thanks to Mariano (happy to say Dr. Dara), for all the scientific and emotional support in these years, my anchor in laboratory and precious friend. Luca and Federica, the days without you in and out of the lab would not be the same, if for good or bad I leave it to you (I'm joking). Thanks, guys, for the shared moments together, your help and your encouragement and for being able to bear and understand my moments of stress, we are a nice bunch of crazy people.

Thanks to my family, my certainty in life. For allowing me to reach this goal too, reassuring and pushing me, with their ways, always, and supporting me, when necessary, I am a lucky daughter and sister. I love you. Thanks to my friends, my outburst valve, essential to maintain mental health during this stressful period full of mixed emotions.

And last but not least, thank you, Manuel, for all the love, the smiles, the sustain, the calm and the energy that you have managed to convey to me in every moment of this journey and when I needed it most. Grateful to have you by my side.